EVALUATION OF THE ANTI FIBROTIC ACTIVITY OF PCBP2 SIRNA IN PRIMARY HEPATIC STELLATE CELLS AND DISCOVERY OF ANTI PD-L1 PEPTIDE AND NANOBODY FOR IMMUNOTHERAPY

A DISSERTATION IN

Pharmaceutical Sciences

and

Chemistry

Presented to the Faculty of the University

of Missouri-Kansas City in partial fulfillment of

the requirements for the degree

DOCTOR OF PHILOSOPHY

by

HAO LIU

M. S., Tianjin University, 2009

Kansas City, Missouri

2018

EVALUATION OF THE ANTI FIBROTIC ACTIVITY OF PCBP2 SIRNA IN PRIMARY HEPATIC STELLATE CELLS AND DISCOVERY OF ANTI PD-L1 PEPTIDE AND NANOBODY FOR IMMUNOTHERAPY

Hao Liu, Candidate for the Doctor of Philosophy Degree

University of Missouri-Kansas City, 2018

ABSTRACT

There are two major research objectives in this dissertation. Our laboratory recently discovered a small interfering RNA (siRNA) that silences the poly (rC) binding protein 2 (PCBP2) gene. It is hypothesized that silencing of the PCBP2 gene in hepatic stellate cells (HSCs) leads to the reversal of the accumulated type I collagen in fibrotic liver. The first research objective is therefore to evaluate whether the PCBP2 siRNA can reverse the alcohol- and cytokine-induced profibrogenic effects on HSCs.

The second research objective is to discover programmed death ligand 1 (PD-L1) specific peptides and nanobodies using phage display. These PD-1/PD-L1 checkpoint inhibitors can be potentially used as immunotherapy agents for cancer.

Chapter 1 introduces the background of the dissertation research and presented the Statement of the Problems and Objectives.

Chapter 2 reviews the mechanisms of liver fibrogenesis and cancer immunotherapy using checkpoint inhibitors.

Chapter 3 details our investigation of the anti-fibrotic effect of the PCBP2 siRNA in rat primary HSCs and HSC-T6 cells. The α-complex protein-2 (αCP2), encoded by the PCBP2 gene, is responsible for the accumulation of type I collagen in fibrotic liver. In this dissertation, we aimed to silence the PCBP2 gene using a siRNA to reverse the alcohol- and cytokines-induced pro-fibrogenic effects on HSCs. Primary rat HSCs and the HSC-T6 cell line was used as fibrogenic models to mimic the initiation and perpetuation stages of fibrogenesis, respectively. Our laboratory recently discovered a PCBP2 siRNA, which can efficiently silence the expression of αCP2 and reduce the stability of type I collagen mRNA in HSC-T6 cells. In this dissertation, we investigated the effects of PCBP2 siRNA on cell proliferation and migration. Expression of type I collagen in primary HSCs was analyzed using quantitative real-time PCR and western blot. In addition, we evaluated the effects of PCBP2 siRNA on apoptosis of the HSCs. Our results showed that PCBP2 siRNA reversed the alcohol- and cytokine-induced multiple pro-fibrogenic effects on primary rat HSC and HSC-T6 cells. The PCBP2 siRNA also reversed the alcohol- and cytokine-induced accumulation of type I collagen as well as cell proliferation and migration. Moreover, the combination of LY2109761, a TGF-β1 inhibitor, and PCBP2 siRNA exhibited a synergistic inhibition effect on the accumulation of type I collagen in HSCs. We therefore concluded that silencing of PCBP2 using siRNA could be a potentially therapeutic strategy for alcoholic liver fibrosis.

Chapter 4 discusses our discovery of several anti-PD-L1 peptides using a phage display peptide library. PD-L1 is overexpressed on a variety of cancer cells, and programmed cell death protein 1 (PD-1) is expressed on T cells. The interaction between

PD-L1 and PD-1 negatively regulates the immune responses of T cells, leading to escape of cancer cells from the attack of T cells. Blocking the PD-L1/PD-1 interaction is therefore a promising strategy to treat cancers by restoring the immune activity of T cells. The FDA has approved several monoclonal antibodies targeting PD-1 or PD-L1 for various cancer immunotherapies. However, large size (150 kDa) of antibodies limits their tumor penetration, especially in solid tumors. There has been a growing interest in developing low-molecular weight checkpoint inhibitors, such as peptides, in the past few years. Using a novel phage biopanning, we discovered several PD-L1-specific peptide antagonists to block the PD-1/PD-L1 interaction. The peptide candidate CLP002 exhibited the highest binding affinity to PD-L1 with an equilibrium dissociation constant (K_D) of 366 nM. The apparent K_D values of CLP002 to PD-L1-positive human cancer cell lines MDA-MB231 and DU145 are 212.9 nM and 184.1 nM, respectively. CLP002 efficiently blocked 85% of the PD-1/PD-L1 interactions with an IC_{50} of 2.17 μM. We verified that CLP002 restored T cell proliferation and prevented T cell apoptosis *in vitro*, when T cells were co-cultured with cancer cells. More importantly, we demonstrated that CLP002 is highly specific for PD-L1, thus minimizing its potential off-target effects in the body. According to the results of the *in vivo* anti-tumor activity study, the CLP002 peptide inhibited tumor growth and increased the survival of the CT26 tumor-bearing mice, suggesting the CLP002 peptide represents a promising drug candidate for cancer immunotherapy.

Chapter 5 describes our work towards discovering anti-PD-L1 nanobodies for cancer immunotherapy using a phage display of single-domain antibody (sdAb) library. Nanobody (also named sdAb or VHH) is an antibody fragment composed of a single

variable domain of the heavy chain on heavy chain only antibody. Nanobody is the smallest antibody fragment (14 kDa) that maintains the similar antigen-binding affinity. We discovered seven anti-PD-L1 nanobodies that blocked the PD-1/PD-L1 interaction. Among them, the nanobody CLV3 showed the highest binding affinity to PD-L1 with a K_D value of 12.37 nM. The nanobody CLV3 also exhibited the highest blockade of the PD-1/PD-L1 interaction with an IC_{50} of 32.3 nM. CLV3 inhibited tumor cell proliferation by binding to PD-L1 on the cancer cell surface and blocking the PD-1/PD-L1 interaction between cancer cells and T cells. Antitumor activity of the nanobody CLV3 was evaluated in a CT26 xenograft mouse model. The nanobody CLV3 significantly inhibited tumor growth and increased the survival of the tumor-bearing mice. The nanobody CLV3 is therefore a promising PD-L1 inhibitor that can be used for cancer immunotherapy.

APPROVAL PAGE

The faculty listed below, appointed by the Dean of the School of Graduate Studies, have examined the dissertation titled "Evaluation of the Anti-Fibrotic Activity of PCBP2 siRNA in Primary Hepatic Stellate Cells and Discovery of Anti-PD-L1 Peptide and Nanobody for Immunotherapy", presented by Hao Liu, candidate for the Doctor of Philosophy Degree, and certify that in their opinion it is worthy of acceptance.

Supervisory Committee

Kun Cheng, Ph.D., Committee Chair

Division of Pharmaceutical Sciences

Zhonghua Peng, Ph.D.

Department of Chemistry

Mridul Mukherji, Ph.D.,

Division of Pharmaceutical Sciences

Russell B. Melchert, Ph.D., R.Ph,

Division of Pharmacology & Toxicology

Xiang-Ping Chu, M.D., Ph.D.

Department of Biomedical Sciences

TABLE OF CONTENTS

LIST OF ILLUSTRATIONS

Figure Page

LIST OF TABLES

ACKNOWLEDGEMENTS

I would like to express my sincere gratitude and deep appreciation to my advisor, Dr. Kun Cheng for his excellent, patient guidance and mentorship and continuous support throughout all the time of research and study.

I would like to thank Dr. Russell B. Melchert of the Division of Pharmacology & Toxicology, Dr. Mridul Mukherji of the Division of Pharmaceutical Sciences, Dr. Zhonghua Peng of the Department of Chemistry, Dr. Xiang-Ping Chu of the Department of Biomedical Sciences, for their valuable guidance and thought insightful suggestions for my research and the dissertation, and kindly serving in my supervisory committee.

I would like to express thanks to my colleagues, Dr. Zhijin Chen, Dr. Wei Jin, Dr. Rubi Mahato, Dr. Ravi Shukla, Ashutosh Barve, Akshay Jain, Zhen Zhao, Yuanke Li and Bahaa Mustafa for their time, support and friendship during my research and study in UMKC.

In addition, I am grateful to other professors, staff members, and fellow students in the Division of Pharmaceutical Sciences for their help and friendship.

Finally, I would like to express my profound gratitude to my family for their support and love.

CHAPTER 1

INTRODUCTION

1.1 Overview

1.1.1 Liver fibrosis

Liver fibrosis is a worldwide health problem and one of the leading causes of morbidity and mortality in western developed countries [1]. Liver fibrosis is a wound-healing process induced by chronic liver injuries, such as hepatitis B, hepatitis C, alcoholic steatohepatitis, nonalcoholic steatohepatitis, alcohol abuse, autoimmune and biliary diseases, and metal poisoning [2]. Activation and proliferation of hepatic stellate cells (HSCs) is the critical milestone during liver fibrogenesis. Activated HSCs differentiate into myofibroblast-like cells, which migrate to the site of liver injury and produce a high amount of extracellular matrix (ECM) and pro-fibrotic cytokines [3].

Liver fibrosis is characterized by abnormal accumulation of ECM in the liver [1, 4]. During liver fibrogenesis, collagen is the most prominent component of the ECM and is mainly produced by activated HSCs [5]. Composition of the ECM changes from collagen type IV to collagen type I and type III during liver fibrogenesis. Activated HSCs, as the main contributor to liver fibrosis, produce over 90% of the collagen in fibrotic liver. As a result, activated HSCs are the key pathogenic cells in liver fibrogenesis.

1.1.2 Cancer immunotherapy and the PD-1/PD-L1 checkpoint pathway

Immunotherapy using checkpoint inhibitors has now evolved into the most promising therapy for cancer patients. Programmed death-ligand 1 (PD-L1) is overexpressed on a variety of cancer cells. The binding of PD-L1 to programmed cell death protein 1 (PD-1), which is expressed on immune cells, leads to immunosuppressive activity of T cells [6]. Once binding to PD-1, PD-L1 induces a negative regulatory effect on T cell immune responses, inhibits T cell activation, reduces T cell proliferation, induces T cell apoptosis, and finally reduces the cytokine release [7]. Blocking the PD-1/PD-L1 interaction therefore disrupts the immune-suppressing pathway and unleashes the anti-cancer immune responses of T cells to destroy cancer cells. Several anti-PD-L1 and anti-PD-1 monoclonal antibodies have been approved by the FDA for various cancer immunotherapies [8].

1.2 Statement of the problems

HSCs interact intensively with other cells in the liver, such as hepatocytes, Kupffer cells, endothelial cells and infiltrated immune cells. Autocrine and paracrine cytokines, growth factors and chemokines in the liver mediate the interactions between HSCs and other cells. Various cytokines including transforming growth factor beta 1 (TGF-β1), platelet-derived growth factor (PDGF) and epidermal growth factor (EGF) play important roles in activating quiescent HSCs. Among them, TGF-β1 is the most potent profibrogenic cytokine for liver fibrosis. It binds to the TGF-β1 receptor and regulates the synthesis and degradation of collagen type I, which is the major component of ECM in a fibrotic liver [10]. PDGF, which is primarily secreted by Kupffer cells, is

considered to be the most potent mitogen to HSCs [11]. Our laboratory previously discovered that exposure of HSC-T6 cells to alcohol leads to upregulation of αCP2, which is the main contributor to the accumulation of collagen type I in HSCs. We have identified a PCBP2 siRNA, which shows promising anti-fibrogenic activity in HSC-T6, a rat hepatic stellate cell line, through silencing the αCP2 protein [9]. In this dissertation, we aimed to determine whether the PCBP2 siRNA can reverse the alcohol- and cytokine-induced fibrogenesis in primary HSCs and HSC-T6 cells.

The PD-1/PD-L1 interaction facilitates the tumor growth by dampening the effector T cell-mediated immune responses. The tumor cell-killing ability of the effector T cells can be retrieved by the antibodies that block the checkpoint pathway. The FDA has approved two PD-1 inhibitors (Pembrolizuman and Nivolumab) and three PD-L1 inhibitors (Atezolizuman,AVelumab, Durvalumab). These blockade antibodies, either bind to PD-1 or PD-L1, have shown enormous promise to resume the T cell killing ability and subsequently improve anti-tumor immune responses towards melanoma, lung cancer, bladder cancer, and lymphoma [9, 10]. Thus, PD-L1-specific inhibitors may be more preferred to block the PD-1/PD-L1 pathway.

While these antibody-based checkpoint inhibitors demonstrated impressive clinical efficacy, they still have several limitations, such as poor tumor penetration due to large size (150 kDa) [11, 12]. The effector T cells are able to migrate deeply into solid tumor tissue, and it is critical for checkpoint inhibitors to reach there to block the PD-1/PD-L1 pathway. However, antibodies cannot penetrate into tumor tissues and therefore may not be able to block checkpoints within solid tumors, leading to suboptimal efficacy [13]. Another drawback of these antibodies is their Fc-mediated activation of cytotoxic

immune responses through macrophages and nature killer cells, which result in the undesirable depletion of T cells in the circulation [11]. Therefore, there has been a growing interest in develop low-molecular weight checkpoint inhibitors in recent years.

1.3 Objectives

The objectives of the dissertation are:

1) To determine whether the PCBP2 reverses the pro-fibrogenic effects of alcohol and cytokines on rat primary HSCs and HSC-T6 cells. Alcohol, TGF-β1, PDGF and EGF were used to activate quiescent HSCs and stimulate the production of type I collagen. mRNA and protein levels of PCBP2 and type I collagen will be measured. We will also investigate proliferation and migration of the HSCs.
2) To investigate whether combination of the small molecule drug, LY2109761, and the PCBP2 siRNA exerts a synergistic inhibition effect on the accumulation of type I collagen in HSCs.
3) To discover PD-L1-specific peptides and nanobodies using phage display biopanning. We will develop a novel biopanning strategy to discover peptides and nanobodies that not only bind to PD-L1 but also block the PD-1/PD-L1 interaction.
4) To evaluate the affinity and specificity of the discovered PD-L1-specific peptides and nanobodies. We will determine the equilibrium dissociation constants (K_D) of the peptides and nanobodies to human PD-L1 using Surface Plasmon Resonance (SPR). We will determine the affinity and specificity of the peptides and

nanobodies to PD-L1 positive cancer cells. We will also use AugoDock Vina to model the interaction between the peptides and PD-L1.

5) To investigate whether these PD-L1-specific peptides and nanobodies restore the T cell proliferation and prevent T cell apoptosis in the presence of cancer cells.
6) To investigate anti-tumor activity of the PD-L1 peptides and nanobodies in CT26 xenograft mouse model. We will determine the expressions of PD-L1 and IFNγ in tumor specimen. We will monitor the density of CD8+ positive cells in tumors using immunohistochemistry (IHC). We will also determine the survival rate of the tumor-bearing mice treated with the peptides and nanobodies.

CHAPTER 2

LITERATURE REVIEW

2.1 Liver fibrosis

Liver fibrosis is a global health problem and one of the leading causes of morbidity and mortality in the world. It is a wound-healing process that results from chronic liver injuries [3]. Liver fibrosis is characterized by the excessive accumulation of extracellular matrix (ECM) in the liver. In healthy liver, there is a balance between synthesis and degradation of ECM, whereas the balance is shifted towards to accumulation of ECM during liver fibrogenesis [14]. Liver fibrosis is mainly caused by alcoholic steatohepatitis, nonalcoholic steatohepatitis, hepatitis B, hepatitis C, autoimmune disorder, biliary diseases, drug induced, helminthic infection, iron and copper overload [2]. Liver fibrosis is a reversible and treatable stage. The end stage is liver cirrhosis, which would lead to liver failure [5].

2.1.1 HCS is the main contributor for liver fibrogenesis

It has been well established that the activation and proliferation of HSCs is the central event in liver fibrogenesis. In the healthy liver, HSCs locate at the Disse space and are the primary storage cells of vitamin A. During the chronic wound-healing process, HSCs transform to myofibroblast-like cells, convert to proinflammatory, contractile and fibrogenesis cells [15]. The HSC activation would turn to “perpetuation”, when the wound healing process is chronic. The activated HSC increase the cell proliferation, migrate to the injury sites, and synthesizes over 50-fold more amount of

ECM. It is reported that the activation is mediated by several cytokines, either autocrine or secreted from other cells [16].

The HSC will be activated when the chronic injury persists. The wound healing reaction turns to dysfunctional, the stimuli cannot be terminated and the cell death remains, which would induce inflammation and promote the fibrogenesis [17]. After chronic liver injury, the HSC experiences a complicated transformation or activation procedure, which the HSC activates from quiescent to activated myofibroblast [15]. Cellular variations, which associated with the HSC activation, consist of morphological alterations, including the presence of the cytoskeletal molecule alpha smooth muscle actin (α-SMA), the loss of vitamin A storage, and an expansion in the development of rough endoplasmic reticulum [3]. Intrinsically, the synthesis of DNA and stellate cell proliferation are enhanced after the HSC activation. Notably, the significant changes in collagen type I and type III were observed. In addition, the level of heat shock protein 47 (HSP47) is also increased, which is reported as a collagen-binding stress protein. The up regulation is diagnosed as a collagen-specific molecule accompany collagen production [18].

2.1.2 Interactions between HSC and other cells

The transformation of quiescent HSC into activated myofibroblasts is associated with the interaction between the HSC and several other cell types. The activation is correlated with particular pathways that within the connection of the wound healing response. It is reported that the hepatocytes, endothelial cell, lymphocytes, macrophages would interact with HCS and then induce the activation. The cellular components are

spread out through the dead hepatocytes, such as the nucleic acid and damage-associated molecular patterns. The cellular components along with the reactive oxygen species, which induce the macrophages (Kupffer cells) activate and secrete pro-inflammatory and pro-fibrogenic cytokines, for example interleukin 1 beta (IL-1β), interleukin 6 (IL-6), tumor necrosis factor alpha (TNFα) and transforming growth factor beta (TGF-β). There are also some pro-inflammatory chemokines, such as pathogen-associated molecular patterns and chemokine ligand 2 (CCL2) [19]. HSC cooperates with macrophages, lymphocytes hepatocytes and endothelial cells leading to the progression of fibrosis development [16, 20].

2.1.3 Cytokines promote the liver fibrosis

The platelet-derived growth factor (PDGF) and TGF-β are the two most critical cytokines in the liver fibrogenesis, mediating the HSC activation and ECM production. PDGF, generally secreted by Kupffer cells, is the prevailing mitogen for fibroblast HSCs [21]. PDGF is a dimeric molecule consisting of 4 different variations of polypeptide chains (A, B, C, and D). The PDGF binds to the cell through tyrosine kinase receptors PDGFR-α and PDGFR-β. The expressions of 4 different PDGF are all increased after the HSC activation [22]. In the fibrotic liver, the chronic wound process is linked with the increased levels of both PDGF and the PDGFR. The signaling protein Ras is engaged by the activated PDGFR, which will further activate the ERK/MAPK pathway. Next, Phosphoinositide 3-kinase (PI3-kinase) pathway is also involved, which is essential for both mitogenesis and chemotaxis [21, 23, 24]. The sustained HSC proliferation induced by PDGF demands for the uptake of extracellular ($Ca2^{+}$) and up regulated intracellular

pH value. The multi-function signaling transcription factor, signal transducer and activator of transcription 1 (STAT1), is also associated to the PDGF pathway. Furthermore, the phosphorylated signaling molecule CREB may also have a key role in the hepatic stellate cell proliferation [25].

TGF-β is one of the most potent cytokines, playing a critical role in immunity, development, carcinogenesis and wound healing. This cytokine serves as an important connection between immune cells and fibrogenesis cells. TGF-β is produced by a series of different cell types. There are three major isoforms, including TGF-β1, TGF-β2 and TGF-β3. TGF-β1 is the most important isoform in fibrogenesis, which is secreted primarily by monocytes and kupffer cells, facilitate the fibrosis development. It is reported that the TGF-β promote the expression of type I and III collagen by Smad pathway [26]. TGF-β1 binds to the receptor, leading to the type II receptor associate with type I receptor and further interact with Smad2 and Smad3. After binding to Smad4, the complex come into the nucleus and regulate the gene transcription [3]. The HSCs also secrete TGF-β in an autocrine manner. TGF-β communicates with pro-inflammatory pathways at different stages, leading to the decreased expression of the TGF-β negative regulator BAMBI. The TGF-β suppresses the function of NK cells, furthermore inhibit the HSC apoptosis, implying the TGF-β also has influence on the immunoregulatory functions [16].

2.1.4 Modulations of the extracellular matrix in liver fibrosis

Hepatic fibrogenesis is characterized with significant alterations in both the amount and components of ECM. After chronic injury, the fibrotic liver accumulates

about 50 times ECM than before [9]. The over expression of ECM is due to the enhanced synthesis and attenuated proteolysis. Reduced function of ECM collagenase MMPs is the major reason, which is because of the increased level of the specific inhibitors (TIMPs).

Researchers have discovered a series of collagens that are overexpressed in the fibrotic liver, which account the major part of ECM [18]. The collagen type I and type III are the two most abundant with significant increases in the injured liver. In the liver microenvironment, enhanced collagen expression is reported at not only mRNA level but also protein level [27]. Collagen type I, as the most abundant content in hepatic fibrosis, is consisting of two α1 and one α2 polypeptide chains. The overexpression of collagen type I in hepatic fibrosis is mainly because of an extension in the half-life of the mRNA of collagen type I, from 1.5 h in quiescent status to about 24 h in activated primary HSCs [28]. There's no significant alteration of the transcription of the collagen α1 gene, which implies the post-transcriptional modification plays a important role in the overexpression of collagen type I [29]. The increased stabilization of the collagen α1 mRNA is due to the RNA binding molecule αCP2, which binds to the 3′-UTR of collagen α1 and significantly increase the stability of the mRNA [30].

It is reported that the expressions of several glycoproteins were also up regulated in liver fibrosis, such as laminin, fibronectin, tenascin, merosin, hyaluronic acid and nidogen [31]. Researchers discovered that expressions of a few proteoglycans are increased, for example dermatan, heparin, perlecan, chondroitin sulfates, biglycan, decorin and syndecan [32]. Alteration of the ECM quantity and composition exerts a mechanical and physical influence, leading to variation of cellular activities such as gene expression, stellate cell migration and growth [33].

In summary, the liver fibrosis is characterized as over accumulation of ECM. HSC is the major producer of the ECM. During the fibrogenesis, the HSC activate, migrate from disse to the injury site with enhanced proliferation and collagen production. The levels of cytokines also increase such as TGF-β and PDGF. In this dissertation, we aim to use PCBP2 siRNA reverse the alcohol- and cytokine- induced fibrogenesis.

2.2 Cancer immunotherapy and PD-1/PD-L1 blockade

2.2.1 Cancer immunotherapy

Immunotherapy has shown enormous promise for cancer treatment and was elected as the Breakthrough of Year 2013 by Science [34]. Checkpoint inhibitor is one of the most important Immunotherapies. Notably, the first checkpoint inhibitor, anti-CTLA4 antibody (ipilimumab), attained a massive improve on the survival rate of patients with metastatic melanoma [35]. The traditional targeting therapies usually have good response on patients at the beginning of treatment but not for long. Immunotherapy is able to improve the patient's survival in long term, though not as many people respond well as the targeting therapies [36].

To initialize the antitumor activity, there are three steps: presenting antigen to dendritic cells, generation of active T-cell responses and reverse the immunosuppression from the tumor cells. The immune activities normally start with the tumor antigen presentation by the dendritic cells, acquired exogenously or from dead tumor cells. Next, the MHC class II and I molecules receive the antigen, respectively [37, 38]. In the lymph nodes, the T cells are activated and transform to effector T cells in the presence of immunogenic maturation stimulus. Otherwise, it will induce the generation of T

regulatory cells instead. Depending on the dendritic cell maturation stimulus and the co-stimulatory signal, the T cell would transform to effector T cells or T regulatory cells [39, 40]. Then, the T cells are released from the lymph node and migrate to the tumor tissue. Notably, the tumor cells suppress the T cell killing ability by the over expression of the negative regulatory ligands such as PD-L1 on the tumor cell surface [39, 41].

Tumor cells mute the immune system through a few complementary mechanisms of immunosuppressive activities. Some factors, such as prostaglandin E2, adenosine, VEGF-A and TGF-β, exhibit immunosuppression to the dendritic cells, further prevent the T cell penetration to the tumor tissue and hinder the T cell activation [42]. Tumor cells are also able to directly bypass the T cell recognition through the inhibition of the MHC molecules or reduce the NKG2D ligands [43]. Notably, over expression of tumor cell surface ligands is reported such as PD-L1, which suppress the T cell function by direct binding of the T cells and tumor cells through the PD-1/PD-L1 interaction [44]. Some leukocytes also inhibit the T cell activity, such as T regulatory cell, B cell, NK cell and myeloid-derived suppressor cell (MDSC). Those cells inhibit the T cell activation through multiple mechanisms, for example IL-10, nitric oxide, arginase, reactive oxidative species and TGF-β [45].

2.2.2 The immunosuppressive effect of PD-1/PD-L1 interaction

PD-1 is a key inhibitory receptor expressed on immune cells, for example T cells. PD-1 typically works to restrain autoimmunity through binding to either ligand, PD-L1 or PD-L2 [46]. This process is helpful to avoid harmful inflammation in normal circumstances. But in tumor, the tumor cell binds to T cell and initiates a negative

signaling by the PD-1/PD-L1 interaction, leading to the inhibition of the T cell functions [6]. PD-L1 is highly expressed on tumor cells. The binding interaction would bring a negative effect to T cells and inhibit the immune response, promoting T-cell exhaustion, anergy, and apoptosis [10]. In addition, it is also reported that the B7-1/PD-L1 interaction will also suppress the T cell activation and cytokine secretion [47].

The PD-1/PD-L1 interaction facilitates the tumor growth by dampening the effector T cell mediated immune response. There are several blockade antibodies approved by FDA. The blockade antibodies, either bind to PD-1 or PD-L1, have shown enormous promise to restore the T cell killing ability and to improve antitumor immune response towards some cancer models [10]. While the immune suppress mechanism makes use of checkpoint that inhibit the effector T cell functions, the tumor cell killing ability may be retrieved by the antibodies, which block the suppressing receptor-ligand interaction so as to mute the checkpoint inhibitory effect. By now, the antibodies have showed potent oncologic efficacy in several cancers and metastasis, like breast cancer and melanoma [48]. However, it is reported that the inadequate expression of PD-L2 would possibly lead to tumor promoting TH2 inflammation, implying the anti PD-1 antibodies would bring an unwanted PD-L2 signal blocking, which is not true for the anti-PD-L1 antibodies [49, 50]. Thus, PD-L1 specific targeting strategy may be preferred over the PD-1 blocking.

Even though therapeutic monoclonal antibodies have shown great promise in the tumor treatment, the blockade antagonists have inevitable limitations, such as deficient tumor tissue penetration [11, 12]. The effector T cells are able to immigrate deep into solid tumor tissue. It would not be favorable for the antibodies to enter tumor tissue due

to their large molecular weight, which will compromise the effect of the therapeutics [13]. Second, it is reported that detrimental Fc-mediated effector would diminish the activity of antibodies [12]. In addition, another limitation of antibodies is the cytotoxic immune responses [11].

Cluster of differentiation 80 (CD80) is reported as another receptor of PD-L1 apart from PD-1. The binding of CD80 with PD-L1 brings inhibitory effect on T cell function. The binding affinity of the PD-L1 to CD80 is around 1.7 μM [47]. The CD80 binding site on PD-L1 partly overlaps with the binding area on PD-L1 to the PD-1 [51]. It is suggested the anti PD-L1 antibody, which blocks the PD-1/PD-L1 interaction, may also hinder the CD80/PD-L1 interaction as well. Anti PD-L1 antibody (10F.9G2) has significant tumor inhibitory effect, since the anti PD-L1 antibody is capable of targeting two different bindings simultaneously [44].

2.2.3 PD-1/PD-L1 blockade antibodies and combinations with checkpoint inhibitors

So far, there are two anti PD-1 antibodies and three anti PD-L1 antibodies have been approved by the FDA. The antibodies bind to PD-1 or PD-L1, block the ligation and further increasing the tumor clearance. It is reported that the anti PD-1 antibody Nivolumab was given to 296 cancer patients, including renal-cell or colorectal cancer, non–small-cell lung cancer, advanced melanoma and castration resistant prostate cancer. About 20-25% of the patients showed positive response to the treatment. 14% reported adverse events. The researchers also observed a correlation between the objective response and the PD-L1 expression [52]. This is in agreement with another research [53]. In that research, tumor patients received the treatment of Atezolizumab, an engineered

humanized anti PD-L1 antibody. About 13-26% of the volunteers showed objective response to the anti PD-L1 antibody treatment. Notably, the researchers observed sustained response only days after the treatment, which is different from the traditional chemotherapy. The small molecule drugs normally have most patients with good objective response at only the beginning. The authors also discovered the tumor regression is related to T-helper type 1 (TH1) gene expression, CTLA4 expression and the absence of fractalkine.

The combinations of chemotherapeutic drugs have been commonly applied for decades. It is beneficial to improve the response and reduce the resistance by using the combinations. It is believed that the combination will also expand the usage of immunotherapy [35]. The anti CTLA-4 antibody only exerted objective response in 10% of the cancer patients, while the combination of anti CTLA-4 antibody with anti PD-1 antibody improved the response in 53% [54, 55]. In another study, researchers investigated the combination of anti 4-1BB antibody and anti PD-1 antibody in melanoma mouse model [34]. The authors discovered potent tumor inhibition effect by using the combination compare to the single antibody treatment. The IFNγ and CD8+ levels were significantly up regulated in tumor tissue. The authors suggested the anti 4-1BB and anti PD-1 antibody combination could induce robust immune response against tumors. Similarly, Ueha et al. combined the anti CD4 antibody plus anti PD-L1 antibody and observed strong tumor inhibition effect on the B16F10 bearing mice [56]. The authors suggested the depletion of CD4+ T cells, including CD25+ T regulatory cells, has a significant effect on the tumor growth. This is because the clearances of CD4+ cells improved cytotoxic T lymphocyte (CTL) proliferation and the penetration of CTL cell

into the tumor tissues. In addition, Mace et al. studied the combination of anti IL-6 and anti PD-L1 antibodies in pancreatic ductal adenocarcinoma (PDAC) [57]. IL-6 is highly expressed in pancreatic cancer, which is released from pancreatic stellate cells. The combination exerted prominent antitumor effect on mice xenograft. They also discovered elevated effector T cells and decreased α-smooth muscle actin level in the tumor tissue.

Some chemotherapeutic small molecule drugs trigger the tumor-associated immune responses by elevating the immunogenic factors, such as PD-L1 expression. Shalapour et al. reported oxaliplatin induced the chemotherapy resistance by the recruitment of immunosuppressive B cell [58]. The PD-L1 expression was induced on the B cells and further inhibited the T cell activation. Then, the researchers treated the tumor bearing mice with the combination of the oxaliplatin and anti PD-L1 antibody. They observed attenuated tumor progression with up regulated CD8+ T cell density. In addition, Wood et al. discovered that the histone deacetylases (HDACs) inhibitor works synergistically with anti PD-L1 antibody for the melanoma model [59]. As the HDAC inhibitor increased the PD-L1 expression during the treatment, the PD-L1 blockade combined with HDAC inhibitor significantly decreased the tumor growth.

The PD-1/PD-L1 blockade plus vaccination has also been studied. The vaccination targeting GM-CSF or Flt3-ligand on mouse melanoma cancer cells combined with checkpoint inhibitors of CTLA-4 and PD-1/PD-L1 interaction exhibited great tumor inhibition [10]. The vaccination showed significant synergistic effect, when combined with antibody. The combination showed more than two fold of the tumor inhibition compare to the vaccination only. Notably, the combination of vaccination plus anti CTLA-4 and anti PD-1/PD-L1 antibodies significantly improved survival rate of the B16

melanoma bearing mice. There were 65% of the mice with tumor-free survival for up to around 90 days after the challenge. In addition, Xue et al. used one huIgG1 antibody DNA vaccine (SCIB1) against mice challenged with B16F1-DR4 tumors. About 40% survival rate of the mice was observed. Then, the researchers combined the vaccine with anti PD-1 antibody and increased the survival rate of the mice to 80%.

2.2.4 Novel checkpoint inhibitors block PD-1/PD-L1 interaction

Nanobody is the antigen binding area on the heavy chain of the heavy chain only antibody [60]. It is small in size (15 KD) and robust but still retains the comparable binding specificity and affinity as antibody, which makes nanobody a great candidate as the checkpoint inhibitor [13]. Recently, one nanobody caplacizumab targeting acquired thrombotic thrombocytopenic purpura (aTTP) received a very promising result from clinical trial phase III [61]. Zhang et al. reported the one nanobody KN035, which targets PD-L1 and suppresses the tumor growth as a checkpoint inhibitor [62]. The authors detected the crystal structures of nanobody and PD-L1 binding complex and discovered the binding area between the KN035 and PD-L1 is overlapped with PD-1. The nanobody competed PD-1 for the PD-L1 binding site, single surface loop of 21 amino acids, which is consisting of two short helices and critical hydrophobic and ionic binding spot with amino acid residues on PD-L1, including Ile54, Tyr56 and Arg113. The authors treated the tumor bearing mice with KN035. Potent antitumor activity was observed at dosage of 0.5 mg/Kg.

Peptide has also been used as candidate for the blockade of the PD-1/PD-L1 interaction. Phage display is a powerful tool to screen the targeting ligand. After 3-5

rounds of selections, the phage colonies are isolated for sequencing. Recently, it is proved that the peptide can also be used a checkpoint inhibitor for immunotherapy [63]. A novel method of biopanning was developed to screen the D amino acid peptide against PD-L1. The authors first performed the biopanning against PD-L1 protien synthesized with D amino acid. Next, the peptide candidates were produced of D amino acids targeting PD-L1 protein with L amino acid. The peptide composed with D amino acids is very stable and embraced strong PD-L1 specificity and significant antitumor activity. The average survival rate of the CT26 bearing mice was increased from 27 days to 44 days.

Small molecule drugs were identified for the blockade of PD-1/PD-L1 interaction [64]. The authors studied the mechanism of small molecule candidates discovered by Bristol-Myers Squibb. Among them, there were two molecules that induced two PD-L1 molecules to form a dimer and further prevent the PD-1/PD-L1 bonding. The candidate stayed in a deep hydrophobic tunnel in the middle of the two PD-L1 molecules and stopped the PD-1/PD-L1 interaction. The authors suggested the small molecule drugs revealed a novel prospect to disrupt the PD-1/PD-L1 interaction.

Aptamers are widely used as therapeutics or targeting ligands. Either RNA aptamers or DNA aptamers are composed of small nucleic acids with great targeting specificity and binding affinity [65]. Lai et al. reported a DNA aptamer, which works the similar mechanism as blockade antibody [66]. The PD-L1 specific aptamer (aptPD-L1) binds to PD-L1 and blocks the PD-1/PD-L1 interaction. The aptPD-L1 successfully inhibited the tumor growth in a mouse model, with significant increased CD8+ T cell detection. The author also observed elevated levels of several mediators, such as IL-2, TNF-α, IFNγ and CXCL9.

In general, the immunotherapy has shown great promise for tumor treatment, especially the checkpoint inhibitor, including the PD-1/PD-L1 blockade. It is reported that cancer cells make use of checkpoint interaction to inhibit the immune response. Since many checkpoints function through ligand-receptor interactions, they can be blocked by monoclonal antibody [67], antibody fragment [62], peptide [63] or small molecule [64]. The PD-1/PD-L1 checkpoint inhibitors have exhibited exciting and long-term therapeutic effects on multiple tumors. The combinations of two different drugs significantly increase the tumor suppression. Compared to the conventional chemotherapy drugs, the immunotherapy may have a great future for the cancer treatment.

CHAPTER 3

SILENCING OF αCP2 REVERSE THE ALCOHOL- AND CYTOKINE-INDUCED FIBROGENESIS IN HEPATIC STELLATE CELLS

3.1 Rationale

Liver fibrosis/cirrhosis is a global health problem that leads to morbidity and mortality. Alcohol abuse is one of the most common causes of liver fibrosis/cirrhosis in western developed countries and accounts for over 50% of the cirrhosis cases [1, 5]. Alcoholic liver fibrosis is characterized by the excessive accumulation of extracellular matrix (ECM) in the liver. While liver fibrosis is reversible and treatable in the initial stage, it becomes irreversible and untreatable in its advanced stages.

The hepatic stellate cells (HSC) play a key role in fibrogenesis and are responsible for the production of the ECM. It is known that the transformation of quiescent HSC to myofibroblast-like cells is a milestone in liver fibrogenesis [68]. ECM secretion is significantly increased when the HSC are activated. These conditions lead to liver fibrosis, which is accompanied by enhanced HSC migration.

HSC activation is divided into two different stages, initiation and perpetuation [3]. The initiation stage involves changes in gene expression and phenotype. Sustained stimulation of HSC over a longer term results in the perpetuation stage, which involves proliferation and fibrogenesis [69]. When they are activated, HSC become more contractile, proinflammatory, and fibrogenic [70]. Additionally, after transformation, activated HSC migrate to the injury sites, where they produce over 50-fold higher levels of ECM, in which collagen type I is the major component [71]. The excessive collagen

accumulation in activated HSC is mainly because of the enhanced stability of collagen type I mRNA [30]. In our previous study [9], HSC-T6, exposed to alcohol for 48 h, demonstrated enhanced αCP2 expression, leading to the prolonged stability of collagen type I mRNA.

In a fibrotic microenvironment, various cytokines including transforming growth factor β1 (TGF-β1), platelet-derived growth factor (PDGF) and epidermal growth factor (EGF) play important roles in stimulating fibrosis and cirrhosis. These cytokines promote cell proliferation and cell migration as well as excessive collagen production. TGF-β1, one of the most potent pro-fibrogenic cytokines, is involved in the initiation and maintenance of fibrogenesis. The TGF-β1-stimulated activation of HSC is reported to be the key fibrogenic response in liver fibrosis [68]. In addition, PDGF, an important cytokine, also promotes collagen production in HSC activation. PDGF and its receptor (PDGFR) are up-regulated after HSC activation and correlated with the degree of fibrosis. Epidermal growth factor (EGF) plays a critical role in liver regeneration and transformation. EGF and EGF receptor (EGFR) are highly over-expressed in fibrotic liver and result in increased HSC migratory capacity and up-regulated matrix metalloproteinase (MMP)-2 activity [72, 73].

In the current study, primary rat HSC and the HSC-T6 cell line were used as fibrogenic models to mimic the initiation and perpetuation stages of fibrogenesis**,** respectively. Furthermore, we used PCBP2 siRNA to explore its effects on liver fibrogenesis induced by alcohol and cytokines.

3.2 Materials and methods

3.2.1 Materials

Dulbecco's modified Eagle's medium (DMEM), Dulbecco's phosphate-buffered saline (DPBS), penicillin and streptomycin were purchased from Mediatech, Inc. (Manassas, VA). Fetal bovine serum (FBS) was purchased from Atlanta Biologicals Inc. (Lawrenceville, GA). Bovine serum albumin (BSA) was purchased from Sigma-Aldrich Corporation (St. Louis, MO). iTaq Universal SYBR Green One-Step Kit was purchased from Bio-Rad (Hercules, Ca). Platelet-derived growth factor (PDGF) and epidermal growth factor (EGF) was purchased from R&D system (Minneapolis, MN). Transforming growth factor (TGF)-β1 was purchased from Sino Biological Inc. (Beijing, China). PCBP2 siRNAs and the scrambled siRNA (negative control siRNA) were obtained from Ambion Inc. (Austin, TX). Lipofectamine-iMAX and TRIzol reagent were obtained from Invitrogen Corp. (Carlsbad, CA). Dead Cell Apoptosis Kit with Annexin V Alexa Fluor® 488 and Propidium Iodide (PI) was purchased from Thermo-Fisher Scientific (Pittsburgh, PA).

3.2.2 Cell culture

The rat hepatic stellate cell line HSC-T6 was kindly provided by Dr. Scott L. Friedman (Mount Sinai School of Medicine, New York, NY), and primary rat HSCs were isolated as we described before [74-76]. The cells were cultured as previously reported [77] in DMEM medium supplemented with 10% FBS, penicillin (100 units/mL) and streptomycin (100 μg/mL) at 37°C in a humidified atmosphere containing 5% CO_2. The medium was changed every other day. Cells were passaged at 80–90% confluence. For

alcohol induction study, HSC were incubated with alcohol in a closed chamber as previously described [9, 78-80].

3.2.3 Isolation of primary rat hepatic stellate cells

Primary rat HSCs were isolated as we described before [74-76]. The animal used protocol was approved by the University of Missouri-Kansas City, Institutional Animal Care and Use Committee. Briefly, Sprague-Dawley rats (~250 g) were anesthetized with isoflurane. The abdomen was opened, and the portal vein was cannulated by using polyethylene tubing. The rat liver was perfused with 2 mL of heparin solution diluted to 20 units/mL to avoid blood clotting. The rat liver was then perfused with 200 mL of Hanks' balanced salt solution at 15 mL/min and then with 250 mL of Hanks' balanced salt solution containing 0.05% type IV collagenase and 0.1% Pronase at 10 mL/min. All solutions were maintained at 37 °C. After the perfusion, the rat liver was removed and immersed in Hanks' balanced salt solution, and all other tissue were removed without damaging the liver. The liver was then cut into small fragments, and the liver cells were released into the medium by mild agitation with forceps. The cell suspension was filtered through sterilized gauze and then centrifuged at 50 × g for 5 min; the supernatant was further centrifuged at 100 × g for 5 min. After that, the supernatant was collected and centrifuged at 500 × g for 10 min. The HSC were further separated using a density gradient centrifugation method. The cells pellet was dispersed into 10 mL of an 11.5% Nycodenz solution and slowly overlaid on 5 mL of a 17.5% Nycodenz solution. This gradient was then covered by 2 mL of PBS. The gradient was then centrifuged at 1450 × g for 17 min, and the top of the second layer contained the purified primary HSC.

3.2.4 Cell cycle analysis and apoptosis assay

The cell cycle analysis and apoptosis assay were performed as described in the previous study with modifications [81]. For the cell cycle assay, twenty-four hours after the PCBP2 siRNA transfection, the cells were incubated with 50 ng/mL PDGF for an additional 12 hours. The cells were collected and fixed with ice-cold 70% ethanol. They were then washed with Dulbecco's PBS and incubated with a propidium iodide/RNase staining buffer for 30 min. The cell cycle analysis was performed using a FACSCalibur flowcytometer (BD Biosciences). For the apoptosis assay, the cells were incubated with alcohol for 48 hours, or transfected with 50 nM of the PCBP2 siRNA for 24 hours and then harvested. All of the cells were treated according to the manufacturer's protocol and analyzed using the FACSCalibur flowcytometer.

3.2.5 siRNA transfection

Cells were transfected using Lipofectamine-iMAX as described before [9, 81, 82]. The cells were seeded in 24-well plates at a density of 10,000-30,000 cells/well 12 h before the transfection. The transfection complex was prepared with 1.25 μL PCBP2 siRNA in 25 μL OPTI-MEM and 1.5 μL Lipofectamine-MAX in 25 μL OPTI-MEM by mixing two 25 μL solutions at room temperature for 5 min to form a complex. The cells were washed with DPBS and then incubated with 50 μL of the siRNA-Lipofectamine complex and 450 μL of OPTI-MEM to produce a final concentration of 50 nM of siRNA. After 6 h incubation, another 500 μL of fresh DMEM was added and incubated for 18 h before further evaluation.

3.2.6 Real-time PCR

Total RNA from the cells was isolated using Direct-zol RNA Miniprep Plus (ZYMO research), and real-time RT PCR was conducted to compare gene expression as reported [83]. The primers were as follows: PCBP2: forward primer: 5'-ACCAATAGCACAGCTGCCAGTAGA-3' and reverse primer 5'-AGTCTCCAACATGACCACGCAGAT-3'; type I collagen mRNA: forward primer 5'-TGGTCCCAAAGGTTCTCCTGGT-3' and reverse primer 5'-TTAGGTCCAGGGAATCCCATCACA-3'; type I collagen pre-mRNA: forward primer 5'-CCAGCCGCAAAGAGTCTACATGTC-3' and reverse primer 5'-TCACCTTCTCATCCCTC CTAA-3'. 18s: forward primer 5'-GTCTGTGATGCCCTTAGATG-3' and reverse primer 5'-AGCTTATGACCCGCACTTAC-3'.

3.2.7 Cell proliferation assay

HSC were seeded into 96-well plate at a density of 7000 cells/well in complete DMEM 12 h before transfection. They were transfected with 50 nM of the PCBP2 siRNA in DMEM with 0.5% FBS and incubated for 6 hours. Then, another 100 μL of DMEM with 0.5% FBS was added, and the incubation was continued for another 18 h. PDGF was then added at 50 ng/mL in completed DMEM containing 10% FBS. After 12 h, MTT was added and incubated for 2 hours, and the values were assessed using a DTX880 multimode detector (Beckman Coulter, Indianapolis IN) [84, 85].

3.2.8 Migration assay

The migration assay was conducted as described with modifications [72]. Transwell chambers with 8 μm polycarbonate membranes (COSTAR, Corning, NY) were coated with matrigel on the top (50 μg/mL) and collagen type I on the bottom (50 μg/mL). The wells were filled with DMEM containing 10% FBS with or without cytokines. HSCs were transfected with PCBP2 siRNA for 24 h in DMEM with 0.5% FBS (serum starvation for 24 h) before migration. The transwell chambers were inserted into the well, loaded with 20,000 cells/chamber and incubated for 4 h to allow migration through the membrane. The cells were fixed with 10% paraformaldehyde and stained with 0.05% crystal violet. All cells remaining on the upper side of the membrane were removed with a cotton swab. Images were taken (200×), and the numbers of cells were counted.

3.2.9 Western blotting

RIPA buffer (150 mM NaCl, 50 mM Tris base pH 8.0, 1 mM EDTA, 1% Triton X-100, 0.1% SDS, 1 mM PMSF and 1 mM Na_3VO_4) with protease inhibitor cocktail (Roche, Indianapolis, IN) was used to lyse cells. The cells were then incubated for 5 min on ice. The lysate was collected by centrifugation at 12,000 × g for 20 min at 4°C. Protein concentration of the supernatant was determined using a BCA protein assay kit (Pierce, Rockford, IL). Equal amounts of protein were loaded into a 12% SDS-PAGE gel. The separated proteins were transferred to a PVDF membrane. After blocking (5% nonfat dry milk solution) the membrane, an anti-type I collagen antibody (Rockland Immunochemical Inc., Gilbertsville, PA) was added and incubated for 2h at room

temperature. A horseradish peroxidase-conjugated secondary antibody and a chemiluminescence detection kit were used. The membrane was also re-probed with an anti-β-actin antibody (Rockland Immunochemical Inc., Gilbertsville, PA) as an internal control [68].

3.2.10 Statistical analysis

Data are expressed as the mean ± standard deviation (SD). Statistical analysis was performed using one-way analysis of variance (ANOVA). Tukey's multiple comparisons test was used as post hoc analysis. $P<0.05$ was considered to be significantly different.

3.3 Results

3.3.1 Silencing PCBP2 reverses the fibrogenic effect of alcohol and cytokines in primary HSC

Primary HSC were treated with 100 mM alcohol for 48 h to induce the pro-fibrotic gene expression [9, 86]. Quantitative real-time PCR was performed to determine the mRNA levels of PCBP2 and type I collagen. As shown in Figure 1A, incubation with 100 mM alcohol for 48 h significantly increased the mRNA levels of PCBP2 and type I collagen by 2.30-fold and 4.65-fold, respectively. Compared to our previous study in HSC-T6 [9], the increase of PCBP2 mRNA is equivalent, however the change of type I collagen mRNA is greater than observed in previous study (4.65-fold for the primary HSC compared to 2.7-fold for the HSC-T6 cells). We suggest that the primary HSC are at the quiescent state and therefore are more sensitive to alcohol treatment than HSC-T6 cell line. In addition, the alcohol treatment has no significant effect on the type I collagen

primary mRNA of the primary HSC, which is consistent with our previous report using HSC-T6 [9]. The alcohol increase the stability of mature mRNA, while there is no statistic significant difference of type I collagen primary mRNA of the primary HSC. Alcohol induces pro-fibrogenic effect in HSC by up-regulating the expression of the αCP2 (PCBP2), which increases the stability of the type I collagen mRNA at the post-transcriptional level [87].

Next, we treated the primary HSC with PCBP2 siRNA followed by the alcohol stimulation. Briefly, primary HSC were transfected with 50 nM PCBP2 siRNA for 24 h, and then the medium containing 100 mM alcohol was replaced every 6 h for a total incubation time of 48 h. As shown in Figure 1A&B, the PCBP2 siRNA remarkably knocked down the expression of PCBP2 (αCP2) in HSC at the mRNA and protein levels [9]. Real-time PCR results demonstrated that after alcohol induction, the silencing effect was up to 85% and 60% for PCBP2 and type I collagen, respectively. The protein expression of type I collagen was silenced to a similar level as that prior to alcohol stimulation (Figure 1B).

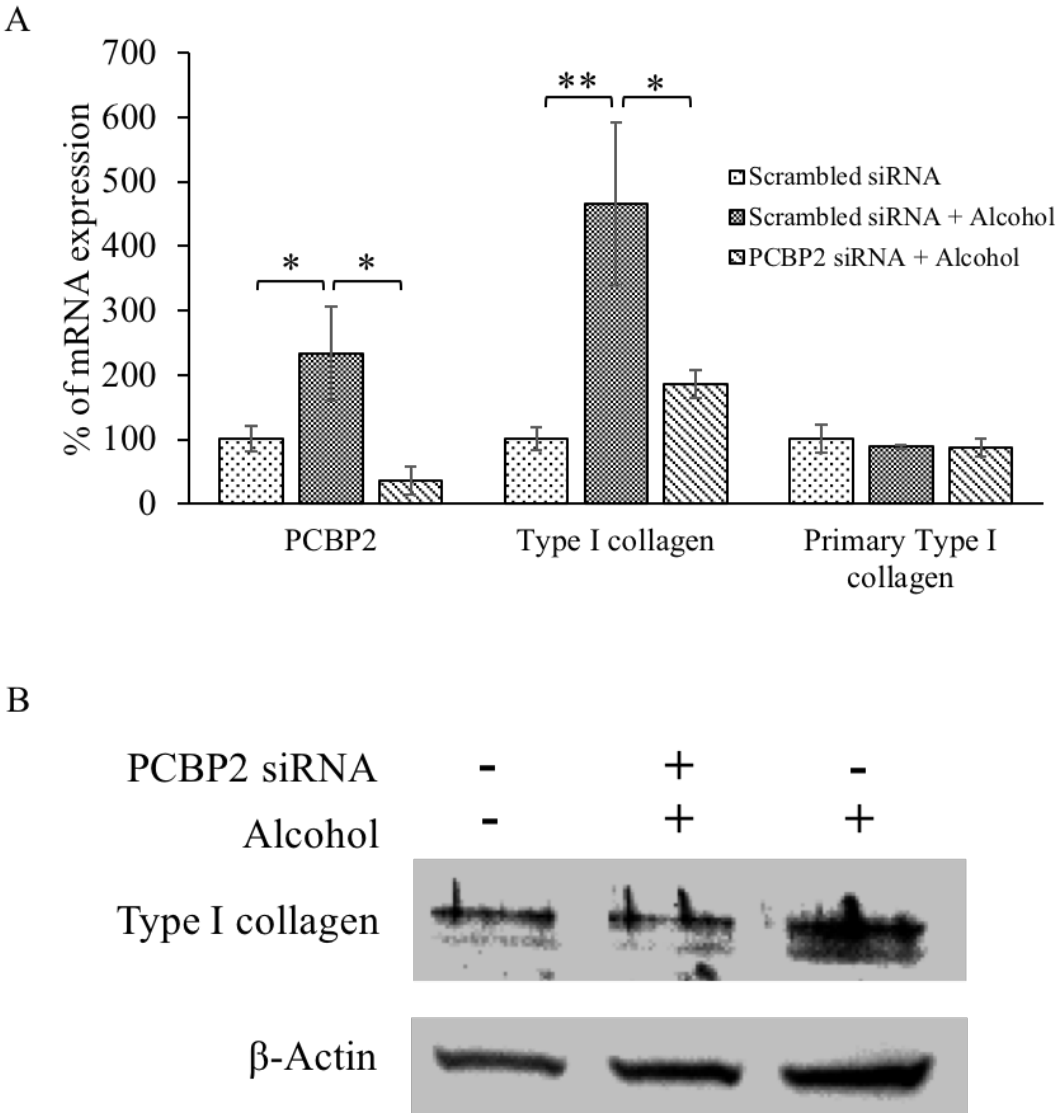

Figure 1. PCBP2 siRNA reverses alcohol-induced expressions of type I collagen in primary HSC. Primary rat HSC were transfected with 50 nM PCBP2 siRNA or scrambled siRNA for 24 h and then treated with 100 mM alcohol for 48 h. (A) The levels of PCBP2 mRNA, type I collagen mRNA, and type I collagen primary mRNA were quantified using real-time RT-PCR. (B) Protein expression of type I collagen was determined using western blot. The results are presented as the mean ± SD (n=3). (*P<0.05; **P<0.01).

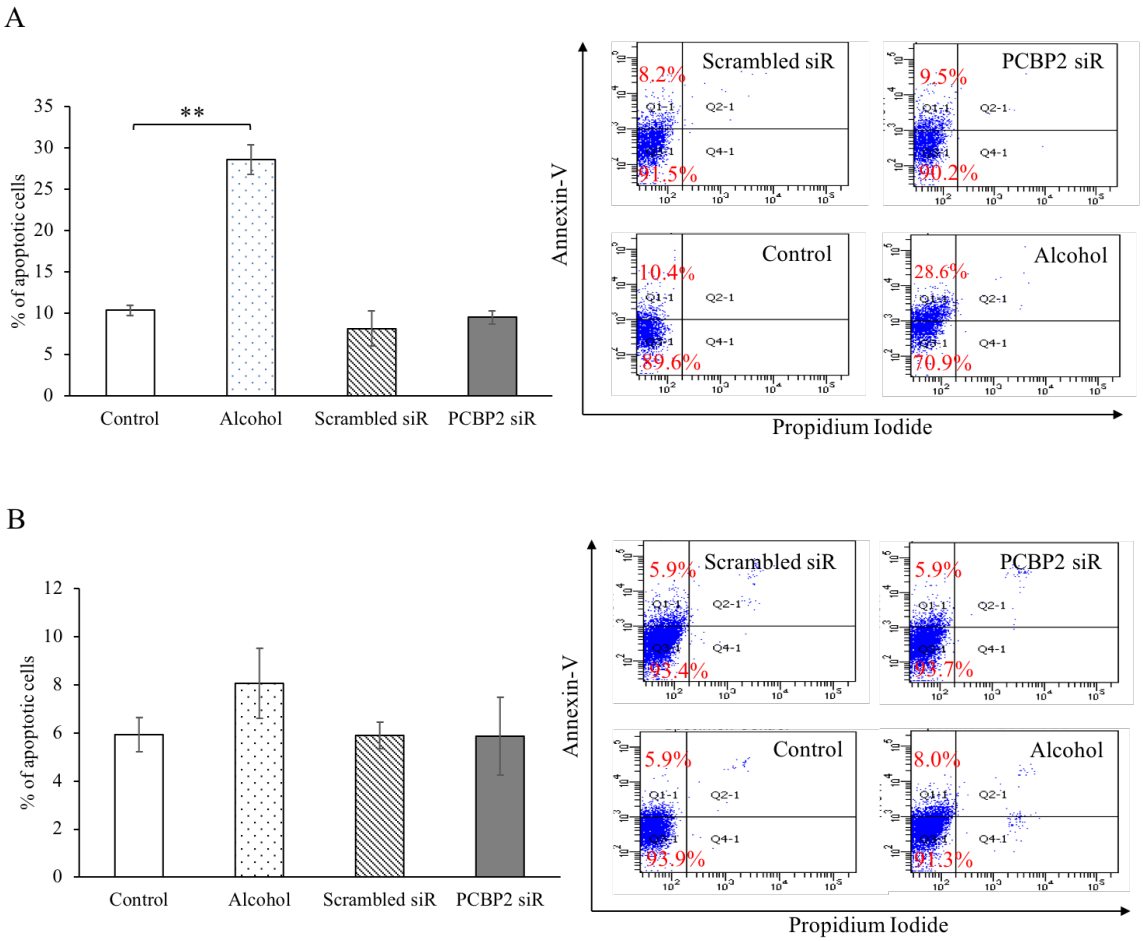

Figure 2. The effect of PCBP2 siRNA and alcohol on apoptosis in primary rat HSC (A) and HSC-T6 cells (B). HSC were treated with 50 nM siRNA for 24 h or 100 mM alcohol for 48 h. The cells were stained with Annexin-V-FITC and propidium iodide and analyzed using flow cytometry. The results are presented as the mean ± SD (n=3). (*P<0.05; **P<0.01).

Flowcytometry was performed to examine the apoptosis of HSC after the inhibition of PCBP2 using siRNA [81]. No significant difference in the numbers of annexin-V-positive apoptotic cells were observed in the PCBP2 siRNA treated group compared to the HSC transfected with scrambled siRNA. As shown in Figure 2, the scrambled siRNA and PCBP2 siRNA induced apoptosis by approximately 8.2% and 9.5%, respectively, in primary HSC (Figure 2A), while 5.9% and 5.9% in HSC-T6 cells (Figure 2B).

We also evaluated the apoptotic effect of alcohol stimulation on primary HSC and HSC-T6 cells (Figure 2). The cells were incubated with DMEM containing 100 mM alcohol for 48 hours, and the percentage of apoptosis in the primary HSC increased from 10.4% to 28.6%. However, 100 mM alcohol did not induce significant apoptotic effect in HSC-T6 (an increase from 5.9% to 8.0%).

Previous studies have demonstrated that TGF-β1 and PDGF could induce the expression of type I collagen [88, 89]. In the current study, we transfected HSC with PCBP2 siRNA three times over six days and then incubated the cells with a medium containing the cytokines. The primary HSC were treated with TGF-β1 (12 ng/mL) or PDGF (10 ng/mL) for 24 h. The expressions of PCBP2 and type I collagen were then determined at mRNA and protein levels. As shown in Figure 3A and C, both TGF-β1 and PDGF upregulated the mRNA level of PCBP2 and type I collagen. On the other hand, treatment of the cells with PCBP2 siRNA can reverse the induction effect of profibrotic cytokines, TGF-β1 and PDGF, on PCBP2 and type I collagen. Similar results were observed at the protein level of type I collagen (Figure 3B and D).

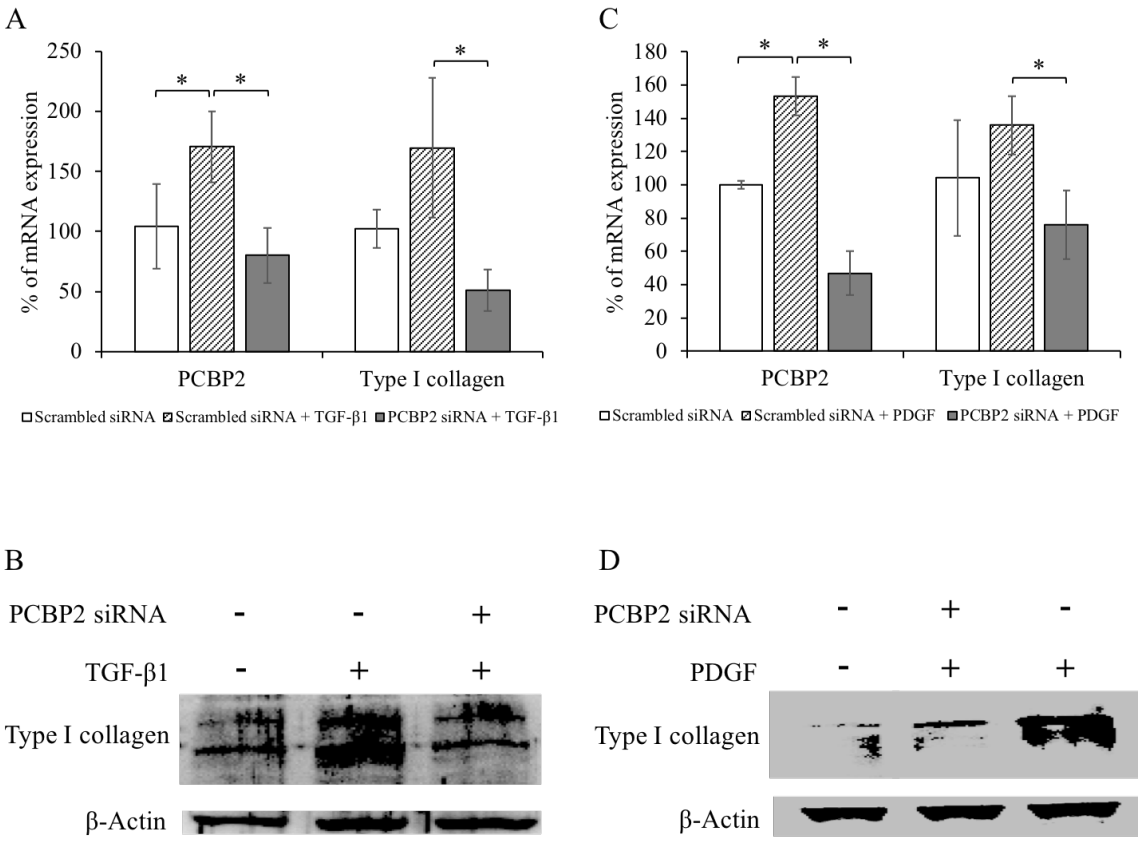

Figure 3. PCBP2 siRNA reverses cytokine-induced expression of type I collagen in primary rat HSC (A, B) and HSC-T6 (C, D) cells. The cells were transfected with 50 nM siRNA for 24 h and then treated with TGF-β1 or PDGF for 12 h. (A, C) mRNA levels of PCBP2 and type I collagen were quantified using real-time RT-PCR. (B, D) Protein expression of type I collagen was determined using western blot. The results are presented as the mean ± SD (n=3). (*P<0.05; **P<0.01).

3.3.2 PCBP2 siRNA reverses the proliferation effect of PDGF

As a result of chronic livery injury, the HSC, as the main ECM-producing cells, activate and transdifferentiate into myofibroblast-like cells and acquire pro-inflammatory properties. As previously reported [90], PDGF is up-regulated during fibrogenesis and is the most potent cytokine for HSC proliferation. In order to evaluate the effect of the PCBP2 siRNA on PDGF-stimulated cell proliferation, both primary HSC and HSC-T6 cells were transfected with 50 nM PCBP2 siRNA in DMEM containing 0.5% FBS for 24 h and then incubated with PDGF for another 12 h. As shown in Figure 4A, proliferation of primary HSC was induced by PDGF, and the stimulatory effect of PDGF was reversed by the treatment of PCBP2 siRNA. Similar results were observed in HSC-T6 cells (Figure 4B). However, the stimulatory effect of PDGF on primary HSC is more significant than on HSC-T6 cells.

Cell cycle analysis was conducted to investigate the anti-proliferation mechanism of the PCBP2 siRNA. Primary HSC treated with PDGF exhibited a decrease in the G0/G1 phase and a block in the G2/M phase (Figure 4C). Following transfection with the PCBP2 siRNA, the percentages of the primary HSC in the G0/G1 and G2/M phases were reversed to normal as compared to the cells without PDGF stimulation. Similar studies were also conducted in HSC-T6 cells (Figure 4D). PDGF also decreased the proportion of cells in the G1/G0 phase but blocked the cells in the S phase rather than the G2/M phase. The PCBP2 siRNA reversed the PDGF-induced cell distributions in the G0/G1 and S phases.

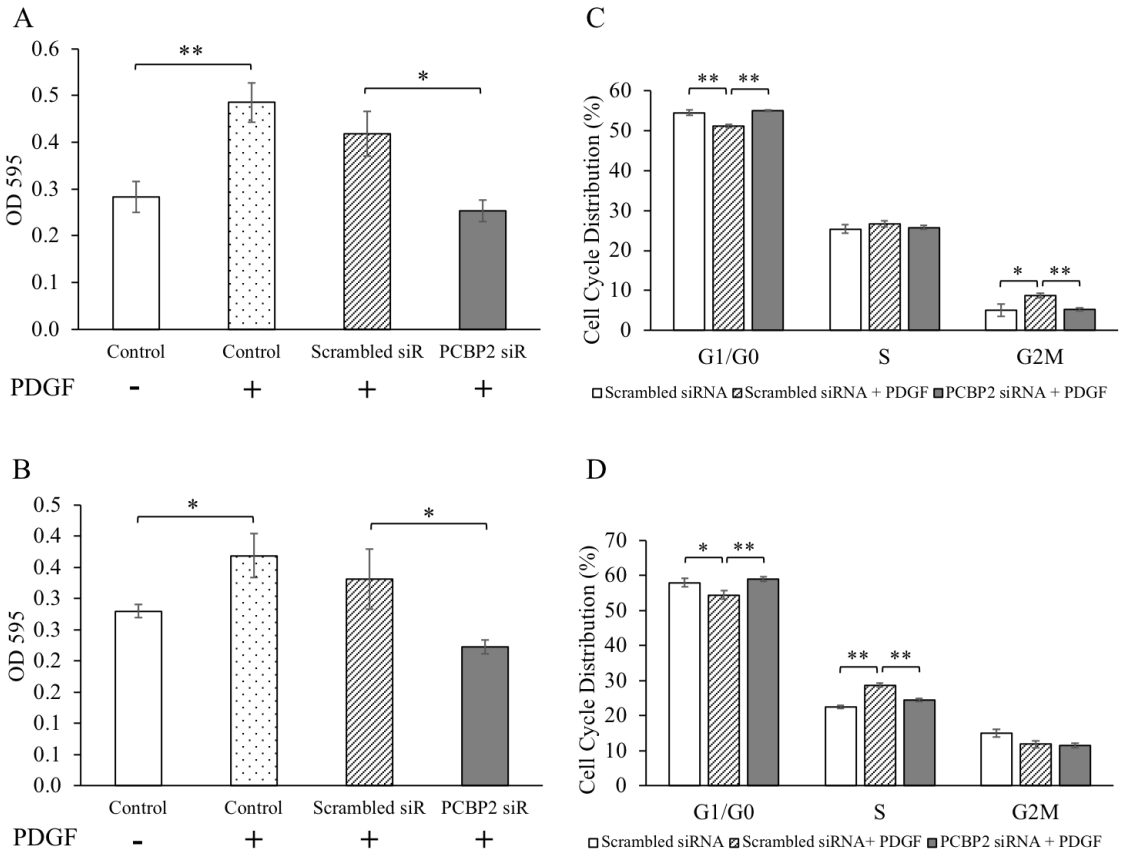

Figure 4. PCBP2 siRNA reverses PDGF-induced cell proliferation in primary rat HSC (A, C) and HSC-T6 cells (B, D). The cells were transfected with 50 nM siRNA for 24 h and then incubated with PDGF for 12 hr. (A & B) Cell proliferation was measured using MTT assay. (C & D) Cell cycle analysis was performed using flow cytometry. The results are presented as the mean ± SD (n=3). (*P<0.05; **P<0.01).

3.3.3 PCBP2 siRNA inhibits the migration effect of cytokines and alcohol

HSC reside in the space of Disse are the major storage site of vitamin A [91]. Following chronic injury of the liver, activated HSC migrate and accumulate at the site of injury, where they produce large amounts of ECM and modulate the degradation rate of ECM. Cytokines such as TGF-β1 [88], PDGF and EGF were previously reported to facilitate HSC migration [72, 90]. In the present study, we evaluated whether PCBP2 siRNA can inhibit the migration effect induced by cytokines and alcohol.

First, we treated HSC with serial concentrations of TGF-β1, PDGF and EGF to determine the optimal concentration that can induce the highest degree of migration of HSC (data not shown). Primary HSC (Figure 5) and HSC-T6 cells (Figure 6) were transfected with PCBP2 siRNA, followed by incubation with the cytokines for 4 h. Scrambled siRNA was used as a negative control in this study. As illustrated in Figure 5, after stimulation with the cytokines, the number of migrated primary HSC increased approximately by 3.3-fold for PDGF, 2.7-fold for TGF-β1 and 4-fold for EGF. By contrast, transfection of the cells with PCBP2 siRNA reversed the stimulatory effect of the cytokines. Similar results were observed in HSC-T6 cells (Figure 6). The number of migrated HSC-T6 cells increased by 2-fold for PDGF, 3-fold for TGF-β1 and 2.5-fold for EGF after stimulation with the cytokine. Transfection with PCBP2 siRNA also reversed the stimulatory effect of cytokines in HSC-T6 cells.

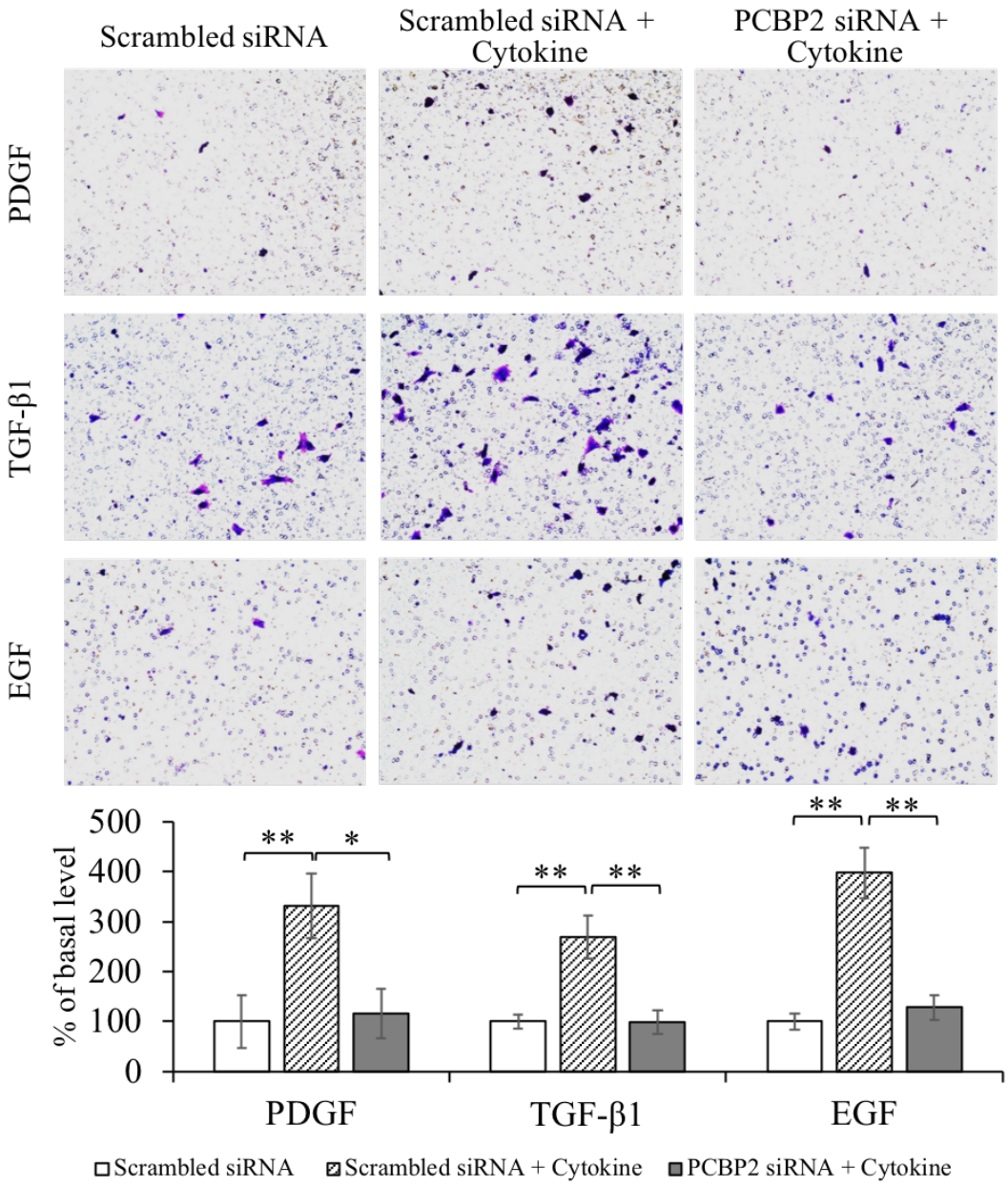

Figure 5. PCBP2 siRNA inhibits cytokine-induced migration effect in primary rat HSC. After transfection with 50 nM PCBP2 siRNA for 24 h, the primary rat HSC were loaded onto transwell chambers and incubated for 4 h to allow migration through the membrane. The migrated cells were stained, and the images were taken at 200× magnification. Six random microscopic fields were counted for each transwell. The cells treated with scrambled siRNA were used as the negative control. The results are presented as the mean ± SD (n=3) (*P<0.05; **P<0.01).

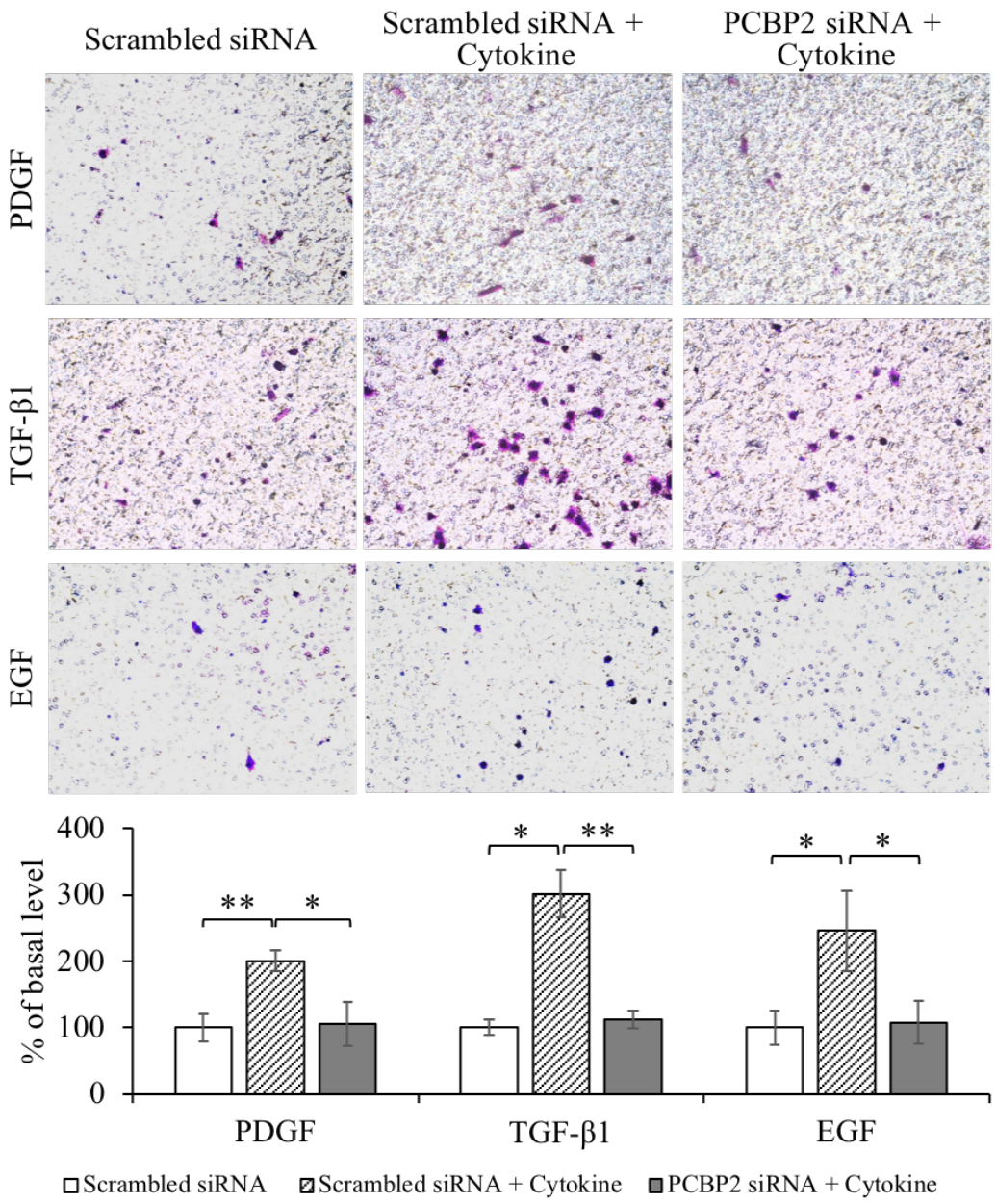

Figure 6. PCBP2 siRNA inhibits cytokine-induced migration effect in HSC-T6 cells. After transfection with 50 nM PCBP2 siRNA for 24 h, HSC-T6 cells were loaded onto transwell chambers and incubated for 4 h to allow migration through the membrane. The migrated cells were stained, and the images were taken at 200× magnification. Six random microscopic fields were counted for each transwell. The cells treated with scrambled siRNA was used as the negative control. The results are presented as the mean ± SD (n=3). (*P<0.05; **P<0.01).

Next, we evaluated the stimulatory effect of alcohol on the migration of primary HSC. As shown in Figure 7, incubation with alcohol for 24 h increased the number of migrated cells by approximately 2-fold, whereas the PCBP2 siRNA was able to completely reverse the stimulatory effect on migration. By contrast, alcohol exhibited more significant effect (4.65-fold increase) on the migration when the incubation time was extended to 48 h. Treatment of the cells with PCBP2 siRNA still attenuated, but cannot complete reverse, the stimulatory effect of alcohol on migration. This could be due to the transit silencing effect of the PCBP2 siRNA during the longer alcohol stimulation period.

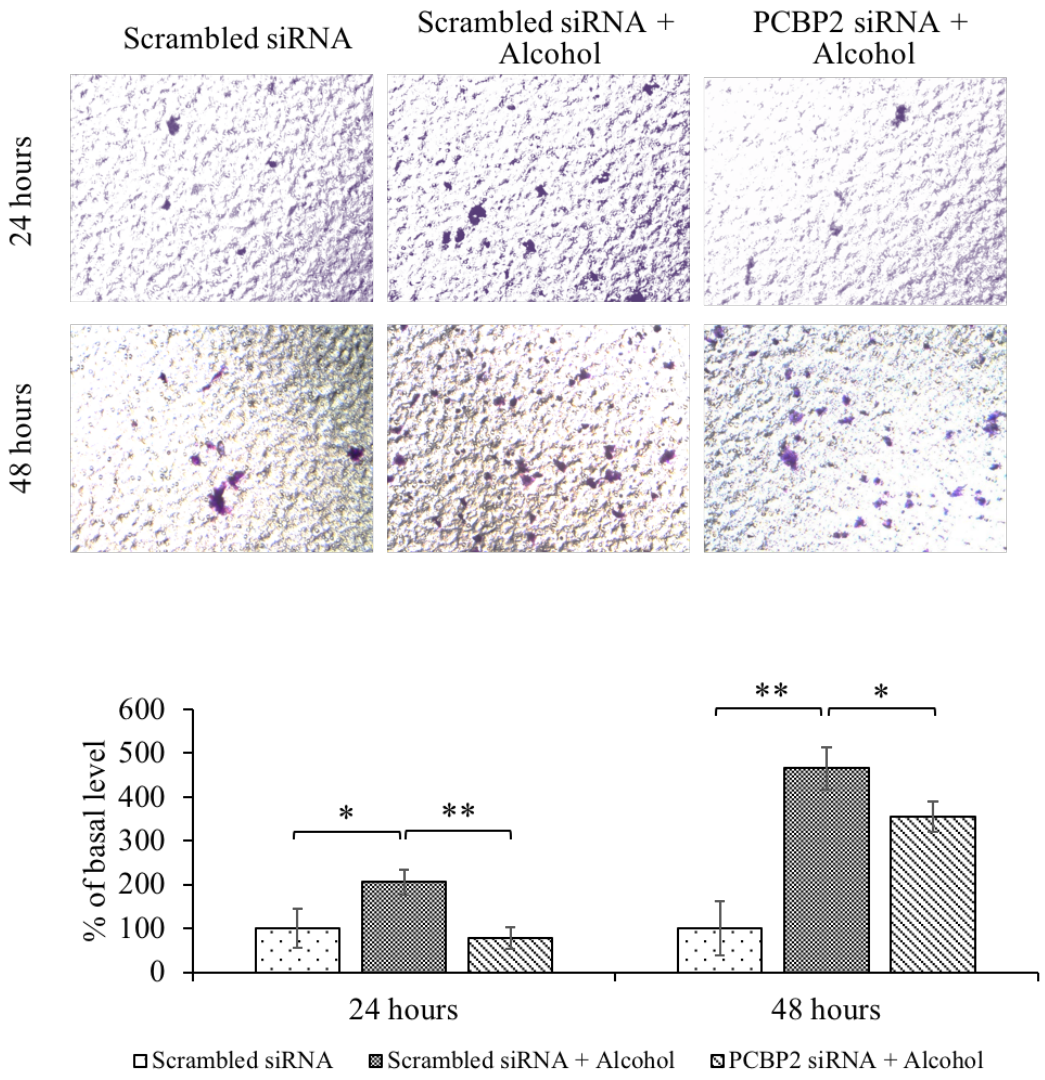

Figure 7. PCBP2 siRNA inhibits alcohol-induced migration effect in primary rat HSC. Primary rat HSC were transfected with 50 nM PCBP2 siRNA for 24 h and then incubated with 100 mM alcohol for 24 h or 48 h. The cells were then loaded onto transwell chambers and incubated for 4 h to allow migration through the membrane. The migrated cells were stained, and the images were taken at 200× magnification. Six random microscopic fields were counted for each transwell. The cells treated with scrambled siRNA was used as the negative control. The results are presented as the mean ± SD (n=3). (*P<0.05; **P<0.01).

3.3.4 Combinational treatment with PCBP2 siRNA and LY2109761

LY2109761 is a small molecule inhibitor of the TGF-β receptor type I/II (TβRI/II) kinases and widely used for various diseases [92, 93]. It has be used to treat pulmonary fibrosis [94] and human hypertrophic scar fibroblasts [95] because of its inhibitory effect on the expression of type I collagen. In this study, we treated HSC with a combination of the PCBP2 siRNA and LY2109761 and then monitored the expression of type I collagen using western blot (Figure 8A). The HSC-T6 cells are activated hepatic stellate cells and accordingly express high levels of type I collagen. While LY2109761 alone can significantly reduce the expression of type I collagen, the combination of LY2109761 and PCBP2 siRNA had a much better inhibition effect on type I collagen. The protein expression of type I collagen in HSC-T6 was reduced to nearly negligible levels by the combination treatment.

We then treated primary HSC (quiescent) with the same combination of PCBP2 siRNA and LY2109761 before subsequent alcohol stimulation (Figure 8B). Compared to HSC-T6, primary HSC are quiescent and therefore express low levels of type I collagen. Incubation with alcohol significantly induced the expression of type I collagen, and the combination treatment reversed the expression level of type I collagen.

Next, we evaluated whether a single transfection of PCBP2 siRNA can also reverse the alcohol-induced expression of type I collagen in primary HSC. As shown in Figure 8C, PCBP2 siRNA alone exhibited a dose-dependent inhibitory effect on the alcohol-induced expression of type I collagen. The combination of LY2109761 with PCBP2 siRNA further reduced the expression of type I collagen to a negligible level.

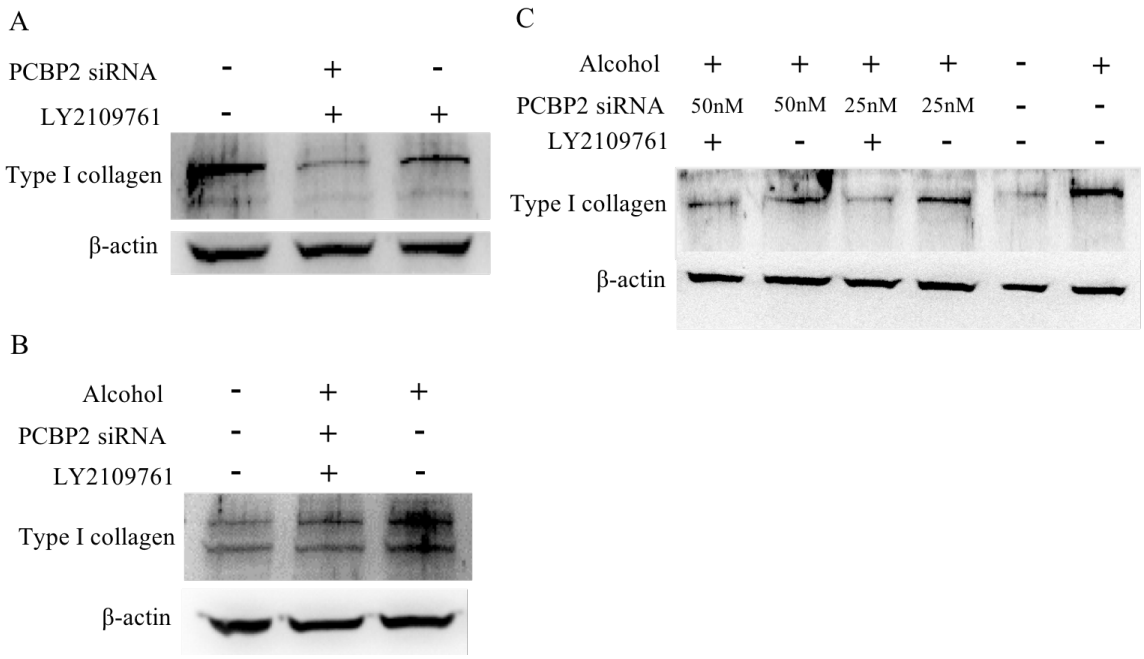

Figure 8. Combinational treatment with PCBP2 siRNA and LY2109761. (A) HSC-T6 cells were transfected with 50 nM PCBP2 siRNA three times on day 1, 3, and 5. LY2109761 (10 μM) was added on day 3, and alcohol (100 mM) was added on day 6. The cells were harvested for western blot analysis of type I collagen on day 7. (B) Primary rat HSC were transfected with 50 nM PCBP2 siRNA three times on day 1, 3, and 5. LY2109761 (10 μM) was added on day 3, and alcohol (100 mM) was added on day 6. The cells were harvested for western blot analysis of type I collagen on day 7. (C) Primary rat HSC were transfected with 25 or 50 nM PCBP2 siRNA for 24 h, followed by incubation with 100 mM alcohol for another 48 h. LY2109761 (10 μM) was added into the medium during the siRNA transfection and alcohol incubation periods. Protein expression of type I collagen was evaluated using western blot.

3.4 Discussion

In our previous study, we demonstrated that synthetic PCBP2 siRNA had a potent silencing effect on the expression of αCP2, which can stabilize the type I collagen α1 (I) mRNA in activated HSC [9]. As an activated hepatic stellate cell line, HSC-T6 reflects a fibroblast-like phenotype that proliferates rapidly in culture [96]. HSC-T6 cells express cytoskeletal proteins such as desmin, alpha smooth muscle actin, glial acidic fibrillary protein, and vimentin, which are typical markers of activated stellate cells. In the current study, primary HSC isolated from normal rats were stimulated with alcohol and cytokines. This model was used to mimic the activation of quiescent HSC in the initiation stage of fibrogenesis. We also used HSC-T6 cells as a model of the perpetuation stage of fibrogenesis.

HSC are the main contributor for ECM accumulation in the process of alcoholic liver fibrosis. HSC transform into active fibroblast cells after continuous exposure to alcohol or other chronic injuries [68]. An increased cytokine release has been reported to occur during the chronic wound-healing process [32, 72, 97-99]. The activated fibroblast cells migrate to the injury sites, where they demonstrate enhanced proliferation and collagen production. In our previous study, we proved that αCP2 and collagen type I were over-expressed in HSC-T6 cells after exposure to alcohol, and PCBP2 siRNA could reverse the collagen accumulation in HSC-T6 [9].

In the current study, we first isolated primary HSC from rat liver and then treated the primary HSC with alcohol. As shown in Figure 1, the mRNA level of PCBP2 and type I collagen were statistically increased. In addition, the type I collagen mRNA level was more significantly increased in the primary HSC than in HSC-T6 cells. We infer that

the primary HSC isolated from a healthy rat were quiescent, and they were therefore more sensitive to the alcohol stimulation. We also demonstrated that treatment of primary HSC with PCBP2 siRNA could significantly suppress the alcohol-induced mRNA levels of PCBP2 and type I collagen and the protein levels of type I collagen (Figures 1 and 8).

It is known that activated HSC produce more type I collagen once the fibrogenesis process is initiated as well as upregulated PDGF and TGF-β1 secretion in the fibrotic environment. In our study, as shown in Figure 3A, type I collagen expression was increased by the PDGF and TGF-β1 stimuli. Treatment with PCBP2 siRNA significantly decreased the expression of type I collagen at the mRNA level and protein level. α-complex protein-2 (αCP2), which is encoded by the PCBP2 gene, binds to the 3′ end of the type I collagen mRNA and increases its stability. This leads to the accumulation of a large amount of collagen in fibrotic liver [9, 100]. Here, we suggested that the treatment of the alcohol- and cytokine-stimulated primary rat HSC with PCBP2 siRNA significantly inhibited collagen accumulation.

PDGF is one of the cytokines with the strongest mitogenic stimulatory effect on HSC proliferation. PDGF and its receptors are highly expressed in cirrhotic liver tissue [101]. As Lin et al. reported, primary rat HSC stimulated with PDGF for 24 h show a dose-dependent increase in cell proliferation [85]. Adachi et al. reported [102] that PDGF activates the NAD(P)H oxidase in HSC, leading to the generation of ROS, which further activates p38 MAPK and induces the proliferation of HSC. Similarly, we found significant proliferation effect on both primary HSC and HSC-T6 with PDGF stimulation (Figure 4A&B). This is also in accordance with a report showing that microRNA-214 (Mir-214) suppresses glioma proliferation by targeting PCBP2 [103]. Mir-214 binds to

the 3'-untranslated region of the PCBP2 mRNA, which leads to the degradation of PCBP2 mRNA. As a result, Mir-214 inhibits the proliferation and growth of glioma cells. On the contrary, the restoration of PCBP2 dramatically reverses these tumor-suppressive effects. PCBP2 was also reported to regulate astrocyte proliferation after spinal cord injury [104] and facilitate the progression of esophageal squamous cell carcinoma (ESCC) by regulating the cellular proliferation and apoptosis [105]. In this study, the HSC cells were transfected with PCBP2 siRNA and then treated with PDGF. The PCBP2 siRNA remarkably blocked the PDGF stimulation on HSC proliferation.

HSC migration is one of the most important features in liver fibrosis. In addition to alcohol, several cytokines were used in this study to mimic the fibrotic environment in the liver. As Yang et al. reported [72], the stimulation of HSC with PDGF, TGF-β1 or EGF results in an enhanced migratory capacity of HSC. Furthermore, TGF-β1 has also been reported to facilitate the migration of HSC in a modified Boyden Chamber model by both chemotactic and haptotactic mechanisms [106]. In addition, PDGF promotes the migration of murine HSC line GRX cells [107]. Alcohol has also been reported to promote migration and invasion of triple-negative breast cancer cells through the activation of p38 MAPK and JNK [108]. In this study, PDGF, TGF-β1, EGF and alcohol were used to induce the migration effect of HSC. We infer that treatment with PCBP2 siRNA could attenuate or reverse the HSC migration induced by alcohol, PDGF, TGF-β1, and EGF, which is consistent with the study of Lin et al., who found that knocking down PCBP2 inhibited glioma cell migration and invasion via Rho GDP Dissociation Inhibitor Alpha (ARHGDIA) [109].

In addition, we also demonstrated that the combination of PCBP2 siRNA with LY2109761 had a potent silencing effect on collagen expression (Figure 8). Both HSC-T6 and primary HSC were used to examine the combination treatment. LY2109761, the TGFβR I/II kinase inhibitor, has been used to treat pulmonary fibrosis and human hypertrophic scar fibroblasts. It has been reported that LY2109761 can strongly inhibit pulmonary fibrosis [94]. It was also found that LY2109761 reduced the expression of pSMAD2 and pSMAD1 and attenuated the gene expression that is involved in the canonical and noncanonical TGF-β signaling, which indicated that LY2109761 has an antifibrogenic effect through the inhibition of the proinflammatory, proangiogenic and profibrotic signals. Furthermore, Wang et al. also reported that LY2109761 suppressed the mRNA levels of type I collagen and TGF-β1 by approximately 86% and 85% in hypertrophic scar-derived fibroblasts, respectively [95]. TGF-β1 enhances collagen expression through its cognate receptors to the Smad proteins, which increase the transcription of their target genes, including procollagen I and procollagen III [3]. Here, we used LY2109761 combined with PCBP2 siRNA to suppress collagen synthesis and inhibit the collagen stability, respectively, which produced a strongly synergistic silencing effect on the accumulation of type I collagen.

In conclusion, in this current study, rat primary HSC and the HSC-T6 cell line was used to model the initiation and perpetuation stages of liver fibrosis. We observed that the expressions of αCP2 and type I collagen was significantly enhanced in the primary HSC and HSC-T6 cells that were exposed to alcohol or fibrogenic cytokines. Notably, we demonstrated that PCBP2 siRNA could inhibit the over-expression of PCBP2 and type I collagen. Moreover, PCBP2 siRNA could also reverse cell

proliferation and migration induced by alcohol and fibrotic cytokines. This study suggests that the PCBP2 siRNA can be used alone or in combination with LY2109761 to reverse alcoholic liver fibrosis.

Results described in chapter 3 have been published in Volume 1, Issues 1, June 2017, Pages 70-79 in Liver Research.

CHAPTER 4

DISCOVERY OF SMALL ANTI-PD-L1 PEPTIDE FOR CANCER IMMUNOTHERAPY

4.1 Rationale

Immunotherapy has shown enormous promise for cancer treatment and was elected as the Breakthrough of Year 2013 by Science [34]. Checkpoint inhibitor is one of the most important Immunotherapies. PD-1 is a key inhibitory receptor expressed on immune cells, for example T cells. PD-1 typically works to restrain autoimmunity through binding to either ligand, PD-L1 or PD-L2. This process is helpful to avoid harmful inflammation in normal circumstances. But in tumor, the tumor cell binds to T cell and initiates a negative signaling by the PD-1/PD-L1 interaction, leading to the inhibition of the T cell functions [6]. PD-L1 is highly expressed on tumor cells. The binding interaction would bring a negative effect to T cells and inhibit the immune response, promoting T-cell exhaustion, anergy, and apoptosis [10]. In addition, it is also reported that the B7-1/PD-L1 interaction will also suppress the T cell activation and cytokine secretion [47].

The PD-1/PD-L1 interaction facilitates the tumor growth by dampening the effector T cell mediated immune response. There are several blockade antibodies approved by FDA. The blockade antibodies, either bind to PD-1 or PD-L1, have shown enormous promise to restore the T cell killing ability, improved antitumor immune response towards some cancer models [10]. The immune suppress mechanism is through checkpoint to inhibit the effector T cell functions. Tumor cell killing ability of T cell may

be retrieved by the antibodies, which block the suppressing interaction. By now, the antibodies showed potent oncologic efficacy in several cancers and metastasis, like breast cancer and melanoma [48]. However, it is reported that the inadequate expression of PD-L2 would possibly lead to tumor promoting TH2 inflammation, implying the anti PD-1 antibodies would bring an unwanted PD-L2 signal blocking, which is not for the anti-PD-L1 antibodies [49, 50]. Thus, PD-L1 specific targeting strategy may be more preferred than the PD-1 blocking.

Even though the therapeutic monoclonal antibodies have shown great promise in the tumor treatment, the blockade antagonists have inevitable limitations, such as deficient tumor tissue penetration [11, 12]. The effector T cells are able to immigrate deep into solid tumor tissue. It would not be favorable for the antibodies to entering tumor tissue due to their large molecular weight, which will compromise the effect of the therapeutics [13]. Second, it is reported that detrimental Fc-mediated effector would diminish the activity of antibodies [12]. In addition, another limitation of antibodies is to cause cytotoxic immune responses [11].

There are a few advantages of synthetic peptide over the antibody antagonists as checkpoint inhibitor candidate, such as better tumor penetrating ability, higher stability, lower costs of production and less immunogenicity [110]. Synthetic peptides have been widely used as targeting moiety and therapeutic reagents to treat various diseases, but peptides serve as checkpoint inhibitor are to be investigated [77]. Here, we would report our discovery of PD-L1 specific peptide as immune checkpoint inhibitor for cancer immunotherapy. As figure 9 shows, the peptide specifically binds to the PD-L1, blockade the PD-1 binding and further restores the immune killing ability.

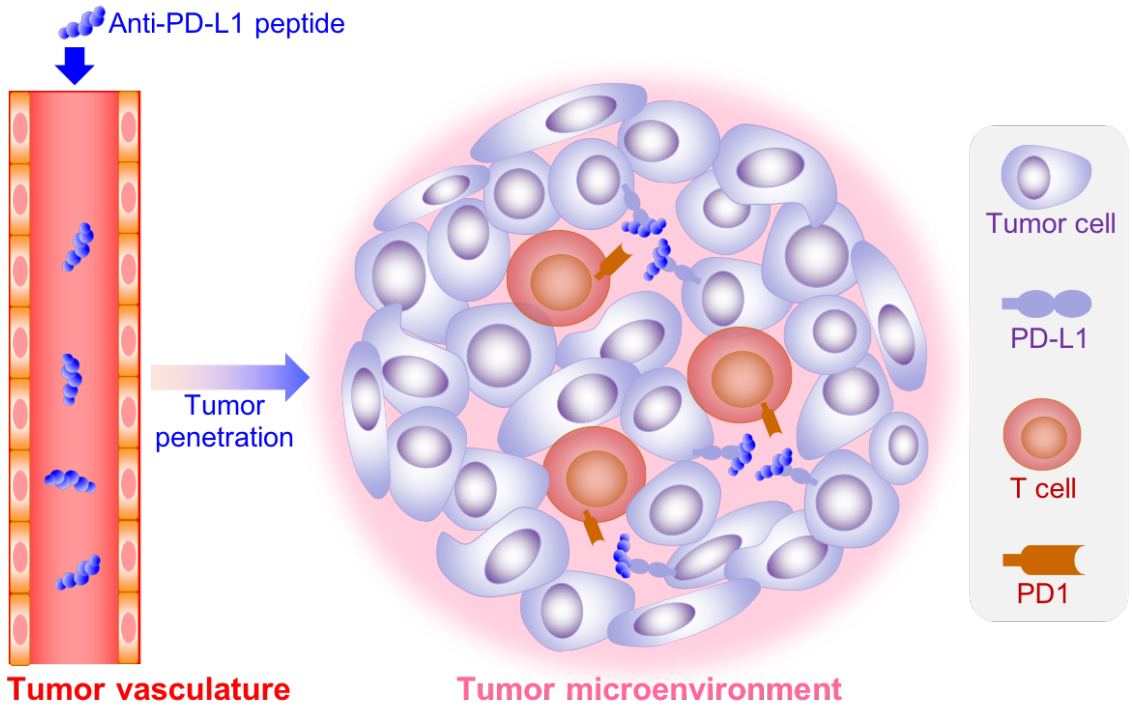

Figure 9. Schematic of the anti-cancer effect of the anti-PD-L1 peptide in tumor microenvironment. After administration, the anti-PD-L1 peptides can efficiently penetrate into tumor microenvironment because of their small size. The peptides bind to PD-L1 expressed on tumor cells and subsequently block the PD-1/PD-L1 interaction between tumor cells and tumor-infiltrating T cells, thus unleashing the anti-cancer immune responses of T cells to destroy cancer cells.

4.2 Materials and methods

4.2.1 Cell culture

The MDA-MB231, DU145, CT26, 4T1 and Jurkat cells were purchased from ATCC. MDA-MB231 and DU145 cells were cultured in DMEM medium with 10% Fetal Bovine Serum (FBS), 100 units/mL penicillin and 100 μg/mL streptomycin. 4T1, CT26 and Jurkat cells were cultured in RPMI1640 medium with 10% FBS, 100 units/mL penicillin and 100 μg/mL streptomycin. All cells were grown at 37°C in a humidified atmosphere containing 5% CO2. The culture medium was changed every other day, and the cells were passaged when they reached 80-90% confluence.

4.2.2 Phage display biopanning

The phage biopanning procedure was followed the previous reports with modifications [77, 111]. Briefly, PD-L1 extracellular domain (ECD) protein (100 ng) was immobilized in a 96-well plate at 4°C overnight. Then the PD-L1 was fully occupied by PD-1 protein at room temperature for 1 hour under gentle shaking. About 1×10^{11} pfu phages in TBST were loaded and incubated for 1 hour. The unbound phages were moved to a second well with only PD-L1 protein coated. TBST was used to wash the second well for ten times. Bound phages were recovered. The eluted phages were then amplified for next round of biopanning.

4.2.3 Blockade of receptor-ligand interaction

Ninety-six-well plates were coated with 100 ng of PD-L1 (G&P Biosciences, human PD-L1 ECD, cat# FCL0784B. mouse PD-L1, cat# FCL3502B) and later blocked

with 2% BSA for 2 hours at room temperature. Various concentrations of peptide were loaded into the wells and incubated for 1 hour at room temperature. Biotinylated PD-1 (G&P Biosciences, human PD-1 ECD, cat# FCL0761B. mouse PD-1, cat# FCL1846) was added and incubated for 1 hour. Streptavidin-HRP (R&D systems) was then added to catalyze the substrate color reaction. The OD450 was recorded and referenced to OD540.

4.2.4 Evaluation of the binding affinity by Surface Plasmon Resonance (SPR)

The binding affinities of the PD-L1 specific peptides for PD-L1 ECD were detected by SPR (BI4500, Biosensing Instrument) [65]. The PD-L1 ECD was diluted to 10 μg/mL with sodium acetate buffer (pH 5.0, GE Healthcare) and was covalently coated onto a CM5 sensor chip (CM Dextran Sensor Chip, Biosensing Instrument) using the standard Amine Coupling Kit (GE Healthcare). Approximately 6500 RU of Pd-L1 were immobilized onto the chip. A second channel was used as a reference. HBS-EP+ buffer (GE Healthcare) was employed at a flow rate of 60 μL/min. A series of concentrations of each peptide (15, 30, 60, 125, 250, 500, 1000, 5000 and 10,000 nM) were prepared in HBS-EP+ running buffer to obtain the K_d values of the peptides . The CM5 sensor chip was regenerated by incubating it with 10 mM NaOH for 20 seconds. The results were analyzed using the software of Bi data analysis software [63].

4.2.5 Apoptosis and proliferation assay

Apoptosis assay was followed the previous report [15, 112, 113]. DU145 cells were mixed with Jurkat cell at ratio 5:1. Peptide was added and incubated for 24 hours. Then, the Jurkat cells were harvested. All the cells were treated per the manufacturer's protocol and analyzed using the FACSCalibur flowcytometer (BD Biosciences).

T cell proliferation was assessed as described in a previous report [114]. Briefly, Jurkat T cells were cultured with medium alone or co-cultured with DU145 cancer cells (ratio 1:5). Then, the co-cultured cells were treated with peptide for 24 hours. T cells were harvest by collecting the supernatant. The proliferation of T cells was accessed by using CellTiter-Glo luminescent cell viability assay (Promega).

4.2.6 Molecular model of the binding of the anti-PD-L1 peptides

Published PD-L1 crystal structures were used as a reference model (PDB ID: 5C3T) [115]. The peptides were aligned to the PD-L1 structure using Autodock Vina. Figures of the PD-L1 and peptide complex were generated using Pymol (Delano Scientific).

4.2.7 Cellular uptake of dye-labeled peptide candidates

The cellular uptake protocol was performed as described in our previous reports with certain modifications [65, 116, 117]. Cells were treated with the non-enzymatic cell dissociation solution (MP Biomedicals) and diluted to a density of 1×10^6 cells/mL in Opti-MEM. The suspended cancer cells were incubated with various concentrations of 5-FAM-labeled peptides for 1 hour at 37°C with gentle rotation. Cells were analyzed using a FACSCalibur flow cytometer (BD Biosciences, Franklin Lakes, NJ).

4.2.8 Enzymatic hydrolysis stability of CLP002

The stability of CLP002 in human and rat serum was determined using methods described in our previous reports [118, 119]. CLP002 peptide, which was dissolved in CH_3CN/H_2O (1:1) buffer, was mixed with 50% (v/v) human serum or 25% (v/v) rat

serum and incubated at 37°C. Thirty microliters of the reaction solution was collected at different time intervals (0, 2, 4, 6 and 24 hours) and mixed with 90 μL of CH_3CN containing 0.1% formic acid to precipitate the serum proteins. The cloudy reaction sample fractions were placed on ice for 15 min and later centrifuged at 12,000 g for 10 min at 4°C. After centrifugation, the supernatants were analyzed by HPLC.

4.2.9 ELISA

PD-L1 and IFNγ elisa kits were purchased from R&D systems, and followed the manufacturer's protocols. The tumor tissues were lysis by RIPA buffer. The protein concentrations were determined by BCA assay. All the tumor samples were diluted to the identical concentration and 100 μL of each sample was loaded. The result was compared at OD 450 and reference OD 540.

4.2.10 Immunohistochemistry (IHC) staining

The anti-CD8a antibody and rabbit specific HRP/DAB (ABC) detection IHC kit were purchased from Abcam and used according to the manufacturer's protocols. The formalin-fixed paraffin-embedded tumor tissue slides were prepared by Kansas City Truman Medical Center. Briefly, the slides were heated in Tris buffer, pH9.0, for 45 min to induce antigen retrieval. After washing, the anti-CD8a antibody was added to the sections and incubated overnight at 4°C. On the second day, a biotinylated goat anti-rabbit secondary antibody was incubated with the sections. The staining was visualized with the DAB chromogen mixture. All images were captured at a magnification of 200×.

4.2.11 Animal study

The animal protocol was approved by the University of Missouri-Kansas City, Institutional Animal Care and Use Committee (IACUC). Five-week old male (50%) and female (50%) Balb/c mice were purchased from Charles Rivers Laboratories (Wilmington, Massachusetts) and housed in a temperature and humidity controlled room on a 12 hour light-dark cycle. Approximately 5×10^5 CT26 cells were subcutaneously injected into the right flank. The mice were intraperitoneally injected with 2 mg/kg peptide daily when the tumor size reached 50-100 mm^3. The anti-mouse PD-L1 antibody (10F.9G2, BioXcell) was administrated as a positive control at a dose of 10 mg/kg every two days. The tumor size was assessed with a caliper and calculated with the formula ½ × a × b × b. For the survival study, the mice were examined daily and deaths were recorded according to the University of Missouri-Kansas City Institutional Animal Care and Use Committee Animal Protocol.

4.2.12 Statistical Analysis

Data are expressed as the mean ± standard deviation (SD). The difference between any two groups was determined by one-way analysis of variance (ANOVA). In animal study, data are expressed as the mean ± standard error of the mean (SEM). The difference between any two groups was determined by two-way analysis of variance (ANOVA). Tukey's multiple comparisons test was used as post hoc analysis. The $P<0.05$ was statistically significant.

4.3 Result

4.3.1 Screening of PD-L1 specific peptide candidates by a novel phage biopanning

In order to discover the peptides not only can bind to PD-L1 specifically but also possess the power to blockade the PD-1/PD-L1 interaction, the phage biopanning procedure was modified from our previous studies [77, 111]. The human PD-L1 extracellular domain (ECD) was coated on 96-well plate into two different wells. On the first well, PD-L1 was saturated with PD-1 protein. In this scenario, all the coated PD-L1 molecules were fully occupied by PD-1. Then, the phage library was loaded into the first well as precleaning step. In order to remove any phage clones, which could bind to the unwanted area (the binding sites out of the PD-1/PD-L1 interaction residues). As all the PD-L1 molecules formed complex with PD-1, the phages could only bind to the area outside the binding residues of PD-L1 protein. The unbound phage clones were transferred to a second well, which was coated with only PD-L1. On the second well, since there was no PD-1, the PD-1 binding area on PD-L1 molecules was exposed and available for phages. Even though the rest area on the PD-L1 was also ready to be bound, we presumed the phage clones, which can bind to the unwanted area, were removed at the previous precleaning step. The unbound phages were washed away and the bound phage clones were eluted. In each biopanning, about 10^{11} pfu phage clones were loaded, and eluted phages were tittered and amplified for the next round of selection. As Figure 10 shows, after 5 rounds of screening, the number of eluted phages increased significantly.

57 single phage colonies were randomly selected for sequencing from the 5^{th} round elute. 4 different peptide sequences were identified and we named them as CLP001

to CLP004. Among the four different peptide sequences, the CLP002 and CLP003 have 21 and 32 repeats respectively, while the CLP001 and CLP004 just have 1 and 3 repeats.

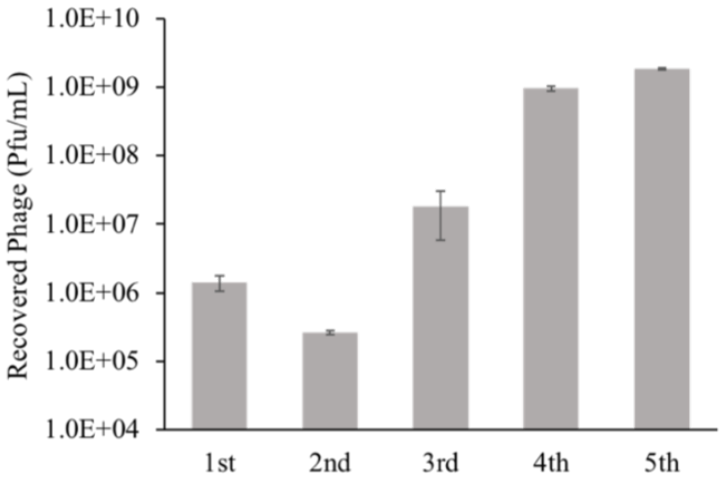

Figure 10. Discovery of anti-PD-L1 peptides using phage display biopanning. The number of recovered phages from each round of biopanning. Results are represented as the mean ± SD (n=3).

4.3.2 Peptide binding affinity and specificity

The binding affinities of the discovered peptides were evaluated using surface plasmon resonance (SPR). Human PD-L1 was immobilized on a CM5 golden chip by the direct amine coupling method. As shown in Table 1 and Figure 11, the K_D values of CLP001, CLP002, CLP003 and CLP004 for human PD-L1 were 534 nM, 366 nM, 117 nM and 544 nM, respectively. CLP003 showed the best binding affinity and the highest frequency after 5 rounds of biopanning. CLP002 showed the second best binding affinity of 366 nM for 21 repeats.

We also examined the equilibrium dissociation constants of the 5-FAM-labeled peptides bound to PD-L1 highly expressed DU145 and MDA-MB231 cancer cells [46, 120, 121]. Cells were incubated with different concentrations of peptides for 1 hour at 37°C. The percentages of cellular uptake were determined using flowcytometry. The equilibrium dissociation constant was analyzed using GraphPad Prism. As illustrated in Figure 12 and Table 2, the peptide CLP003 showed the highest binding affinity with an apparent K_D value of 54.37 nM for MDA-MB231 cells and 43.57 nM for DU145 cells. The binding affinity of CLP002 was 212.9 nM for MDA-MB231 cells and 184.1 nM for DU145 cells.

In addition, we verified the specificity of the peptide candidates. First, albumin was immobilized on the sensor chip. The bindings of the peptide candidates were evaluated. As shown in Figure 11, the response did not increase as we injected gradient concentrations. There is no binding between the peptides and the albumin protein. Next, the cellular uptake of the dye labeled peptides on human breast cancer cell MCF7 was detected. As Figure 12 shows, there was large difference of the binding curves, when the

PD-L1 deficient cancer cells were used [122]. We observed significant reduced cellular uptake compare to the PD-L1 over expressed cancer cells.

Table 1. Binding affinity of the selected peptides against human PD-L1

Peptides	K_a ($M^{-1}S^{-1}$)	K_d (S^{-1})	K_D (nM)
CLP001	5186 ± 212	$(2.81 \pm 0.50) \times 10^{-3}$	534 ± 54
CLP002	4521 ± 666	$(1.45 \pm 0.92) \times 10^{-3}$	366 ± 150
CLP003	$(2.26 \pm 2.03) \times 10^{4}$	$(1.62 \pm 0.11) \times 10^{-3}$	117 ± 80
CLP004	5140 ± 390	$(2.75 \pm 0.20) \times 10^{-3}$	544 ± 81

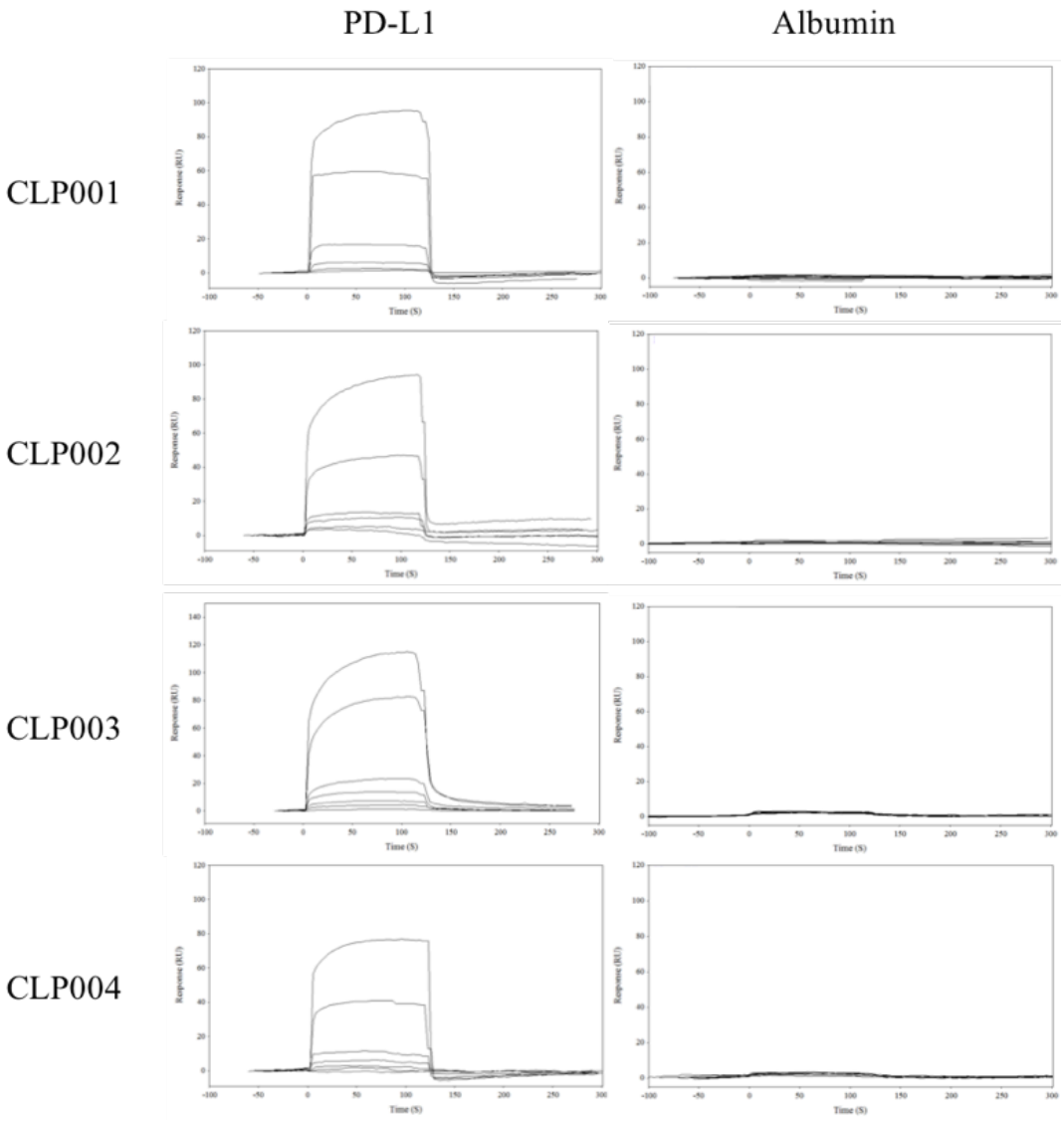

Figure 11. Surface plasmon resonance (SPR) sensograms of the peptides binding to human PD-L1 and bovine serum albumin. All sensograms were baseline-adjusted and reference cell-subtracted.

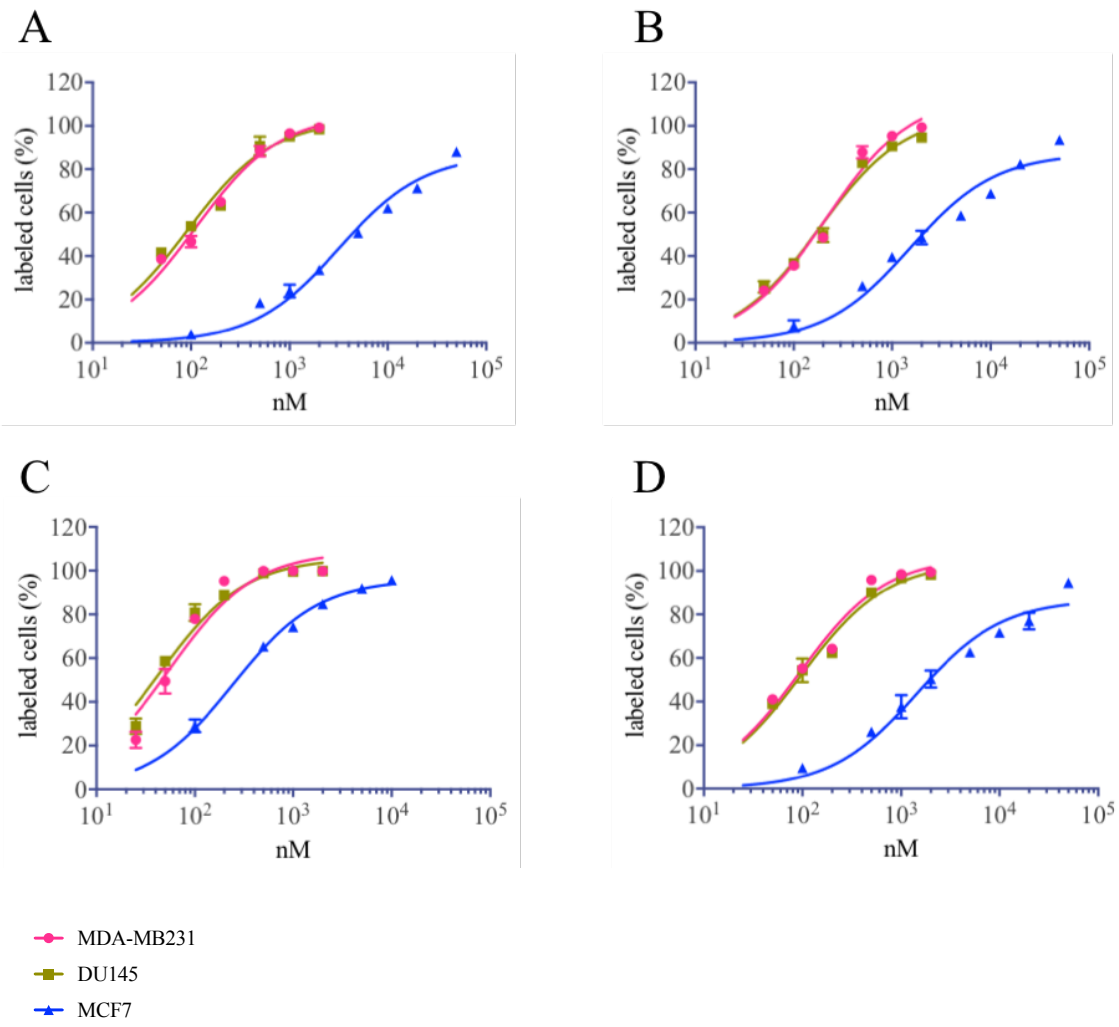

Figure 12. Binding affinity of the PD-L1-specific peptides in human cancer cells. (A) CLP001. (B) CLP002. (C) CLP003 and (D) CLP004. MDA-MB231 and DU-145 are PD-L1-positive cells, and MCF-7 is PD-L1-negative cell line. A series of concentrations of 5-Fam labeled peptides were incubated with the cancer cells for 1h. The labeled cells were analyzed by flow cytometry.

Table 2. Apparent equilibrium dissociation constant (K_D) of the peptides to human cancer cells

Peptides	MDA-MB231	DU145	MCF7
CLP001	110.70 nM	90.89 nM	3167 nM
CLP002	212.9 nM	184.10 nM	1523 nM
CLP003	54.37 nM	43.57 nM	246 nM
CLP004	93.68 nM	97.24 nM	1432 nM

4.3.3 Enzymatic hydrolysis stability of CLP002

The proteolytic stabilities of CLP002 were determined in human and rat serum. The reverse phase HPLC method was used to evaluate the hydrolysis of CLP002 at different time points (0, 2, 4, 6 and 24 hours). As shown in Figure 13A to 13B, CLP002 was degraded to approximately 48% after 6 hours and 22% after 24 hours of incubation with 50% human serum. Since the serum proteins were precipitated with acetonitrile, only free peptide was detected. CLP002 exhibited relatively poor stability in rat serum (Figure 13C). The peptide was almost completely digested within 2 hours.

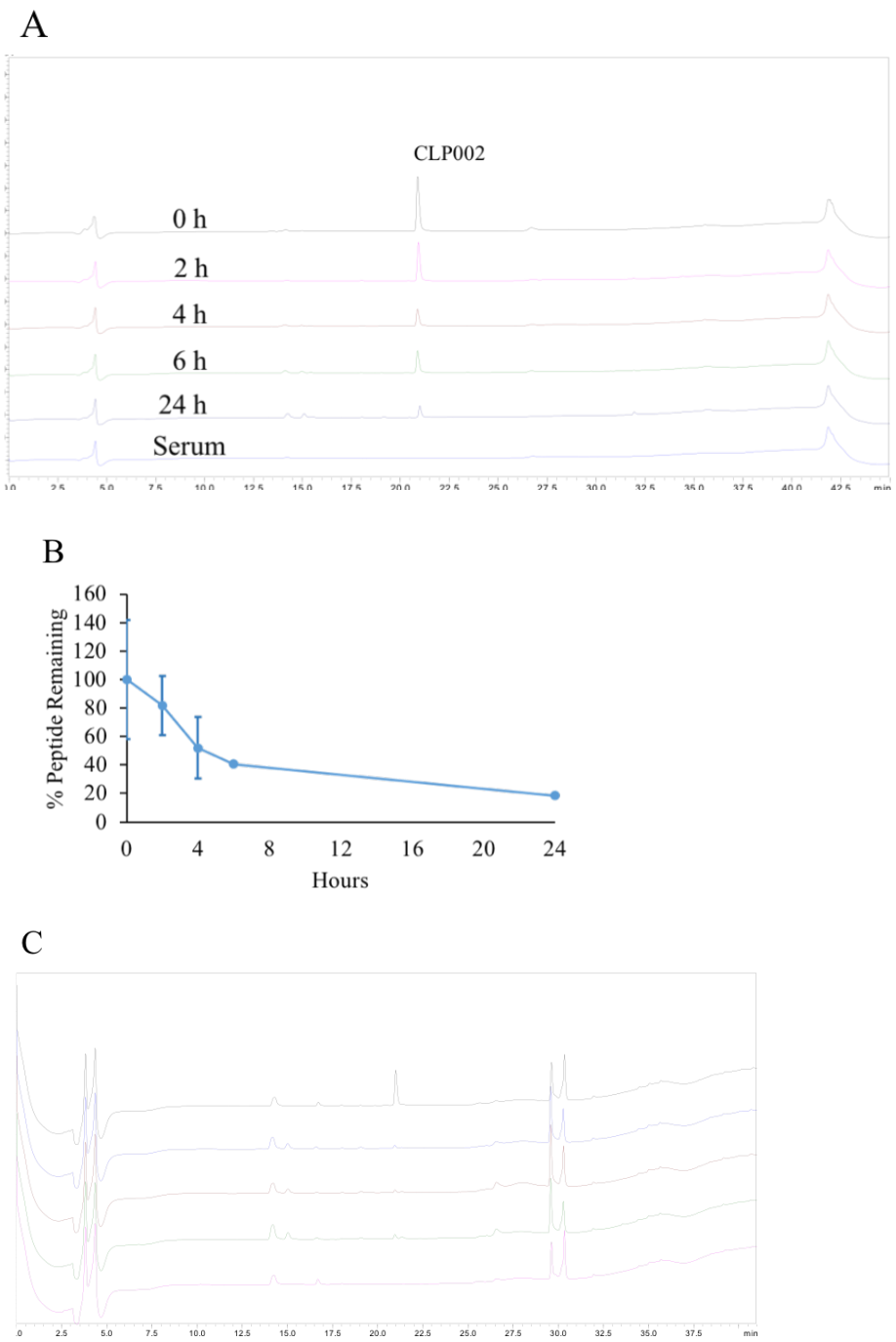

Figure 13. Stability of the CLP002 peptide in serum. (A) HPLC chromatograms (λ = 220 nm) of the CLP002 peptide in 50% human serum after different time intervals. (B) The percent of the CLP002 peptide remaining in 50% human serum. (C) HPLC chromatograms (λ = 220 nm) of the CLP002 peptide in 25% rat serum.

4.3.4 Blockade of PD-L1/PD-1 interaction

A blocking assay was developed to verify the blocking efficiency of all four peptide candidates. An anti-human PD-L1 antibody (R&D Systems, cat# AF156) was used as a positive control in this assay. As shown in Figure 14A, the anti-human PD-L1 antibody blocked the PD-1/PD-L1 interaction with an IC_{50} of 36.76 nM, which is consistent with the report from the company. Next, we determined the blocking efficiencies of four peptides at 10 μM (Figure 14B). CLP002 showed the highest blocking efficiency, whereas CLP001 did not block the interaction. We next calculated the half maximal inhibitory concentration (IC_{50}) of the peptides using human PD-L1 protein and PD-L1-overexpressing DU145 cancer cells. As shown in Figure 15 and Table 3, CLP002 exerted the best blocking effect (85%) with an IC_{50} of 2.17 μM when the plate was coated with the human PD-L1 protein, The blocking effect was 80% with an IC_{50} of 1.43 μM, when the plate was coated with DU145 cells. The IC_{50} of the CLP003 peptide was 2.22 μM with 60% blocking efficiency against the human PD-L1 protein, and the IC_{50} was 3.05 μM with a 56% blocking efficiency against DU145 cancer cells.

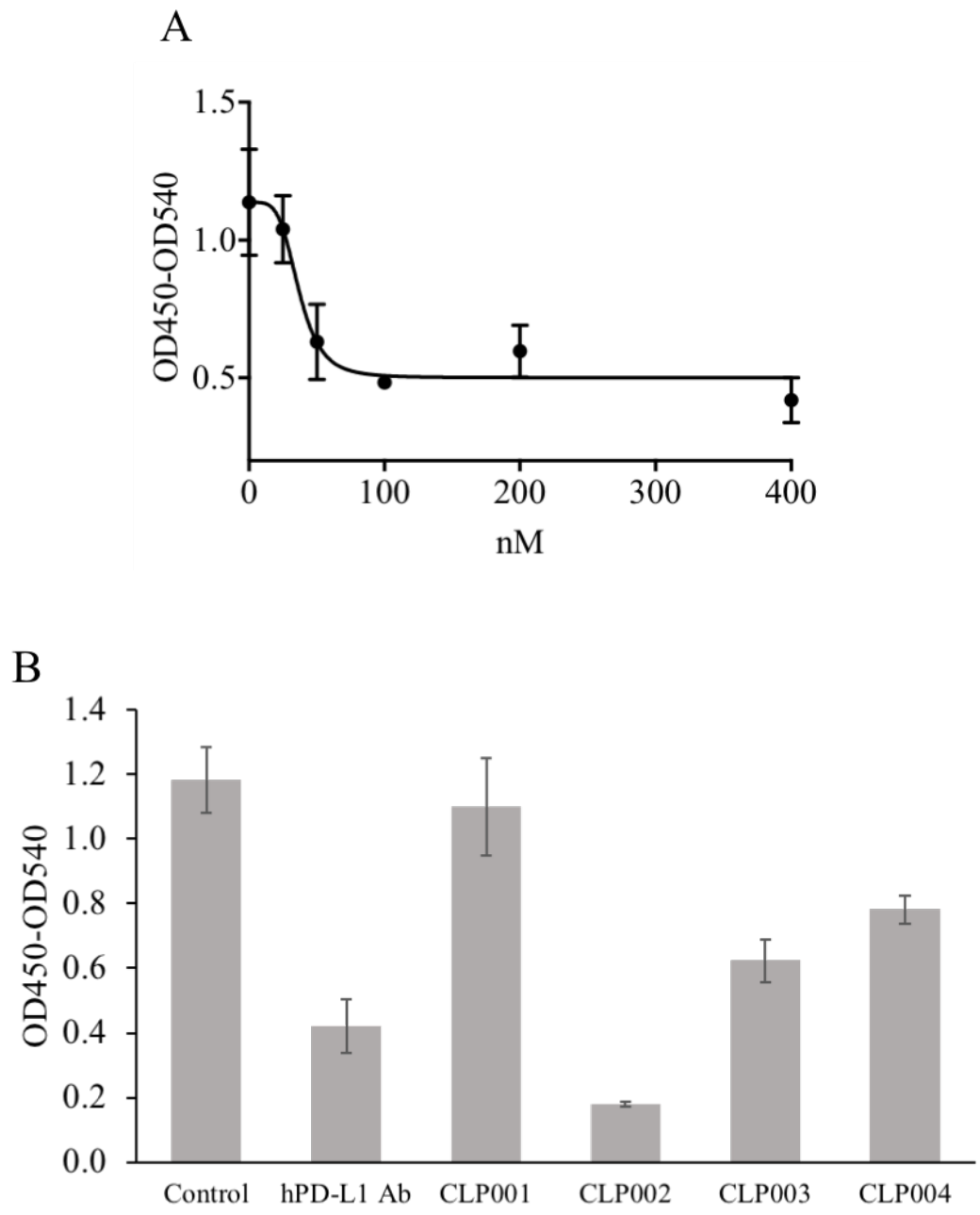

Figure 14. Blockade of the PD-1/PD-L1 interaction by peptides and antibody. (A) The anti-human PD-L1 antibody (R&D, cat# AF156) blocks 63% of the PD-1/PD-L1 interactions with an IC_{50} of 36.76 nM. (B) Blocking activities of the PD-L1-specific peptides and anti-human PD-L1 antibody at 10 μM. The results are presented as the mean ± SD (n=3).

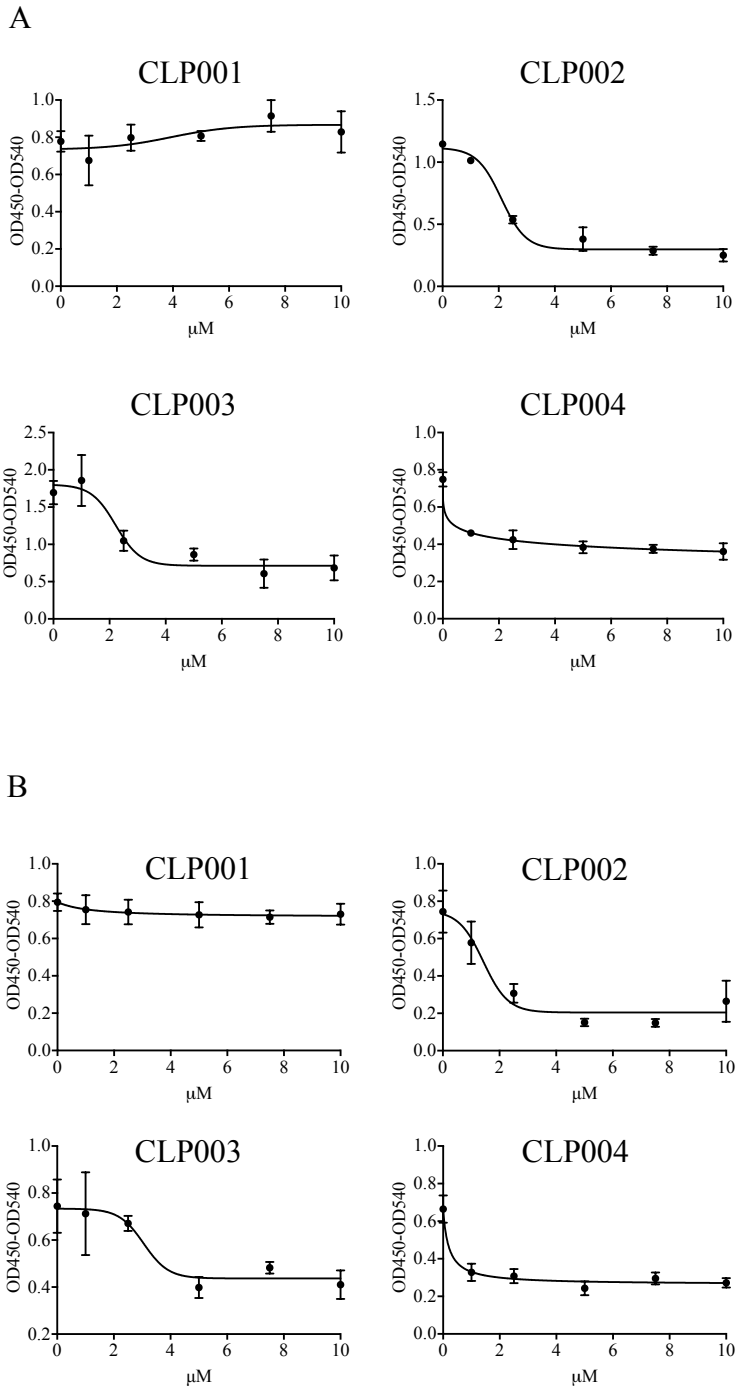

Figure 15. Blocking profiles of the peptides against human PD-L1 ECD protein (A) and DU145 cells (B). Human PD-L1 protein and PD-L1-positive DU145 cells were coated on 96-well plates. Various concentrations of the peptides were loaded to each well to verify the blocking effect. The results are presented as the mean ± SD (n=3).

Table 3. Blocking efficiency of the peptides against human PD-L1 protein and human cancer cell line DU145

Peptide	Target	IC50	Block Efficiency
CLP001	hPD-L1 protein	NA	0%
	DU145 cancer cell	NA	0%
CLP002	hPD-L1 protein	2.17 μM	85%
	DU145 cancer cell	1.43 μM	80%
CLP003	hPD-L1 protein	2.22 μM	60%
	DU145 cancer cell	3.05 μM	56%
CLP004	hPD-L1 protein	1.17 μM	52%
	DU145 cancer cell	0.20 μM	60%
hPD-L1 Ab	hPD-L1 protein	36.76 nM	63%

Next, the blocking efficiency of the peptides against mouse PD-L1 was evaluated. As shown in Figure 16, the blocking efficiencies of peptides and an anti-mouse PD-L1 antibody (BioXcell, 10F.9G2) were compared at 10 μM. CLP002 blocked 71% of the PD-1/PD-L1 interactions, while CLP003 inhibited approximately 46% of the interactions, compared to the blocking efficiency of anti-mouse PD-L1 antibody (92%). We next determined the IC_{50} values of the peptides to block the mouse PD-1/PD-L1 interaction. As shown in Figure 17 and Table 4, the IC_{50} for CLP002 was 1.51 μM with a 71% blocking efficiency, while the IC_{50} of CLP003 was 1.96 μM with a 46% blocking efficiency. There is no significant difference of the binding affinities between the two peptides. Because CLP002 displayed the highest blocking efficiency, we used CLP002 as the best candidate PD-1/PD-L1 blocking peptide in subsequent studies.

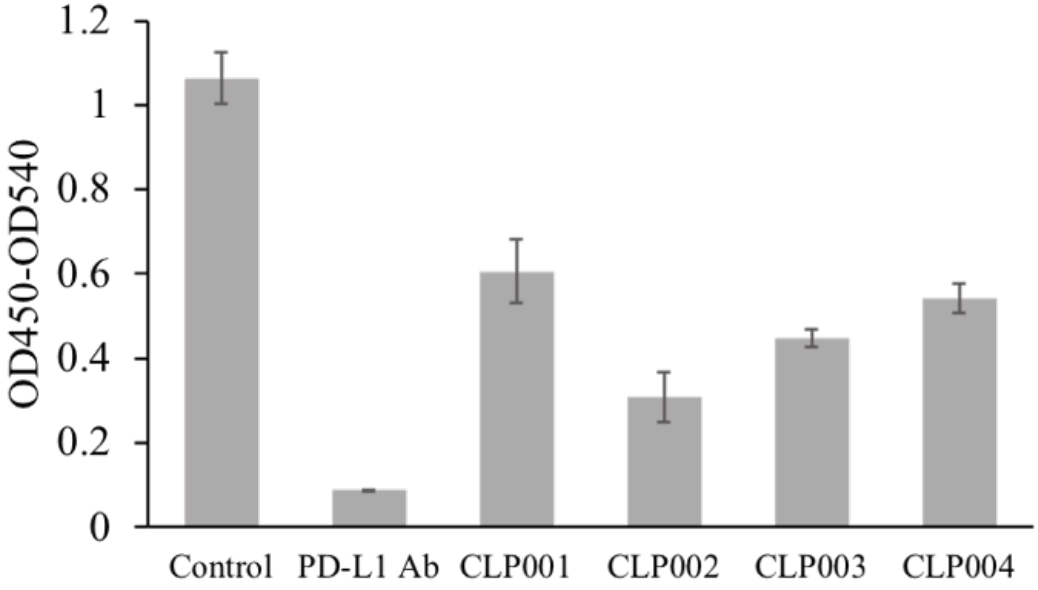

Figure 16. Blocking activity of the peptides against the mouse PD-1/PD-L1 interaction. Mouse PD-L1 protein was coated on a 96-well plate, followed by incubation with the peptides and antibody at 10 μM. After washing with PBS, biotinylated mouse PD-1 was added, and streptavidin-HRP was then added to catalyze the substrate color reaction. The results are presented as the mean ± SD (n=3).

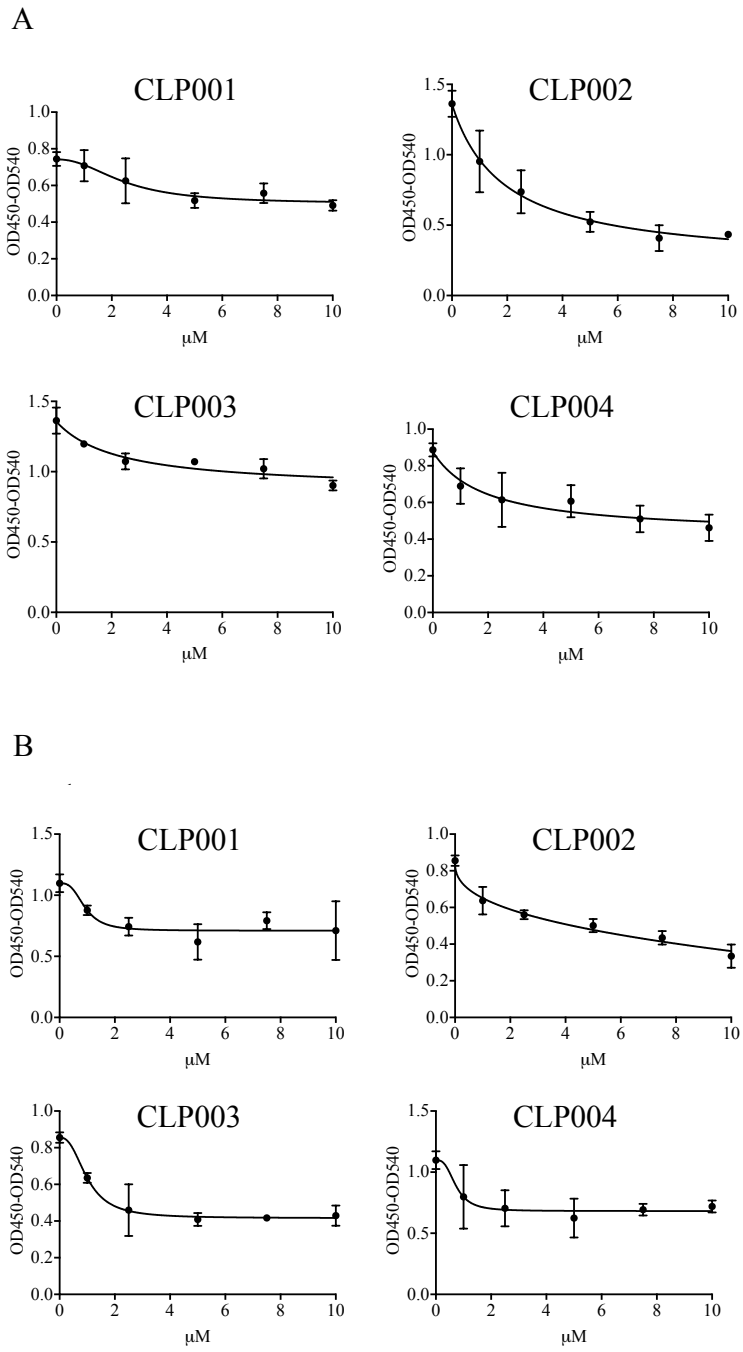

Figure 17. Blocking profiles of the peptides against mouse PD-L1 ECD protein (A) and mouse 4T1 cells (B). Mouse PD-L1 protein and PD-L1-positive 4T1 cells were coated on 96-well plates. Various concentrations of the peptides were loaded to evaluate the blocking effect. The results are presented as the mean ± SD (n=3).

Table 4. IC_{50} and blocking efficiency of the peptides against mouse PD-L1 protein and 4T1 cells

Peptide	Target	IC50	Block Efficiency
CLP001	mPD-L1 protein	2.43 μM	34%
CLP001	4T1 cancer cell	0.91 μM	35%
CLP002	mPD-L1 protein	1.91 μM	68%
CLP002	4T1 cancer cell	2.44 μM	61%
CLP003	mPD-L1 protein	2.26 μM	46%
CLP003	4T1 cancer cell	1.00 μM	50%
CLP004	mPD-L1 protein	1.91 μM	48%
CLP004	4T1 cancer cell	0.73 μM	34%

4.3.5 Docking

Interactions between peptides and the human PD-L1 extracellular domain (PDB ID# 5C3T) were analyzed by Autodock Vina integrated into PyRx software [123]. Figures of the PD-L1 and peptide complex were generated using Pymol. As illustrated in Figure 18, CLP002 and CLP003 specifically bound to PD-L1 at the site where the PD-L1 interacts with PD-1 (yellow area). The residues responsible for the PD-1/PD-L1 interaction were determined based on a previous report [115]. The CLP002 and CLP003 contact areas overlapped with the PD-1/PD-L1 interaction site (pink area). CLP002 forms 10 hydrogen bonds and 5 Pi interactions with PD-L1, and all of them are shared in the PD-1/PD-L1 interaction. CLP003 forms 9 hydrogen bonds and 7 Pi interactions, and only one of which is not shared with the PD-L1/PD-1 interaction. CLP001 did not bind to the PD-1/PD-L1 interaction site. For the CLP004, there is a large area of the contact residues of the CLP004 against PD-L1 were out of the PD-1/PD-L1 binding area. The blocking effect of CLP004 was less than the CLP002.

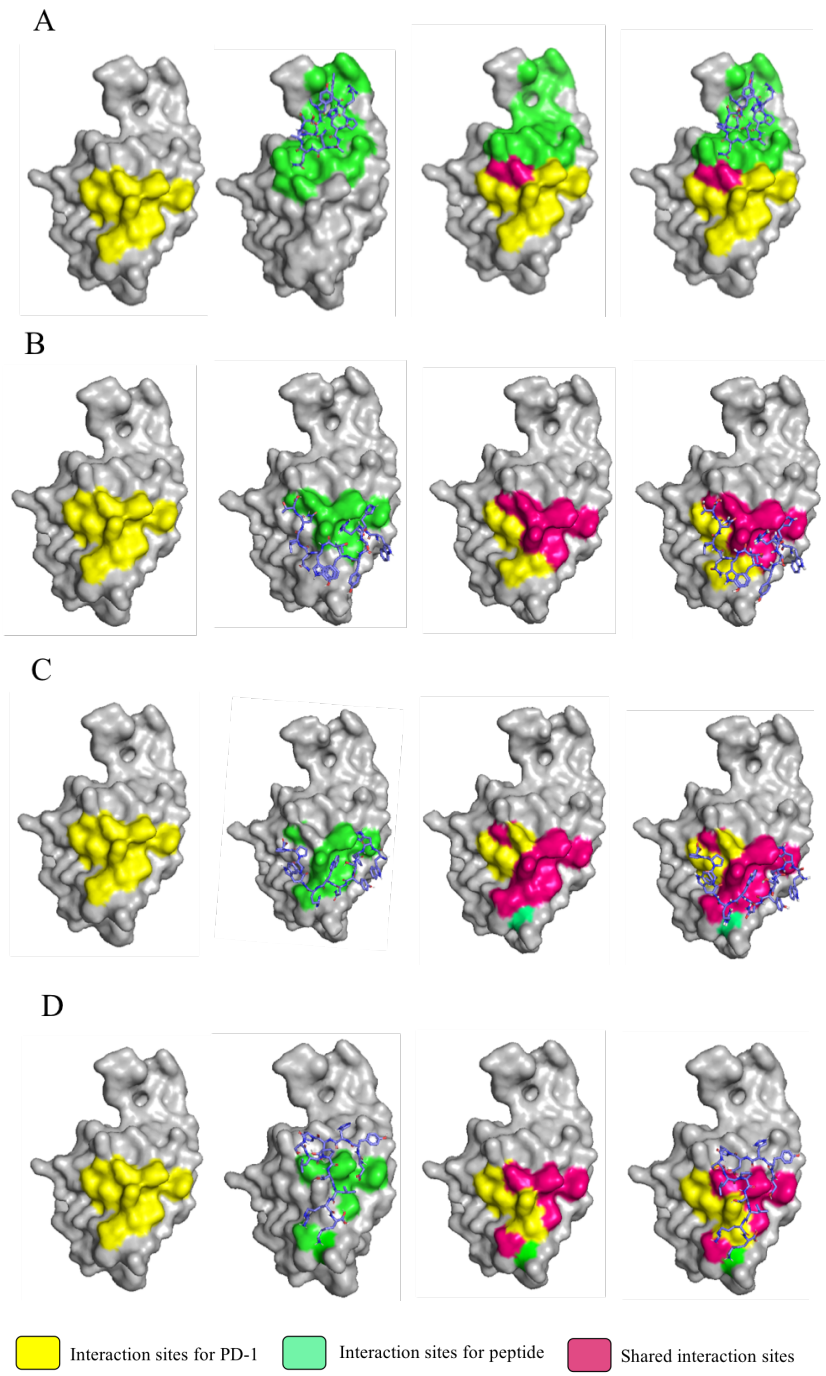

Figure 18. Modeling of the interaction between the peptides and human PD-L1 (PDB ID: 5C3T). (A) Interaction between CLP001 and PD-L1. (B) Interaction between CLP002 and PD-L1. (C) Interaction between CLP003 and PD-L1. (D) Interaction between CLP004 and PD-L1. The binding site for human Pd-1 protein is highlighted in yellow.

4.3.6 CLP002 restores the T cell proliferation and prevents T cell apoptosis

As shown in Figure 19A, we co-cultured Jurkat T cells with DU145 cancer cells. The tumor cells significantly inhibited T cell proliferation. The co-cultured cells were then treated with different peptides and PD-L1 antibody. No difference was observed, when CLP001 was added. As we discussed previously, the CLP001 was not able to block the human PD-1/PD-L1 interaction. The cancer cells inhibited the Jurkat cells proliferation through the PD-1/PD-L1 interaction. Next, the co-cultured cells were treated with CLP002 or PD-L1 antibody. Both treatments successfully restored the Jurkat cell proliferation, which is consistent with previous reports. Freeman et al. reported that human PD-L1 suppressed the proliferation of T cells in a dose-dependent manner. However, T cell proliferation was not inhibited in PD-1 knockout T cells [114]. It is also reported that HIF-1α targets PD-L1 in myeloid-derived suppressor cells (MDSCs). The blockade of the PD-1/PD-L1 interaction by using HIF-1α improves T cell proliferation and function [124].

As shown in Figure 19B, the apoptosis of Jurkat T cells increased from 2.3 % to 15.1 %, when the T cells were co-cultured with DU145 cells. Apoptosis was effectively inhibited to 10.2%, when the co-cultured cells were treated with CLP002 but not CLP001. This is because CLP001 only binds to the PD-L1 but fails to block the PD-1/PD-L1 interaction. As reported in a previous study [112], PD-L1 overexpression on tumor cells promotes T cell apoptosis. Researchers have observed increased apoptosis of cytotoxic T lymphocytes after incubation with melanoma cancer cells. The authors did not observe apoptosis of the immune cells, when the PD-L1 was knocked out in melanoma tumor cells. Notably, tumor-promoted apoptosis was significantly reduced by a PD-1 antibody. Consistent with the reported findings, we also observed a decrease in

the number of apoptotic T cells in response to the CLP002 treatment. CLP002 blocked the receptor-ligand interaction and prevented T cell apoptosis *in vitro*.

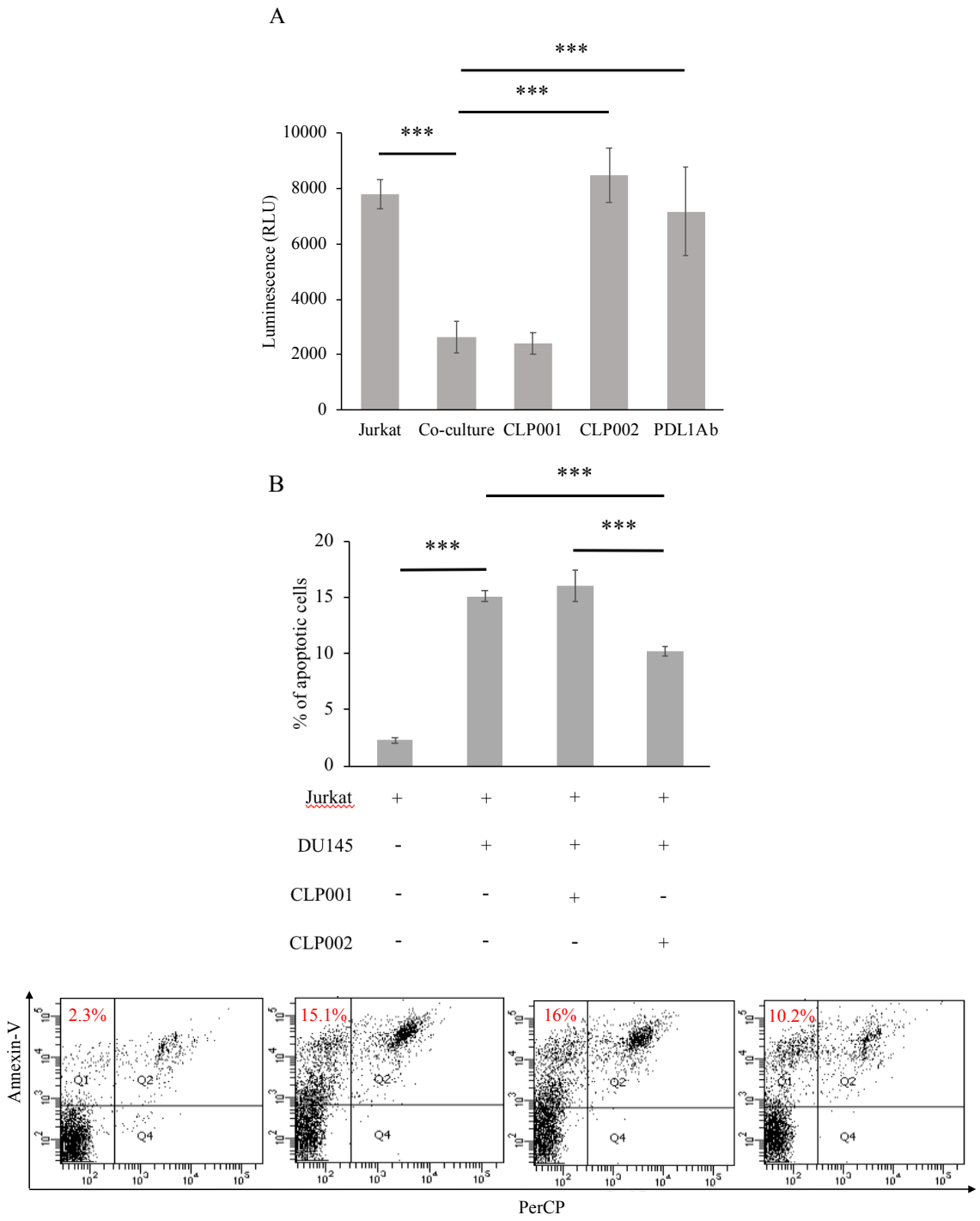

Figure 19. The CLP002 peptide restores T cell proliferation and prevents T cell apoptosis. Jurkat T cells were co-cultured with DU145 cells in a ratio 1:5, followed by incubation with the CLP002 peptide for 24 h. CLP002 restore Jurkat T cell proliferation (A) and reduces apoptosis of the Jurkat cells (B). The results are presented as the mean ± SD (n=3). (*P<0.05; **P<0.01, ***P<0.001).

4.3.7 In vivo study

We next evaluated the therapeutic efficacy of the anti PD-L1 peptides using the CT26 tumor model, which has been widely used to evaluate the activity of PD-1/PD-L1 inhibitors in mice [63, 125-127]. As shown in Figure 20A, 5×10^5 CT26 cells were subcutaneously injected into the right flank of each mouse. The mice were randomly divided into five different groups (10 mice/group, 50% female, 50% male) [128]. Once the average tumor volume reached 50-100 mm^3, the peptides (2 mg/kg) were administrated intraperitoneally daily, as described in a previous study [63]. An anti-mouse PD-L1 antibody (BioXcell, 10F.9G2) was administered intraperitoneally every other day at 10 mg/kg as previously reported [56, 127, 129]. As Figure 20B to 20E showed, both peptides (CLP002 and CLP003) and the antibody effectively suppressed tumor growth. We observed a significant difference in the tumor volumes of mice treated with peptides and the antibody beginning on day 10 for the female mice and day 12 for the male mice. As shown in Figure 21, the tumor weights of the PD-L1 antibody, CLP002 and CLP003 group were significantly different from the saline group in both female and male animals. In general, CLP002 exerted a better tumor inhibitory effect than CLP003, which was similar to the antibody. It is noteworthy to mention that the peptides were screened against the human PD-L1 protein, which, in fact, would compromise the anti-tumor activity of the peptides in a mouse model. By contrast, the antibody is against the mouse PD-L1 protein. We therefore would be cautiously optimistic with the activities of the peptides in future clinical studies.

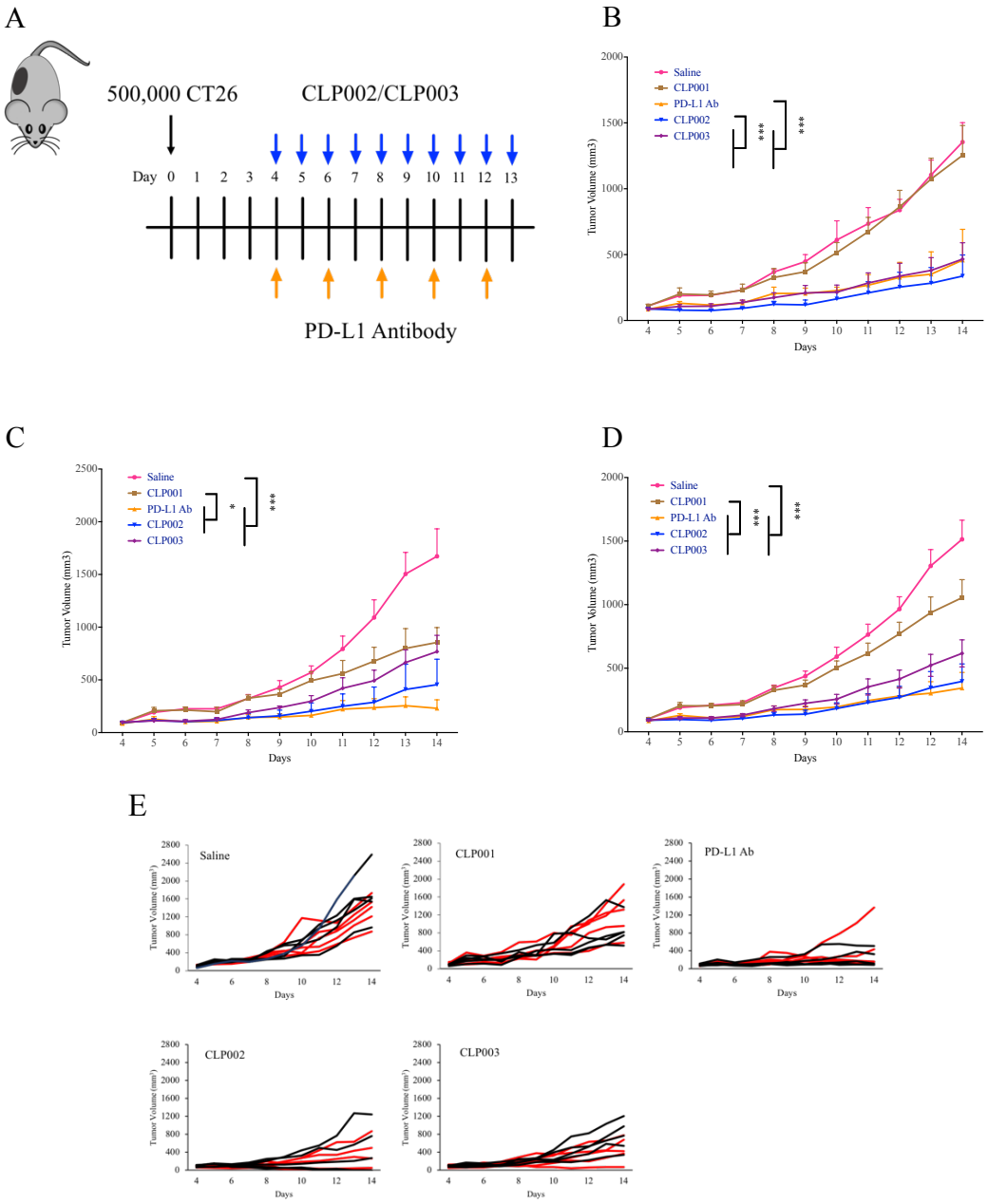

Figure 20. Anti-tumor effect of the peptides and antibody. (A) Schedule of the activity study. CT26 cells (0.5×10^6) were subcutaneously injected into the right flank of the mice. Once the tumor volume reached 50-100 mm^3, the peptides (2 mg/Kg) were injected daily and the anti PD-L1 antibody (10 mg/Kg) was injected every other day. Tumor growth curves of female mice (B), male mice (C), and all the mice (D). (E) Tumor growth curves of individual mice in each group. The results are presented as the mean ± SEM. (*P<0.05; **P<0.01, ***P<0.001).

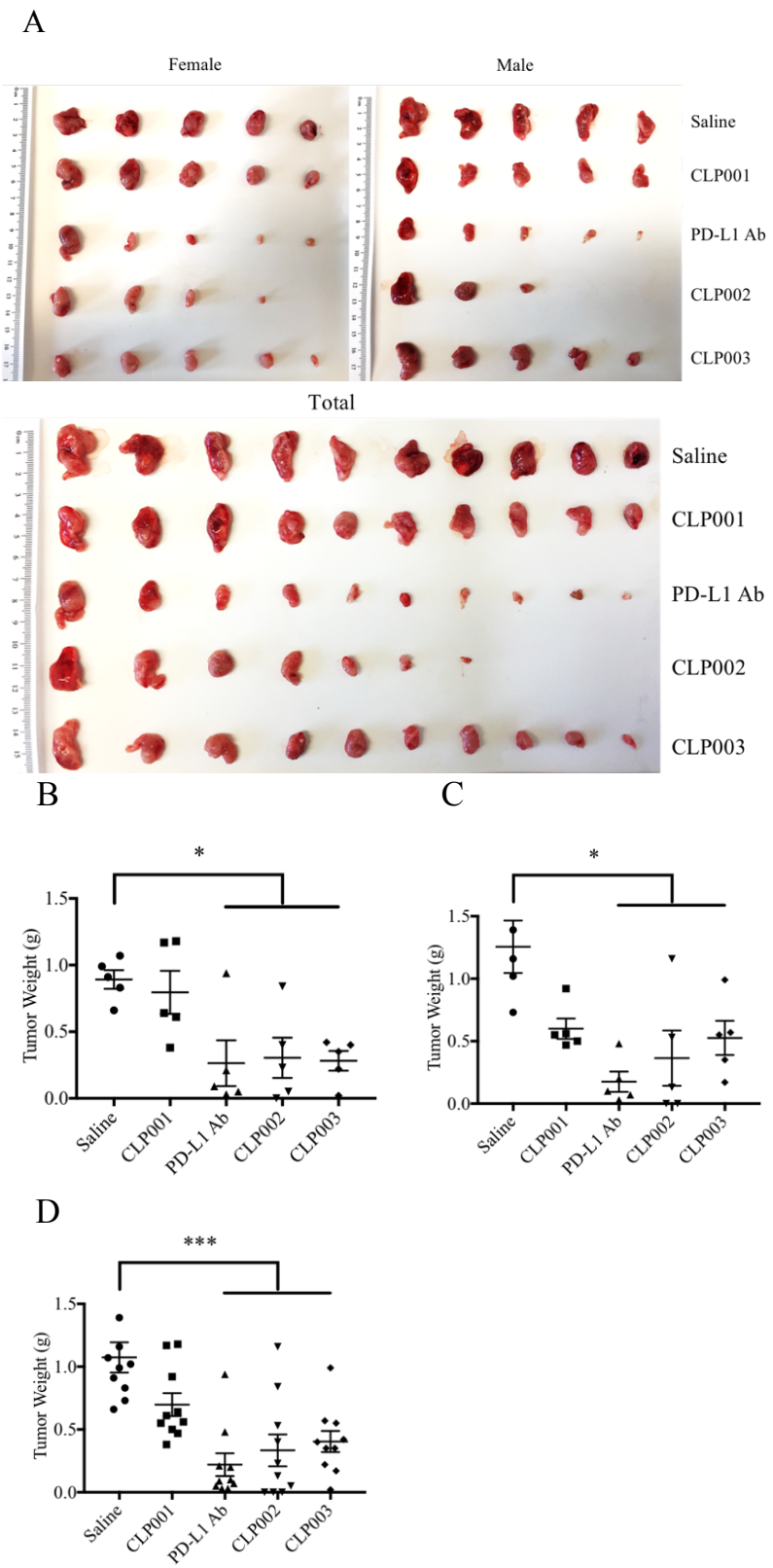

Figure 21. The PD-L1-specific peptides inhibits tumor growth. (A) Tumor tissues of the mice. Tumor weights of the female mice (B), male mice (C), and all the mice (D). (*P<0.05; **P<0.01, ***P<0.001).

Next, we determined the IFNγ, PD-L1 and IL-6 levels in the CT26 tumor tissues. As shown in Figure 22, the positive control (anti-PD-L1 antibody) and peptides increased the expression of IFNγ and PD-L1 in the CT26 tumor tissues. According to previous reports [34, 67, 130], the relationships between cytotoxic T lymphocyte function and treatment result is mediated by the secretion of interferon. IFNγ triggers PD-L1 expression on cancer cells [131]. High PD-L1 expression is required for the immune escape of tumor cells as the tumor cells detect T cells based on the high level of IFNγ secreted from the immune cells. The interferon will induce PD-L1 expression on the tumor cell surface, which inhibits cytotoxic T lymphocyte activation and function. Accordingly, the anti-PD-L1 antibody or CLP002 treatment represents a mechanism to suppress tumor growth. IL-6 levels were also determined. The peptide treatment successfully inhibited IL-6 secretion in tumors. IL-6 is often up regulated along with tumor growth [57]. It is reported that reduced expression of IL-6 was observed from cancer patients, who received anti PD-L1 antibody MPDL3280A [53]. In agreement with the previous report, we discovered a decreased IL-6 from the mouse tumor tissues after the treatment of CLP002 and CLP003. In addition, by using the IL-6 and PD-L1 checkpoint inhibitors, Mace et al. discovered significant tumor suppression in a pancreatic cancer mouse model [57]. The researchers suggested that the IL-6/STAT3 pathway facilitates immunosuppressive cells and negatively influences the T cell balance, such as myeloid-derived suppressor cells (MDSCs) and T regulatory cells, which will benefit the tumor growth. They also reported that the IL-6 is critical for the tumor progression. Knockout of IL-6 will hinder the tumor growth.

We also performed immunohistochemical staining for CD8 in the tumor tissues. As shown in Figure 23, both the positive control antibody and peptide candidates significantly increased the CD8 density in tumor tissues. As reported in the study by Tumeh et al., the CD8 level in the tumor is inversely correlated with the tumor size in patients who showed a response to the anti-PD-1 antibody, while CD8 was not detected in the tumor tissues from patients who did not respond to the treatment [67]. As the marker of the effector T cells, CD8 density is directly associated with the therapeutic outcome. In this scenario, the blockade of PD-1/PD-L1 interaction will allow more CD8+ activated T cells in the tumor. Consistent with the previous report, we observed significantly increased CD8 levels after the treatment in the groups of antibody, CLP002 and CLP003, which showed statistical difference of the tumor volume and weight compared to the saline group.

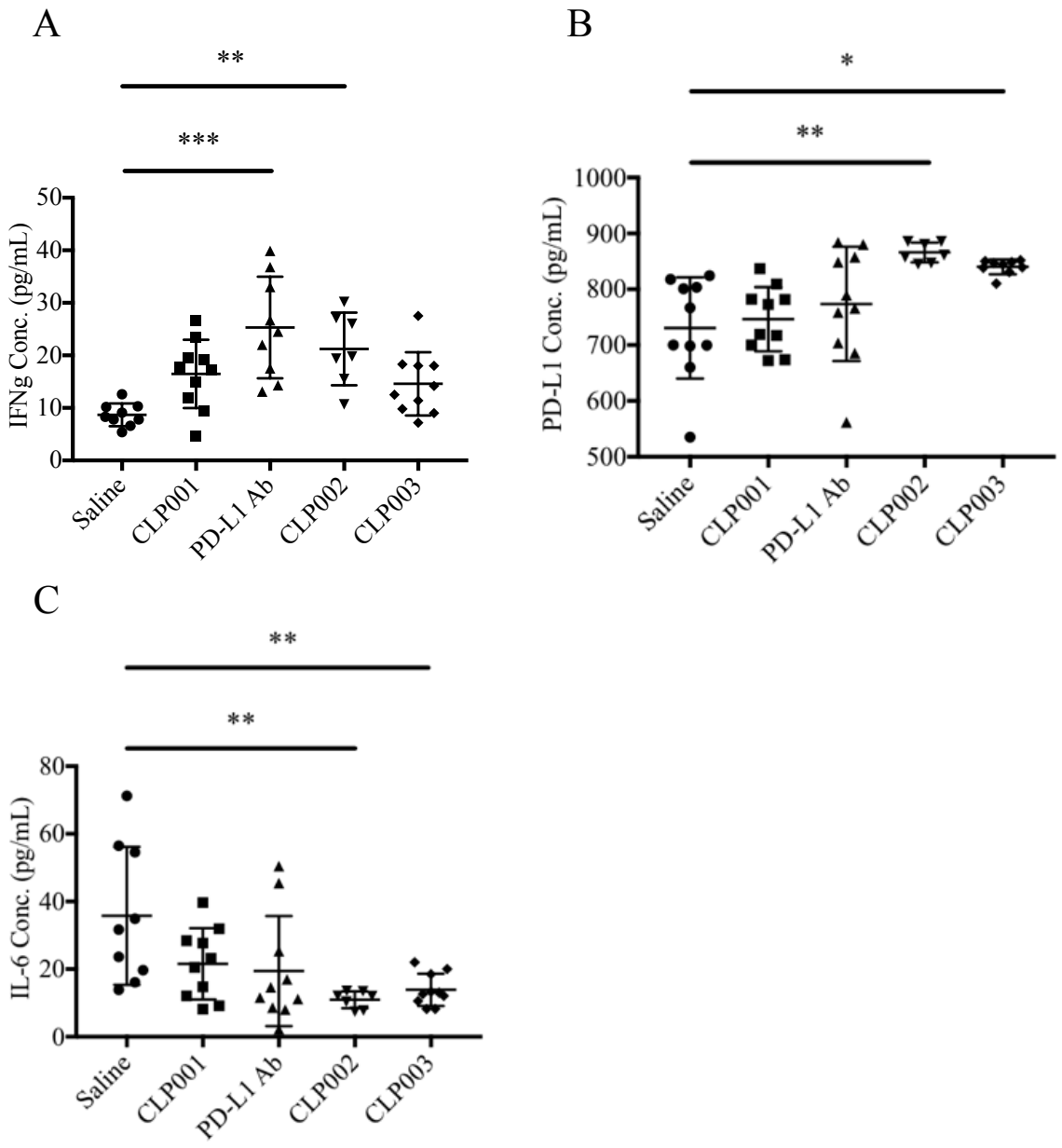

Figure 22. The PD-L1-specific peptides induce the expressions of PD-L1 and cytokines associated with antitumor immune response. The tumor tissues were lysed and total protein concentrations were determined using BCA assay. The expressions of IFNγ (A), PD-L1 (B) and IL-6 (C) were measured with ELISA. (*P<0.05; **P<0.01, ***P<0.001).

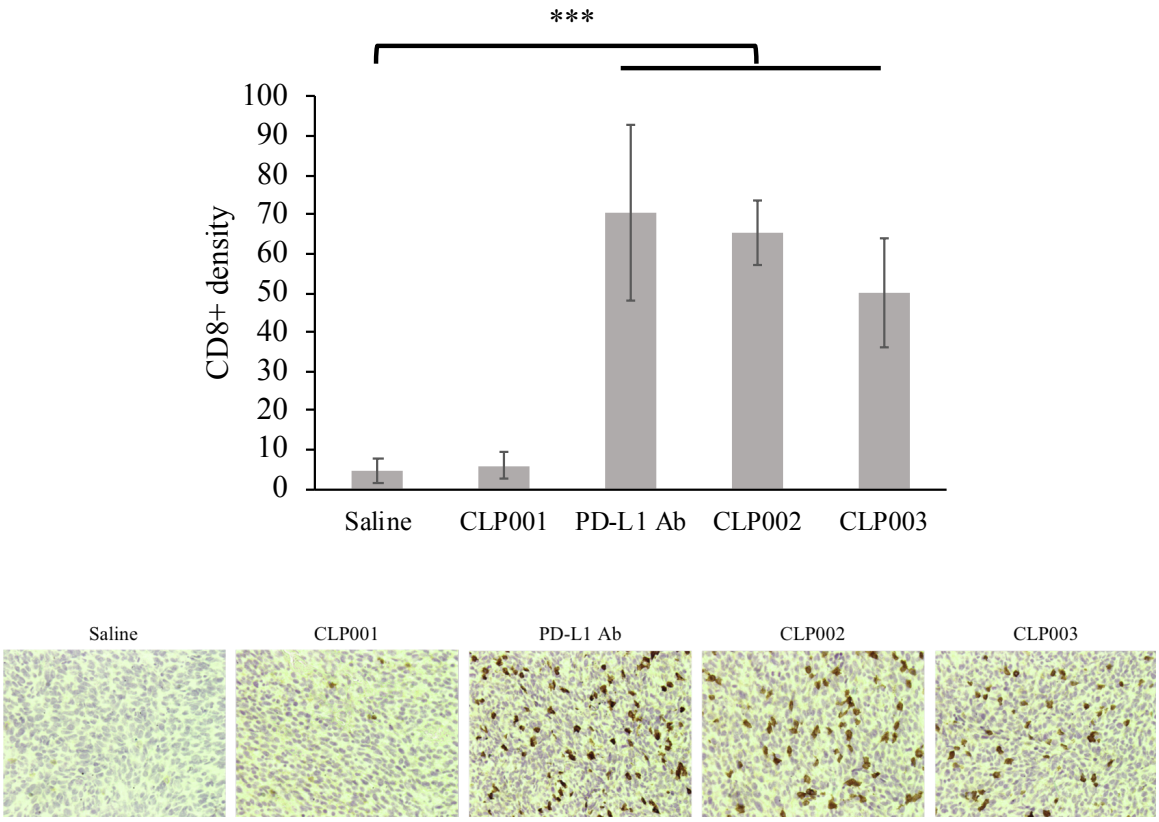

Figure 23. Immunohistochemical analysis of CD8+ T cells in tumor specimen. Representative examples of CD8 chromogenic staining from tumor specimen. The numbers of CD8+ T cells in each specimen were also quantitated. The results are presented as the mean ± SD (n=3). (*P<0.05; **P<0.01, ***P<0.001).

For the survival study, mice were intraperitoneally injected with CLP002 and CLP003 daily or the anti-mouse PD-L1 antibody every other day from day 4 to day 17 (Figure 24A). CLP002 inhibited tumor growth and improved the survival of tumor-bearing mice compared with control animals. CLP003 exerted a similar effect to the positive control antibody. Both CLP003 and the PD-L1 antibody modestly improved the survival of tumor-bearing mice. As shown in Figure 24B, 90% of mice in the saline group had died by day 17. Only 20% of the mice in the CLP002 group were dead by day 17. Eight mice showed a response to the CLP002 treatment, and 4 mice exhibited better inhibition of tumor growth than the others. We also noticed a significant increase in the tumor growth rate after the treatment was withdrawn. Similar tumor growth curves were obtained for the CLP003 and positive control antibody groups. Both treatments slowed tumor growth.

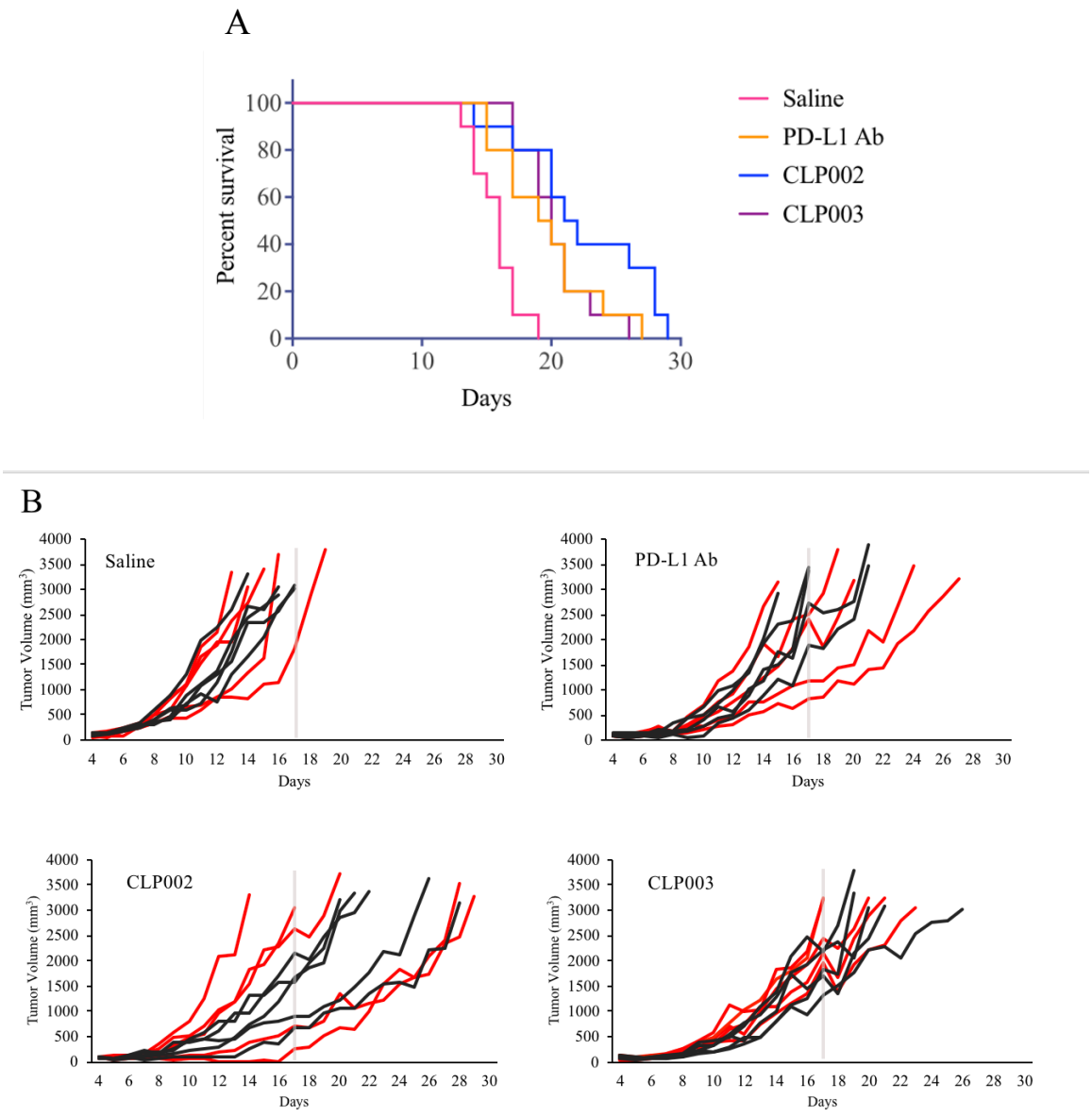

Figure 24. Survival curves of the mice treated with the PD-L1-specific peptides and PD-L1 antibody. CT26 tumor-bearing mice were randomly divided into 4 groups (10 mice per group, 50% female and 50% male). The mice were treated with the antibody or peptides from day 4 to day 17. (A) PD-L1 antibody and peptides improve survival rate of the mice. (B) Tumor growth curves of individual mice in each group.

4.4 Discussion

In the current study, we discovered 4 different peptides targeting human PD-L1 using a novel phage display biopanning method. Precleaning step was designed to remove the phage clones, which bind to any sites outside of the PD-1/PD-L1 contact residues. After 5 rounds of selections, CLP002 was verified to be the best antagonist candidate because it significantly blocked the PD-1/PD-L1 interaction both *in vitro* and *in vivo*.

A blockade assay was generated to verify the blocking efficiency of the peptides. The CLP002 showed the highest blocking effect, which was about 85% of the PD-1/PD-L1 interaction. Then, we investigated the blocking efficiency against PD-L1 positive human/mouse cancer cells. The CLP002 exhibited potent blocking ability on cell-based PD-1/PD-L1 interaction. It blockaded about 80% interaction on DU145 cells and 61% on 4T1 cells. The docking result confirmed the CLP002 blockaded PD-1/PD-L1 interaction. The binding site of CLP002 is overlapped with the PD-1/PD-L1 binding residues. CLP002 competed with PD-1 for the PD-L1 binding and blocked the interaction.

In the tumor microenvironment, PD-L1 is overexpressed on tumor cells. The tumor cells inhibit T cell activation and lead to an exhausted phenotype and impaired effector T cell functions by promoting the PD-1/PD-L1 interaction [112, 132, 133]. In addition, PD-1 expressed at high levels in multiple other cells, such as natural killer (NK) cells and B cells [114, 134]. PD-1/PD-L1 binding suppresses the T cell proliferation and induces T cell apoptosis and cytokine secretion [48]. We verified that CLP002 binds to PD-L1, blocks the PD-1/PD-L1 interaction, restores T cell proliferation and prevents T cell apoptosis *in vitro* and increases the IFNγ level *in vivo*.

In the animal study, we observed similar tumor growth rates in female and male mice. We used an anti-mouse PD-L1 antibody (10F.9G2), which has been widely used as the PD-L1 inhibitor in various animal studies, as a positive control [10, 56, 129, 135]. Consistent with a previous report [126], mice treated with the PD-L1 antibody showed a slower tumor growth rate. Compared to the control antibody, mice treated with CLP002 exhibited a considerable inhibition of tumor growth, although CLP002 was screened against human PD-L1, which only exhibits 76% sequence identity with mouse PD-L1. Tumor volume and tumor weight were compared. We observed significant difference between the saline and the treatment groups. The peptide antagonist also significantly prolonged the survival of the tumor-bearing mice compared to either the saline-treated mice or the antibody-treated mice. Notably, the tumor growth rate was significantly increased after the treatment was withdrawn, confirming the inhibitory effect of the peptide antagonist. Next, we compared PD-L1 expression and cytokine levels in tumors. As Mandai et al reported [130], the IFNγ initially triggered immune response through the T cell activation. However, PD-L1 expression is also elevated by the secreted interferon, which suppress the T cell activation and facilitates the tumor progression. In tumor microenvironment, the tumor cells counteract to the effector T cells through the up regulated IFNγ, which promotes the PD-L1 expression on the tumor cell surface. Consistent with a previous report [34], we observed the IFNγ levels increased after the treatment from both the antibody and peptides. Since IFNγ induces the PD-L1 expression on tumor cells, we observed increased PD-L1 levels of the treated tumor tissue. As Tumeh et al reported [67], there's a strong correlation between the CD8+ density and the PD-L1 expression from the melanoma patients. The high CD8+ density accompanied

with elevated PD-L1 level. The authors discovered increased CD8+ levels in patients who respond to the PD-1 antibody treatment, comparing to very low CD8+ detection from the progressive tumors, who did not show response to the checkpoint inhibitor treatment. In this study, we observed increased levels of CD8+ from the treated groups associated with up regulated PD-L1 and IFNγ expression in tumors, which is in agreement with the previous reports. We observed significant differences of the markers after the treatment, which confirmed the anti-tumor effects of both the PD-L1 antibody and the peptide.

In general, we discovered the anti-human PD-L1 peptide CLP002 that functions as an immune checkpoint inhibitor. The peptide specifically binds to PD-L1 with high affinity and blocks the PD-1/PD-L1 interaction. According to the results of the *in vivo* study, the peptide antagonist inhibits tumor growth and increases the survival of tumor-bearing animals, suggesting the CLP002 represents a good drug candidate for cancer immunotherapy.

CHAPTER 5

A NOVEL NANOBODY TARGETING PD-L1 FOR CANCER IMMUNOTHERAPY

5.1 Rationale

Cancer immunotherapy is the approach designed to boost the immune system for therapeutic benefits in treating cancers [35]. Cancer cells use checkpoint interactions to suppress the immune response, particularly to inhibit T cells. Since most of the checkpoints are regulated by ligand-receptor interactions, the negative regulation on T cells can be blocked by checkpoint inhibitors.

T cells are activated after the recognition of the antigen-MHC complex by the T cell receptor along with a co-stimulatory signal. Programmed cell death protein 1 (PD-1) expression is up regulated by T cell activation. When bound to programmed death ligand 1 (PD-L1), the checkpoint complex will attenuate T cell activation through the phosphorylation of protein tyrosine phosphatase 2 (SHP2) and subsequently inhibiting T cell proliferation, inducing T cell apoptosis and ultimately reducing cytokine release [136]. Currently, two anti-PD-1 antibodies and three anti-PD-L1 antibodies have been approved by the FDA. Antibodies bind to either the receptor or the ligand and block the PD-1/PD-L1 pathway to restore the T cell killing ability. Compared to antibody fragments, the whole antibody still has several limitations, such as inefficient tumor tissue penetration [13]. Smaller nanobodies travel faster through the tumor blood vessels and densely accumulate in the tumor extracellular matrix [137, 138]. Upon reaching the tumor microenvironment, high affinity antibodies exhibit limited penetration depth in the tumor tissue because of their large molecular weights [139]. Another drawback of

antibodies is immunogenicity, which is not been reported against nanobody in mouse or human [11, 140, 141].

A nanobody (domain antibody or VHH) is the antigen-specific variable region of the heavy chain from heavy-chain antibodies [60]. Over the last two decades, researchers have expressed increasing interest in nanobodies. The molecular weight of nanobodies is approximately 15 KD, which is actually the smallest naturally occurring antibody fragment. Antibody-dependent cellular cytotoxicity is not observed in nanobodies because the lack of the Fc region [142]. The nanobodies have many advantages, such as great stability, low immunogenicity, ease of production and high binding affinity, making nanobodies promising candidates for cancer immunotherapy [13]. Target-specific nanobodies have been obtained through immune reactions or various libraries, such as phage display, yeast display, bacterial display, ribosome display, and intracellular 2 hybrid selection and others [60, 143, 144]. Phage display is the preferred method, and the library clones are prepared for expression in phages because of their robustness. In general, 2-4 rounds of selection are required to enrich the target-specific phage clones against immobilized target protein on a plate. After screening, the gene sequences of the enriched clones are obtained to analyze the amino acid sequences of the nanobodies [145, 146].

In the current study, a library of human antibody fragment repertories was used for biopanning against the human PD-L1 extracellular domain (ECD) [147]. After four rounds of selection, the resulting nanobodies were used to block the PD-1/PD-L1 interaction *in vitro* and *in vivo*.

5.2 Methods

5.2.1 Cell culture

DU145, 4T1, CT26 and Jurkat cell lines were purchased from ATCC. DU145 cells were cultured in DMEM medium with 10% Fetal Bovine Serum (FBS), 100 units/mL penicillin and 100 μg/mL streptomycin. 4T1, CT26 and Jurkat cells were cultured in RPMI1640 medium with 10% FBS, 100 units/mL penicillin and 100 μg/mL streptomycin. All cells were grown at 37°C in a humidified atmosphere containing 5% CO2. The culture medium was changed every other day, and the cells were passaged when they reached 80–90% confluence.

5.2.2 Phage display biopanning

The phage biopanning procedure was followed the previous reports with modifications [77, 111, 147]. Briefly, 1×10^{12} pfu phages in MPBS (5% milk in PBS) were incubated with human PD-L1 extracellular domain protein immobilized in a 96-well plate at room temperature for 1 hour under shaking. Unbound phages were removed by washing with PBST (0.1% Tween 20) for ten times. Bound phages were recovered by trypsin. The recovered phages were then amplified for next round biopanning. After 4 rounds of biopanning, 45 single colonies were amplified. The DNA was isolated for sequencing.

5.2.3 Blockade of receptor-ligand interaction

One hundred nanograms of PD-L1 ECD (G&P Biosciences, human PD-L1 ECD, cat# FCL0784B; or mouse PD-L1, cat# FCL3502B) were coated on 96-wells plate

overnight at 4°C and blocked with 2% BSA for 2 hours at room temperature. Nanobodies were loaded in each well and incubated for 1 hour at room temperature. Next, the unbound nanobody was removed by washing. Biotinylated PD-1 (G&P Biosciences, human PD-1 ECD, cat# FCL0761B; or mouse PD-1, cat# FCL1846) was loaded in each well and incubated for 1 hour. Streptavidin-HRP (R&D system) was later added and incubated for 20 min. The substrate was added and incubated for 20 min to develop the color reaction. Absorbance at 450nm and reference at 540nm were recorded, when the stop solution was added.

5.2.4 Surface plasmon resonance (SPR)

The binding affinities between human PD-L1 ECD and anti-PD-L1 nanobodies were measured by SPR (BI4500, Biosensing Instrument) at 25°C. The purified PD-L1 was diluted in 10 mM sodium acetate buffer (pH 5.0). The diluted PD-L1 was soon covalently immobilized to a new sensor chip (Sensor Chip CM5, Biosensing Instrument) via primary amine group, using the standard Amine Coupling Kit (GE Healthcare). The target PD-L1 immobilization levels were 6000 RU. A second channel was blank as a reference, without any modification. Measurements were performed at a flow rate of 60 μL/min in HBS-P+ buffer (GE Healthcare). To get the data for kinetic and affinity analysis, a concentration gradient of nanobodies (1.95, 3.9, 7.8, 15.6, 31.2, 62.5, 125, 250, 500 and 1000 nM) was freshly prepared in running buffer with at least 5 concentrations, the concentration range was optimized per different analytes. The sensor chip surface was regenerated with 10 mM NaOH at a flow rate of 60 μL/min for 20 seconds to completely remove the tightly-bound residual nanobodies [63].

5.2.5 Apoptosis and proliferation assay

The dead cell apoptosis kit with annexin V alexa fluor 488 & propidium iodide (PI) was purchased from ThermoFisher. The apoptosis assay was followed the previous report [15, 117, 148]. 300,000 DU145 cells were cocultured with 60,000 Jurkat cell in 6-well plate. Nanobody was added and incubated for 24 hours. Then, the Jurkat cells were harvested. All the cells were treated per the manufacturer's protocol and analyzed using the FACSCalibur flowcytometer (BD Biosciences).

The T cell proliferation was measured by using CellTiter-Glo luminescent cell viability assay (Promega). First, the Jurkat T cells were mixed with PD-L1 over expressed DU145 cancer cells at ratio 1:5. Peptide or PD-L1 antibody was then added to the cells mixture and incubated for 24 hours. After that the T cells were collected. And T cell proliferation was performed according to the manufacturer's protocol.

5.2.6 Enzyme-linked immunosorbent assay (ELISA)

PD-L1, interferon gamma (IFNγ) and interleukin 6 (IL-6) elisa were purchased from R&D systems, and performed according to the manufacturer's manuals. The tumor tissues were lysis by RIPA buffer and homogenized. The concentrations of the tumor tissue protein were evaluated by BCA assay. All samples were loaded at identical amount of protein. OD 450 and reference OD 540 were recorded.

5.2.7 IHC staining

The anti-CD8a antibody and rabbit specific HRP/DAB (ABC) detection IHC kit were purchased from Abcam and performed according to the manufacturer's manuals. The formalin-fixed paraffin-embedded tumor tissue slides were prepared by Kansas City

Truman Medical Center. Briefly, the slides were heated for 45 mins in Tris buffer pH9.0 to induce antigen retrieval. After wash, the anti-CD8a antibody was loaded and incubated overnight at 4°C. On the second day, the biotinylated goat anti rabbit secondary antibody was loaded. The staining color reaction was generated by adding the DAB chromogen mixture. All the results were taken at magnification 200×.

5.2.8 Animal study

The animal protocol was approved by the University of Missouri-Kansas City, Institutional Animal Care and Use Committee (IACUC). Five-week old male (50%) and female (50%) Balb/c mice were purchased from Charles Rivers Laboratories (Wilmington, Massachusetts) and housed in a temperature and humidity controlled room with a 12 hours light-dark cycle. 5×10^5 CT26 cells were mixed with equal volume of matrigel and injected subcutaneously on the right flank. The mice were treated with peptide at 2 mg/kg for a daily intraperitoneally injection, when the tumor size grow to 50-100 mm^3. Anti-mouse PD-L1 antibody (10F.9G2, BioXcell) was administrated as a positive control at 10 mg/kg (200 μg/mouse) in every two days. The tumor size was assessed with a caliper and calculated with formula ½ × a × b × b. For the survival study, the mice were check daily and treated as dead according to the University of Missouri-Kansas City Institutional Animal Care and Use Committee Animal Protocol.

5.2.9 Statistical Analysis

Data are expressed as the mean ± standard deviation (SD). The difference between any two groups was determined by one-way analysis of variance (ANOVA).

$P<0.05$ was statistically significant. For *in vivo* study, data are presented as the mean ± standard error of the mean (SEM). The statistic significance between any two groups was determined by two-way analysis of variance (ANOVA). Tukey's multiple comparisons test was used as post hoc analysis. The $P<0.05$ was statistically significant.

5.3 Result

5.3.1 Biopanning of anti PD-L1 nanobodies blocking PD-1/PD-L1 interaction

In order to discover the particular phage clones that can specifically bind to PD-L1 and further hinder the binding between the PD-1 and PD-L1, we performed 4 rounds of biopanning against the human PD-L1 extracellular domain (ECD) instead of whole PD-L1 molecule [149]. We used the extracellular domain, PD-1 binding region, but not the whole molecule for the biopanning to focus the screening to a smaller area, reduced the possibility of unwanted targeting phages. As shown in Figure 25A, we observed a significant increase of the recovered phage number after 4 rounds of biopanning. And then 45 different colonies of the phage clones were randomly selected and sent for sequencing. We discovered 9 different sequences and named them as CLV1 to CLV9. Among the 9 candidates, the CLV4 and CLV7 have multiple stop codons in the gene sequences. The other 7 gene sequences were inserted into vector pET-22b (+). The vectors were transformed to E Coli. (BL21 (DE3)) by heat shock method. The nanobodies were expressed and purified by using Ni-NTA affinity chromatography. As shown in Figure 25B, the purity of the nanobody was accessed by SDS-PAGE. All 7 different nanobodies were expressed and used in the subsequent studies.

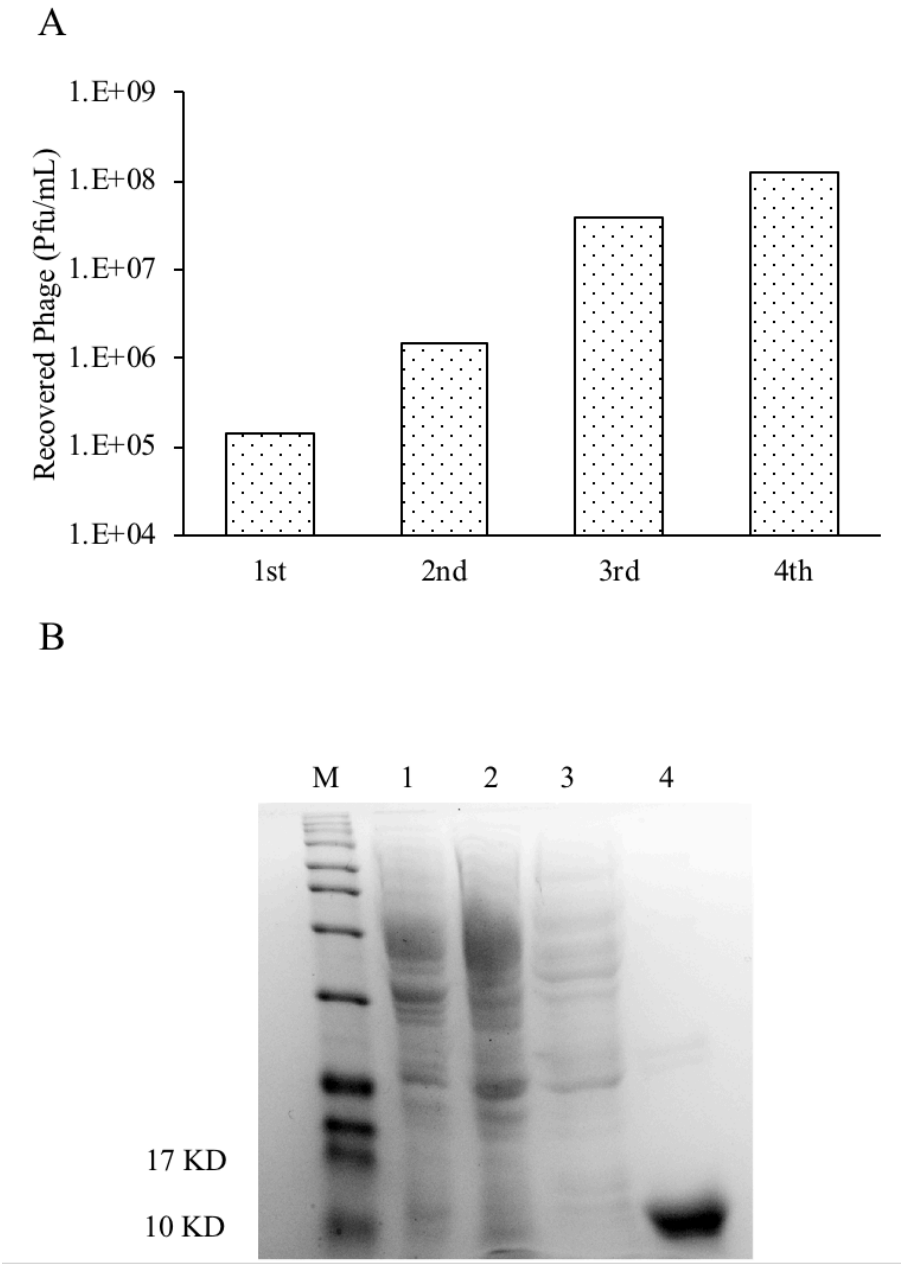

Figure 25. Discovery of anti-PD-L1 nanobodies using phage display. (A) The number of eluted phages after each round of biopanning. (B) The CLV3 nanobody was expressed in E Coli. (BL21 (DE3)), and the cell lysate (lane 1), flow-through (lane 2), washing buffer (lane 3), and elution buffer (lane 4) were analyzed using SDS-PAGE.

5.3.2 Binding affinity of nanobodies against human PD-L1

We investigated the binding affinities of 7 nanobody candidates using surface plasmon resonance. Human PD-L1 ECD was coated on a CM5 sensor chip by the direct amine coupling method. As shown in Table 5, the dissociation constants of the nanobodies bound to human PD-L1 ECD ranged from 12.37 to 228.61 nM, which is in reported range [150]. CLV3 exhibited the highest binding affinity, although it is not the most frequent repeated sequence obtained from the biopanning results.

Table 5. Molecular weights and binding affinities of the nanobodies against human PD-L1

VHH	Mw (Da)	K_a ($M^{-1}S^{-1}$)	K_d (S^{-1})	K_D (nM)
CLV1	13,391	$(2.52 \pm 0.65) \times 10^4$	$(5.02 \pm 1.31) \times 10^{-3}$	198.82 ± 1.36
CLV2	12,918	4874 ± 2498	$(2.47 \pm 1.33) \times 10^{-4}$	65.42 ± 39.27
CLV3	13,573	$(2.98 \pm 1.53) \times 10^5$	$(3.37 \pm 2.07) \times 10^{-3}$	12.37 ± 5.65
CLV5	13,137	$(2.05 \pm 1.89) \times 10^4$	$(5.53 \pm 6.16) \times 10^{-3}$	228.61 ± 88.76
CLV6	12,700	$(1.62 \pm 0.73) \times 10^6$	0.025 ± 0.005	16.63 ± 4.99
CLV8	13,099	$(3.15 \pm 1.13) \times 10^4$	$(5.26 \pm 1.90) \times 10^{-3}$	166.73 ± 1.67
CLV9	13,632	$(6.59 \pm 2.08) \times 10^4$	$(1.15 \pm 0.31) \times 10^{-3}$	17.72 ± 1.13

5.3.3 Nanobody-mediated blockade of the PD-L1/PD-1 interaction

A PD-1/PD-L1 blocking assay was developed to evaluate the blocking efficacy of all nanobody candidates. The efficiencies at which the nanobodies blocked the PD-1/PD-L1 interaction were compared at 1 μM. As shown in Figure 26A, all nanobodies showed blocking effect. Among the nanobodies, CLV3 exhibited the highest blocking ability, as it blocked 74% of the PD-1/PD-L1 interactions at 1 μM. In the next step, different concentrations of CLV3 were loaded to calculate the IC_{50} of CLV3 against the human PD-1/PD-L1 interaction. The IC_{50} was 44.25 nM, with a 70% blocking efficiency (Figure 26B). We also evaluated the blocking effect of CLV3 in PD-L1 over-expressing human prostate cancer DU145 cells. The IC_{50} of CLV3 against the PD-1/PD-L1 interaction on DU145 cells was 32.3 nM, and the nanobody blocked 76.5% of the interactions (Figure 26C).

Next, we investigated the effect of CLV3 on blocking the mouse PD-1/PD-L1 interaction. As shown in Figure 26D, CLV3 blocked approximately 68% of the interaction with an IC_{50} of 15.5 nM. By contrast, the anti-mouse PD-L1 antibody (BioXcell, 10F.9G2) blocked approximately 67% of the interaction with an IC_{50} of 35.2 nM (Figure 26E). The nanobody retained a comparable blocking ability as the whole antibody, although the molecular weight of the nanobody is only approximately 15 KD.

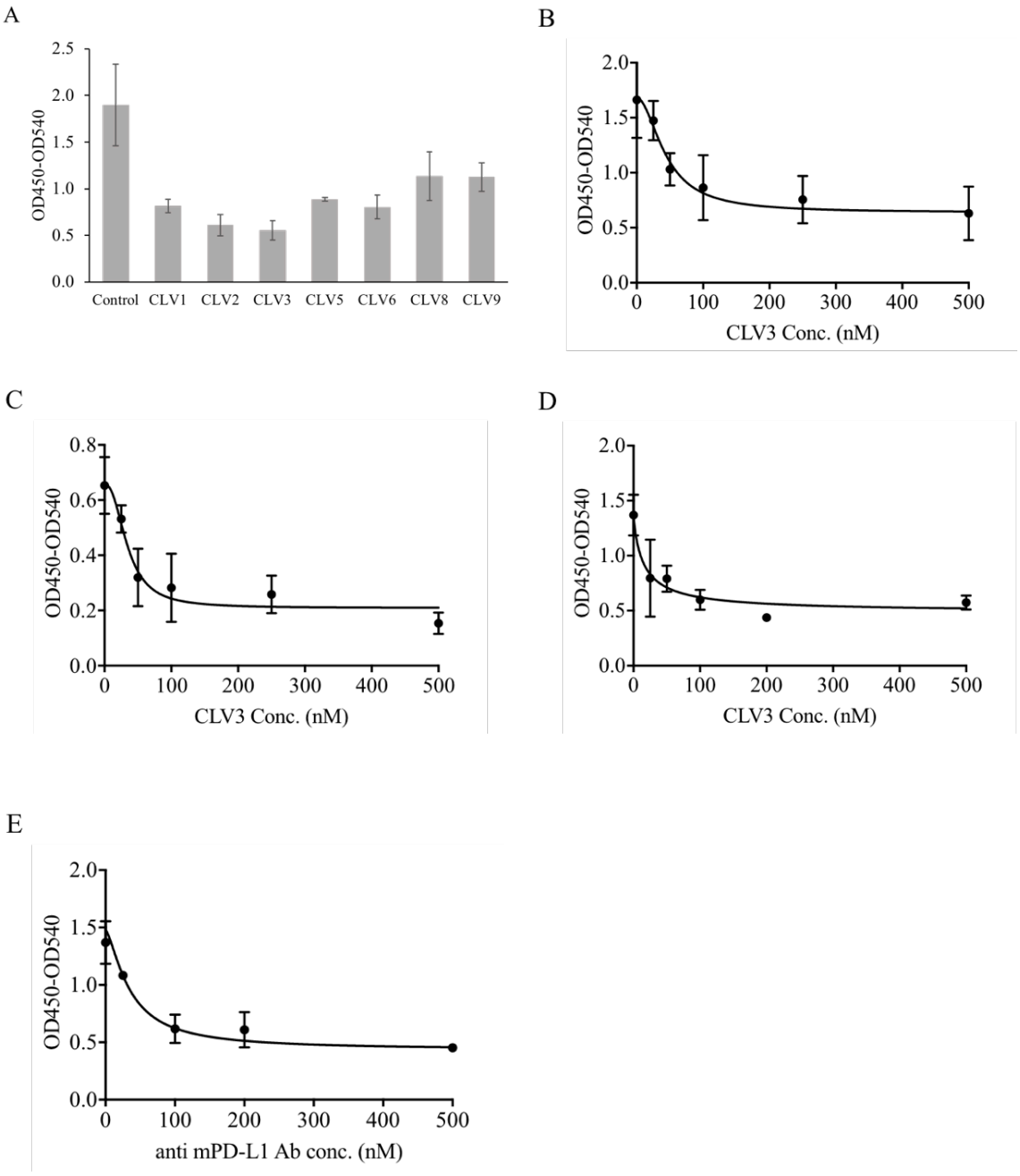

Figure 26. Blocking effect of the nanobodies against the human PD-1/PD-L1 interaction. (A) Blockade efficiency of the selected nanobodies at 1 μM. The CLV3 nanobody shows the highest blocking efficiency. (B) Blocking profile of CLV3 against human PD-L1 ECD. (C) Blocking profile of CLV3 against PD-L1-positive human prostate cancer DU145 cells. (D) Blocking profile of CLV3 against mouse PD-L1. (E) Blocking profile of an anti-mouse PD-L1 antibody against mouse PD-L1. The results are presented as the mean ± SD (n=3).

5.3.4 CLV3 restores the T cell proliferation and restricts the apoptosis induced by cancer cells

We co-cultured Jurkat T cells with DU145 cancer cells. As shown in Figure 27A, the proliferation of Jurkat cells was inhibited in the presence of DU145 cells. Next, we added CLV3 to the co-cultures and incubated them for 24 hours. CLV3 significantly increased the proliferation of Jurkat T cell in the presence of DU145 cells. As reported in a previous study [114], T cell proliferation was restrained by the PD-1/PD-L1 pathway in a dose-dependent manner. The researchers did not observe the inhibition of T cell proliferation, when PD-1 was silenced in T cells. Similarly, Noman et al. reported increased T cell proliferation and function when the PD-1/PD-L1 interaction was blocked [124].

Next, we investigated whether CLV3 inhibited T cell apoptosis in co-cultures of Jurkat T cells with DU145 cells. As shown in Figure 27B, the percentage of apoptotic Jurkat T cells increased after co-culture. Next, CLV3 was added to the co-cultured cells and incubated for 24 hours. CLV3 bound to PD-L1, which is expressed on DU145 cancer cells, and blocked the interaction to PD-1. We observed reduced apoptosis of T cells after treatment with CLV3. As previously reported [112], tumor-associated PD-L1 induced cytotoxic T lymphocyte apoptosis. The authors first cultured the T cells together with melanoma cells and discovered that the tumor cells promoted T cell apoptosis, but apoptosis was not observed in PD-L1 knockout melanoma cells. Next, the researchers treated the co-cultured T cells with an anti-PD-1 antibody, and apoptosis was significantly reduced. Inspired by the previous study, we confirmed the blocking effect of CLV3 on the PD-1/PD-L1 interaction *in vitro*.

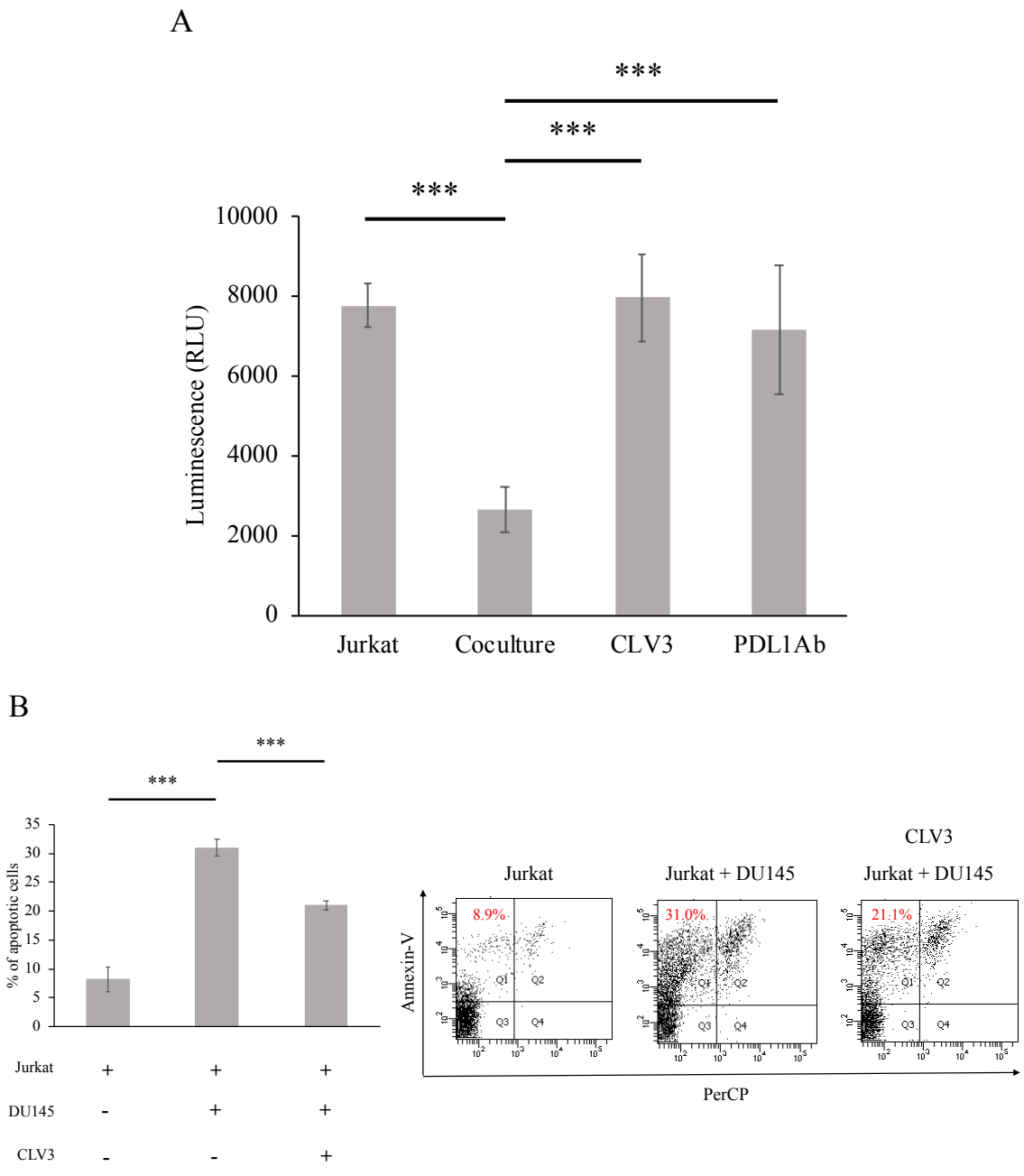

Figure 27. CLV3 restores T cell proliferation and prevents T cell apoptosis. Jurkat T cells were co-cultured with DU145 cells in a ratio 1:5, followed by incubation with the CLV3 nanobody for 24 h. CLV3 restore Jurkat T cell proliferation (A) and reduces apoptosis of the Jurkat cells. The results are presented as the mean ± SD (n=3). (*P<0.05; **P<0.01, ***P<0.001).

5.3.5 CLV3 inhibits the growth of CT26 solid tumors

An animal study was performed to evaluate the anti-tumor effect of CLV3. Equal numbers of male and female Balb/c mice were used in each group [128]. As shown in Figure 28A, CT26 cells, a mouse original colon cancer cell line, were injected into the right flank of the mice and waited 4 days to let the tumor grow [127]. The treatment started when the average tumor volume reached 50-100 mm^3 [63]. CLV3 was administered at a dose of 200 μg (10 mg/kg) daily [125]. One anti-mouse PD-L1 antibody was used as a positive control [56, 127, 129]. The antibody was administered at a dose of 10 mg/kg every other day [49, 52]. As shown in Figure 28B-28D, a significant difference in the tumor growth rate was not observed between male and female mice. CLV3 significantly inhibited tumor growth in mice of both genders. The treatment exerted a substantial effect on the tumor volume and weight in mice of both genders. We observed a better inhibitory effect of CLV3 at 10 mg/kg than at 5 mg/kg on the tumors in both female and male mice. When the mice received 10 mg/kg CLV3, the inhibition of tumor growth by CLV3 and the positive control anti-PD-L1 antibody was similar (Figure 28D). The mice received the treatment for 10 days and were euthanized on day 14. The tumor tissues were collected (as shown in Figure 29A). The tumor weights were compared between different groups. As Figure 29B illustrated, among the female mice, only the antibody group showed a significant difference in tumor weight. Although a lower tumor weight was observed in the CLV3-treated mice, the difference was not statistically significant. For the male mice, the CLV3 and antibody groups showed significant differences in tumor weight. We obtained the same result when we combined the female and male mice together.

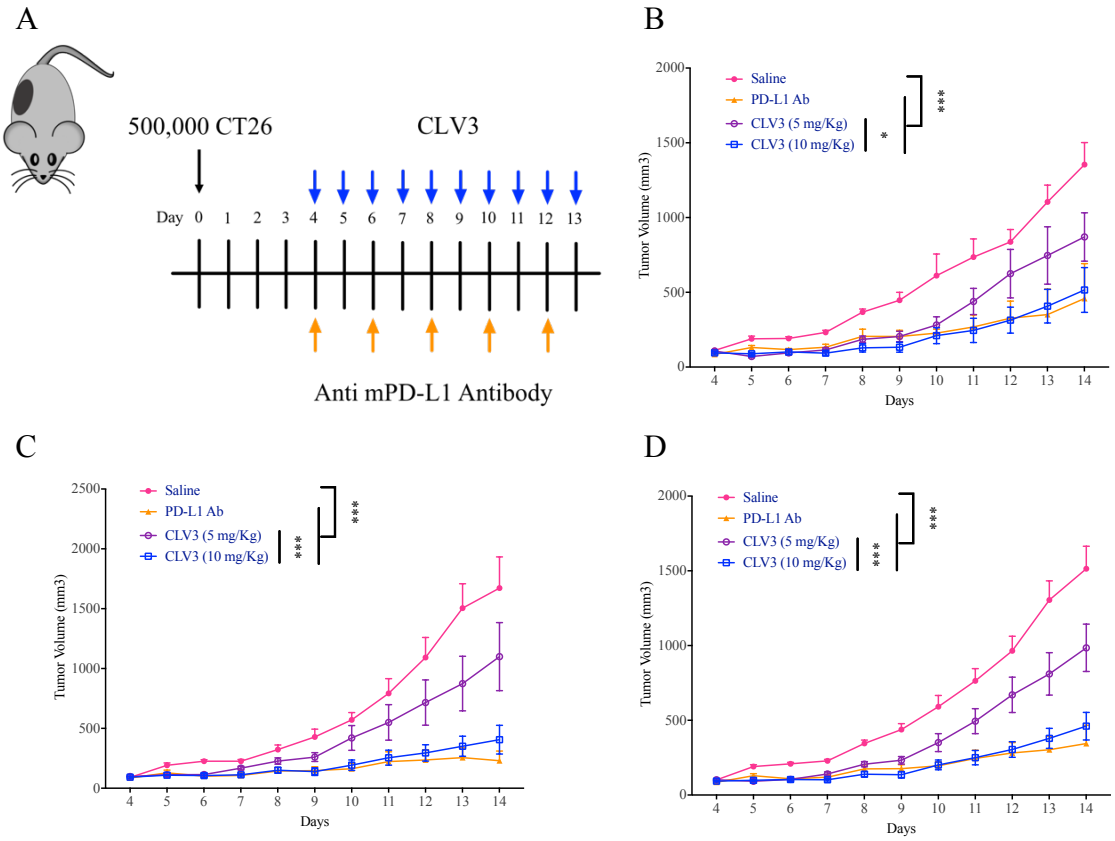

Figure 28. Anti-tumor effect of the CLV3 nanobody. (A) Schedule of the activity study. CT26 cells (0.5×10^6) were subcutaneously injected into the right flank of the mice. Once the tumor volume reached 50-100 mm^3, CLV3 (5 mg/kg or 10 mg/kg) was injected daily, and the antibody (10 mg/kg) was injected every other day. Tumor growth curves of female mice (B), male mice (C), and all the mice (D). The results are presented as the mean ± SEM. (*P<0.05; **P<0.01, ***P<0.001).

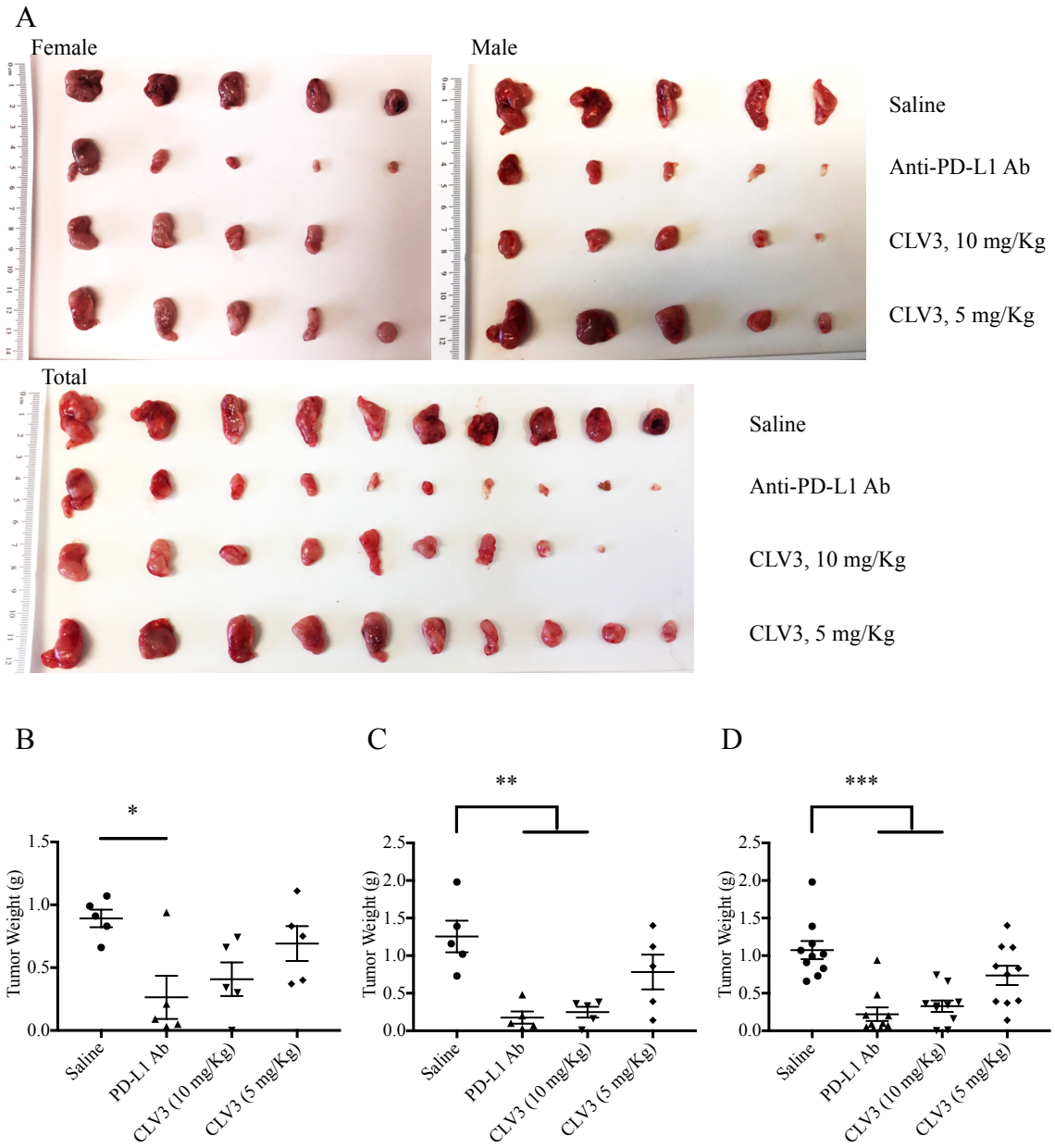

Figure 29. The CLV3 nanobody inhibits tumor growth. (A) Tumor tissues of the mice. Tumor weights of the female mice (B), male mice (C), and all the mice (D). (*P<0.05; **P<0.01, ***P<0.001).

The IFNγ, PD-L1 and IL-6 levels in tumor tissues were evaluated by ELISA. As shown in Figure 30, the PD-L1 antibody significantly increased IFNγ expression on tumor cells. CLV3 also significantly altered the level of IFNγ. Direct contact with CD8+ T cells and secreted IFNγ is strongly associated with increasing PD-L1 expression on tumor cells *in vitro* and *in vivo* [151]. The researchers knocked down the IFNγ receptor and discovered decreased PD-L1 expression on tumor cells, better CD8+ T cell infiltration, and an improved survival rate of the tumor bearing mice [131]. According to Mandai et al., the PD-L1 expression on the tumor cell surface was induced by the secreted IFNγ present in the tumor imcroenvironment. The negative regulation of the PD-1/PD-L1 interaction muted the immune attack from cytotoxic T lymphocytes [130]. In the current study, we observed up-regulated levels of IFNγ in tumor tissues. Next, we also investigated the PD-L1 expression level. We observed increased PD-L1 expression on tumor cells after treatment, which is consistent with previous reports [34, 67]. Our strategy is to use the PD-L1-specific nanobody to block the PD-1/PD-L1 interaction. We observed significant inhibition of tumor growth and improved survival. Then, we evaluated the IL-6 concentrations in tumors. The treatments successfully decreased the IL-6 levels in tumors compared to the saline group. Herbst et al. reported a decrease in the level of IL-6 in cancer patients treated with the anti-PD-L1 antibody MPDL3280A [53]. Mace et al. used IL-6 and PD-L1 blocking antibodies to successfully suppress tumor progression in xenograft mouse models of pancreatic cancer [57]. The authors postulated that the IL-6/STAT3 pathway favors the immunosuppressive cells and dysregulates the T cell balance, such as myeloid-derived suppressor cells (MDSCs) and T regulatory cells, promoting the tumor progression. The authors postulated that IL-6 is essential for tumor

growth. Knockdown of IL-6 thoroughly inhibited tumor progression. We also compared the CD8+ T cells in the tumor tissues by immunohistochemistry. Both the anti-PD-L1 antibody and nanobody significantly increased the density of CD8+ cells (Figure 31). In the previous research [53, 67], a significant increase in the number of CD8+ T cells was observed in patients who showed a response to the PD-1 antibody treatment. Meanwhile, CD8+ T cells were not detected in patients who did not respond to the treatment. In another study, Curran et al. observed a significant increase in the number of CD8+ T cells in a B16 melanoma tumor model after treatment with combination of anti-PD-L1 antibody and Fvax vaccination [10]. In agreement with the previous reports, the elevated CD8 density is directly correlated with the therapeutic effect.

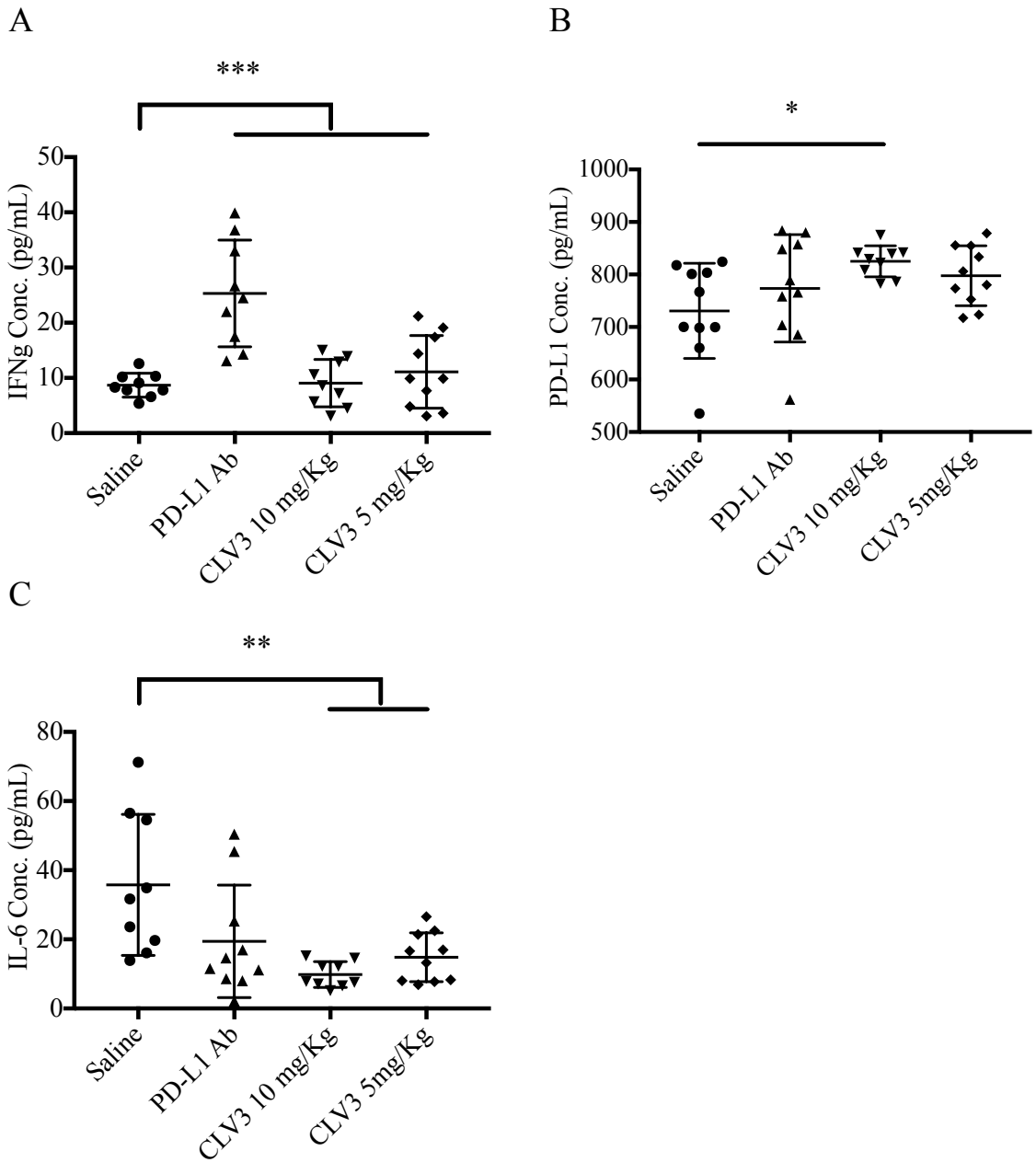

Figure 30. The CLV3 nanobody induces the expressions of PD-L1 and cytokines associated with antitumor immune response. The tumor tissues were lysed and total protein concentrations were determined using BCA assay. The expressions of IFNγ (A), PD-L1 (B), and IL-6 (C) were measured with ELISA. (*P<0.05; **P<0.01, ***P<0.001).

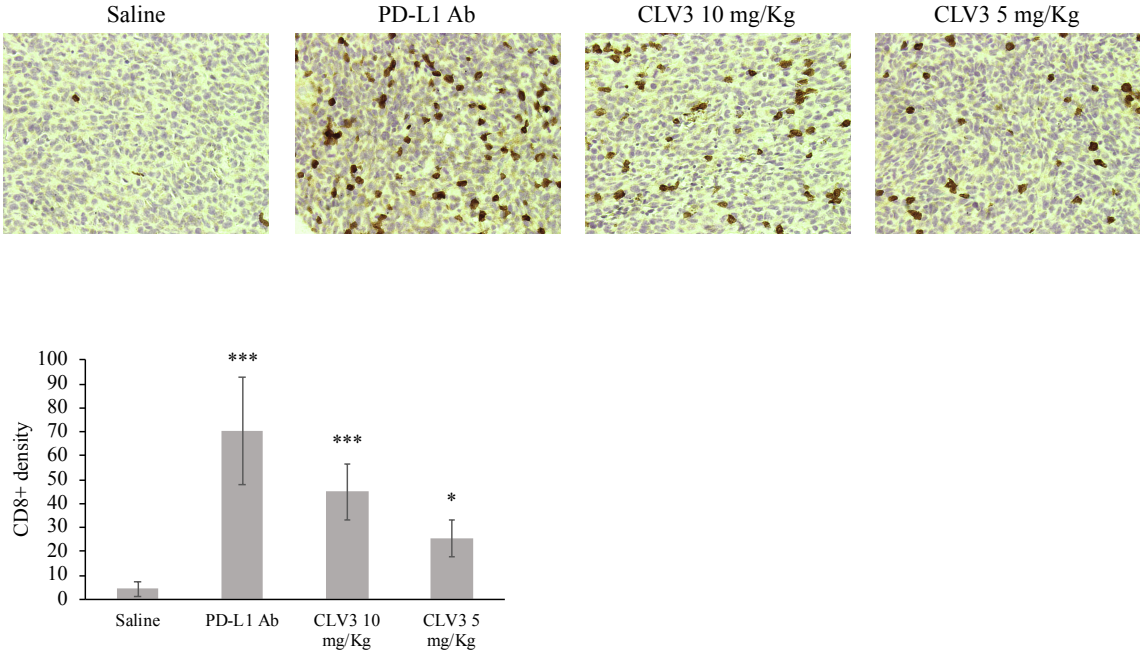

Figure 31. Immunohistochemical analysis of CD8+ T cells in tumor specimen from the mice treated with CLV3. Representative examples of CD8 chromogenic staining from tumor specimen. The numbers of CD8+ T cells in each specimen were also quantitated. The results are presented as the mean ± SD (n=3). (*P<0.05; **P<0.01, ***P<0.001).

We next investigated the survival of CT26 tumor-bearing mice. The mice were treated with CLV3 or the anti-PD-L1 antibody at a dose of 10 mg/kg for 2 weeks. The injections were performed from day 4 to day 17. As shown in Figure 32, both treatments increased the survival rate of mice compared to the saline group. By day 17, most of the mice in saline group died (Figure 32B). Six mice in the PD-L1 antibody group died after the withdrawal of the treatment (Figure 32C). Only one CLV-3 treated mouse died before day 17 (Figure 32D). Nine mice showed a response to the CLV treatment. CLV3 significantly increased the survival rate of the tumor-bearing mice.

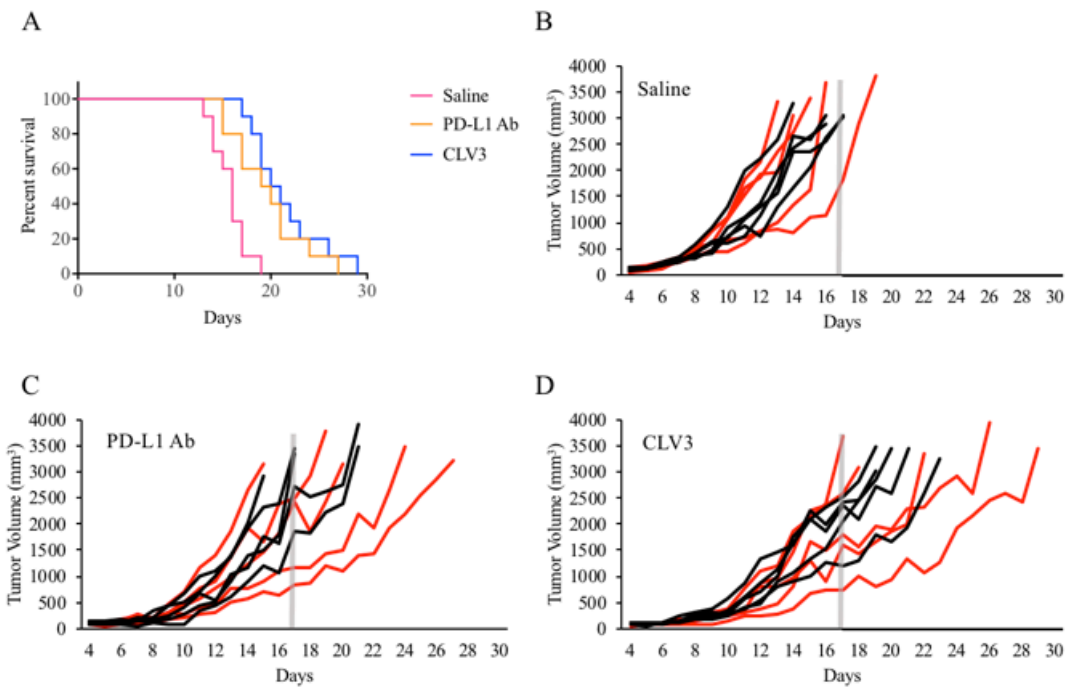

Figure 32. Survival curves of the mice treated with the CLV3 nanobody and PD-L1 antibody. CT26 tumor-bearing mice were randomly divided into 4 groups (10 mice per group, 50% female and 50% male). The mice were treated with the nanobody or antibody from day 4 to day 17. (A) PD-L1 antibody and nanobody improve survival rate of the mice. (B, C, D) Tumor growth curves of individual mice in each group.

5.4 Discussion

Currently, two anti-PD-1 and three anti-PD-L1 antibodies have been approved by the FDA. The antibodies block the PD-1/PD-L1 interaction and subsequently restore the immune cell killing ability [35, 136]. However, blockade of PD-L2 will stimulate TH2-mediated inflammation, implying that PD-L2 blockade would be a side effect of anti-PD-1 antibodies but not the anti-PD-L1 antibodies [49, 50]. PD-L1-specific blockade would be preferred to PD-1 blockade [62]. Compared to antibody, a nanobody, the smallest naturally occurring antibody fragment, is very robust, with low immunogenicity, easy production and high binding affinity. Nanobodies have a limited retention time in the circulation. Even though the short half-life is just about 30 min to 2 hours, researchers discovered nanobodies bound to the target after 24 hours [152, 153]. The nanobody is suggested to carry payload to focus on the tumor and reduce the systemic exposure, because of rapid system clearance and sustained half-life in target tissue. In addition, the production of nanobody is much easier than the antibody. The nanobody is easily expressed in bacteria with a high yield, which makes the nanobody a promising candidate for the up scale production [60]. Thus, a nanobody represents a promising candidate as a checkpoint inhibitor for cancer immunotherapy. A promising result from one phase III clinical trial of a nanobody targeting acquired thrombotic thrombocytopenic purpura (aTTP) was recently reported [61]. As a result, the PD-L1-targeting nanobody would be a good candidate for cancer immunotherapy.

In the current study, we discovered 7 different nanobodies that blocked the PD-1/PD-L1 interaction between tumor cells and immune cells. Among all nanobody candidates, CLV3 showed the best binding affinity to PD-L1 and the most potent ability

to block the PD-1/PD-L1 interaction. We evaluated the blocking effect *in vitro* and *in vivo*. CLV3 inhibited tumor cell proliferation by binding to PD-L1 on the cell surface and further blocking the PD-1/PD-L1 interaction between the cancer cell and T cell. Moreover, CLV3 decreased Jurkat cell apoptosis caused by the cocultured cancer cell *in vitro*.

CLV3 successfully inhibited tumor growth and increased the survival rate of tumor-bearing mice compared to the control group. We observed significantly increased CD8+ T cell numbers in tumor tissues after treatment. The IFNγ, PD-L1 and IL-6 levels were also detected. The CLV3 nanobody increased the IFNγ and PD-L1 levels and decreased the IL-6 level. As in previous report [67], PD-L1 expression was up regulated after the treatment. The PD-L1 level was associated with the CD8 density in the tumor tissue. The researchers suggested that the CD8 detection directly influenced the therapeutic outcome during the immunotherapy. Consistent with the previous report, we observed a significant tumor inhibition, correlated with statistically elevated CD8 detection in the tumors. Thus, we suggest the CLV3 nanobody represents a potentially useful anti-PD-L1 inhibitor.

CHAPTER 6

SUMMARY AND CONCLUSIONS

Liver fibrosis, as a world wide health problem, has attracted enormous attention. Hepatic fibrosis is due to the excessive accumulation of the extracellular matrix along with a series of modulations, including the activation of the HSC, increased the cytokine release and the modulation of ECM content. Alcoholic liver fibrosis is one of the major causes of liver fibrosis, which accounts for 50% of the liver cirrhosis. In fibrogenesis, the TGF-β and PDGF play important roles in stimulating fibrogenesis, promoting cell proliferation and migration and producing excessive collagen. In our previous study, we have identified a PCBP2 siRNA, which shows promising anti-fibrogenic activity on collagen synthesis through silencing the αCP2 protein [9]. In this dissertation, we determined that PCBP2 siRNA can reverse alcohol- and cytokine- induced fibrogenesis in primary HSCs. Moreover, the combination of LY2109761, a TGF-β1 inhibitor, and PCBP2 siRNA exhibited a synergistic inhibitory effect on the accumulation of type I collagen in HSC.

PD-L1 is highly expressed in multiple cancer cells. The interaction of PD-L1 to PD-1 leads to immunosuppressive activity. PD-1 is found on immune cells, including T lymphocytes. The PD-1/PD-L1 binding induces a negative regulatory effect on T cell immune responses [7]. Blocking the interaction is therefore a novel treatment approach for cancer. Anti-PD-L1 monoclonal antibody and anti-PD-1 monoclonal antibody have been approved by the FDA for cancer immunotherapy [8]. We recently discovered that PD-L1 is also highly expressed on HSC-T6 cells, which makes PD-L1 a potential target to induce apoptosis of activated HSC by blocking the PD-L1/PD-1 interaction.

In this dissertation, the PD-L1 specific peptides and nanobodies were discovered by phage display. Both the peptides and nanobodies bind to PD-L1 and further block the PD-1/PD-L1 interaction. The checkpoint inhibitors could prevent the PD-1/PD-L1 induced the apoptosis of T lymphocytes and enhance the T cell proliferation *in vitro*. The anti tumor efficacy was also evaluated by using CT26 xenograft mouse model. Both CLP002 and CLV3 were able to inhibit the tumor growth and significant improve the survival of the tumor bearing mice. The CD8 densities in the tumor tissues were evaluated. We discovered a significant increase of the CD8 density compare to the control group. Thus, both the CLP002 and CLV3 may provide novel anti PD-L1 drug candidates for immunotherapy.

In future studies, we will determine whether the binding of PD-L1 on HSC-T6 to PD-1 will suppress the immune responses. Our goal is to determine whether the PD-L1 expression in hepatic stellate cells could be utilized as a potential target for liver fibrosis immunotherapy. The selected PD-L1 specific ligands (peptides & nanobody) will be used in combination with PCBP2 siRNA. Our hypothesis is to use the PCBP2 siRNA to reverse the collagen accumulation and PD-L1 ligand to induce apoptosis of activated HSCs. The therapeutic effect will be determined by a rat model of liver fibrosis. We will also investigate the modifications of the PD-L1 specific peptide. Dimerization and cyclic peptide will be synthesized to improve the blocking efficiency and the stability of peptide in serum. The dimerization of the nanobody will also be determined. The chemotherapy drug will be linked to the nanobody. The immunotherapy effect of the nanobody drug conjugate will be evaluated in future.

APPENDIX

LETTER OF PERMISSION

Dear Hao Liu
We hereby grant you permission to reprint the material detailed below at no charge **in your thesis** subject to the following conditions:

1. If any part of the material to be used (for example, figures) has appeared in our publication with credit or acknowledgement to another source, permission must also be sought from that source. If such permission is not obtained then that material may not be included in your publication/copies.

2. Suitable acknowledgment to the source must be made, either as a footnote or in a reference list at the end of your publication, as follows:

   "This article was published in Publication title, Vol number, Author(s), Title of article, Page Nos, Copyright Elsevier (or appropriate Society name) (Year)."

3. Your thesis may be submitted to your institution in either print or electronic form.

4. Reproduction of this material is confined to the purpose for which permission is hereby given.

5. This permission is granted for non-exclusive world **English** rights only. For other languages please reapply separately for each one required. Permission excludes use in an electronic form other than submission. Should you have a specific electronic project in mind please reapply for permission

6. This includes permission for UMI to supply single copies, on demand, of the complete thesis. Should your thesis be published commercially, please reapply for permission.

Yours sincerely

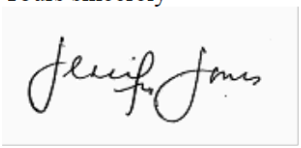

Jennifer Jones
Permissions Specialist

REFERENCES

1. Friedman, S.L., *Liver fibrosis -- from bench to bedside.* J Hepatol, 2003. **38 Suppl 1**: p. S38-53.
2. Friedman, S.L., *Mechanisms of hepatic fibrogenesis.* Gastroenterology, 2008. **134**(6): p. 1655-69.
3. Hernandez-Gea, V. and S.L. Friedman, *Pathogenesis of liver fibrosis.* Annu Rev Pathol, 2011. **6**: p. 425-56.
4. Walker, L.O. and C.Y. Cheng, *Maternal empathy, self-confidence, and stress as antecedents of preschool children's behavior problems.* J Spec Pediatr Nurs, 2007. **12**(2): p. 93-104.
5. Cheng, K. and R.I. Mahato, *Gene modulation for treating liver fibrosis.* Crit Rev Ther Drug Carrier Syst, 2007. **24**(2): p. 93-146.
6. Iwai, Y., et al., *Involvement of PD-L1 on tumor cells in the escape from host immune system and tumor immunotherapy by PD-L1 blockade.* Proc Natl Acad Sci U S A, 2002. **99**(19): p. 12293-7.
7. Mahoney, K.M., G.J. Freeman, and D.F. McDermott, *The Next Immune-Checkpoint Inhibitors: PD-1/PD-L1 Blockade in Melanoma.* Clin Ther, 2015. **37**(4): p. 764-82.
8. Black, M., et al., *Activation of the PD-1/PD-L1 immune checkpoint confers tumor cell chemoresistance associated with increased metastasis.* Oncotarget, 2016. **7**(9): p. 10557-67.

9. Shukla, R.S., et al., *PCBP2 siRNA reverses the alcohol-induced pro-fibrogenic effects in hepatic stellate cells.* Pharm Res, 2011. **28**(12): p. 3058-68.

10. Curran, M.A., et al., *PD-1 and CTLA-4 combination blockade expands infiltrating T cells and reduces regulatory T and myeloid cells within B16 melanoma tumors.* Proc Natl Acad Sci U S A, 2010. **107**(9): p. 4275-80.

11. Maute, R.L., et al., *Engineering high-affinity PD-1 variants for optimized immunotherapy and immuno-PET imaging.* Proc Natl Acad Sci U S A, 2015. **112**(47): p. E6506-14.

12. Dahan, R., et al., *FcgammaRs Modulate the Anti-tumor Activity of Antibodies Targeting the PD-1/PD-L1 Axis.* Cancer Cell, 2015. **28**(3): p. 285-95.

13. Xenaki, K.T., S. Oliveira, and P.M.P. van Bergen En Henegouwen, *Antibody or Antibody Fragments: Implications for Molecular Imaging and Targeted Therapy of Solid Tumors.* Front Immunol, 2017. **8**: p. 1287.

14. Schuppan, D. and Y.O. Kim, *Evolving therapies for liver fibrosis.* J Clin Invest, 2013. **123**(5): p. 1887-901.

15. Liu, H., et al., *Silencing of alpha-complex protein-2 reverses alcohol- and cytokine-induced fibrogenesis in hepatic stellate cells.* Liver Res, 2017. **1**(1): p. 70-79.

16. Seki, E. and R.F. Schwabe, *Hepatic inflammation and fibrosis: functional links and key pathways.* Hepatology, 2015. **61**(3): p. 1066-79.

17. Rehermann, B., *Pathogenesis of chronic viral hepatitis: differential roles of T cells and NK cells.* Nat Med, 2013. **19**(7): p. 859-68.

18. Tsukada, S., C.J. Parsons, and R.A. Rippe, *Mechanisms of liver fibrosis.* Clin Chim Acta, 2006. **364**(1-2): p. 33-60.

19. Trautwein, C., et al., *Hepatic fibrosis: Concept to treatment.* J Hepatol, 2015. **62**(1 Suppl): p. S15-24.

20. Mederacke, I., et al., *Fate tracing reveals hepatic stellate cells as dominant contributors to liver fibrosis independent of its aetiology.* Nat Commun, 2013. **4**: p. 2823.

21. Lechuga, C.G., et al., *PI3K is involved in PDGF-beta receptor upregulation post-PDGF-BB treatment in mouse HSC.* Am J Physiol Gastrointest Liver Physiol, 2006. **291**(6): p. G1051-61.

22. Moreno, M. and R. Bataller, *Cytokines and renin-angiotensin system signaling in hepatic fibrosis.* Clin Liver Dis, 2008. **12**(4): p. 825-52, ix.

23. Aleffi, S., et al., *Upregulation of proinflammatory and proangiogenic cytokines by leptin in human hepatic stellate cells.* Hepatology, 2005. **42**(6): p. 1339-48.

24. Bataller, R., et al., *NADPH oxidase signal transduces angiotensin II in hepatic stellate cells and is critical in hepatic fibrosis.* J Clin Invest, 2003. **112**(9): p. 1383-94.

25. Friedman, S.L., *Cytokines and fibrogenesis.* Semin Liver Dis, 1999. **19**(2): p. 129-40.

26. Inagaki, Y. and I. Okazaki, *Emerging insights into Transforming growth factor beta Smad signal in hepatic fibrogenesis.* Gut, 2007. **56**(2): p. 284-92.

27. Friedman, S.L., et al., *Isolated hepatic lipocytes and Kupffer cells from normal human liver: morphological and functional characteristics in primary culture.* Hepatology, 1992. **15**(2): p. 234-43.

28. Sato, M., S. Suzuki, and H. Senoo, *Hepatic stellate cells: unique characteristics in cell biology and phenotype.* Cell Struct Funct, 2003. **28**(2): p. 105-12.

29. Siegmund, S.V. and D.A. Brenner, *Molecular pathogenesis of alcohol-induced hepatic fibrosis.* Alcohol Clin Exp Res, 2005. **29**(11 Suppl): p. 102S-109S.

30. Lindquist, J.N., et al., *Regulation of alpha1(I) collagen messenger RNA decay by interactions with alphaCP at the 3'-untranslated region.* J Biol Chem, 2004. **279**(22): p. 23822-9.

31. Arthur, M.J., *Fibrogenesis II. Metalloproteinases and their inhibitors in liver fibrosis.* Am J Physiol Gastrointest Liver Physiol, 2000. **279**(2): p. G245-9.

32. Li, D. and S.L. Friedman, *Liver fibrogenesis and the role of hepatic stellate cells: new insights and prospects for therapy.* J Gastroenterol Hepatol, 1999. **14**(7): p. 618-33.

33. Wynn, T.A., *Common and unique mechanisms regulate fibrosis in various fibroproliferative diseases.* J Clin Invest, 2007. **117**(3): p. 524-9.

34. Chen, S., et al., *Combination of 4-1BB agonist and PD-1 antagonist promotes antitumor effector/memory CD8 T cells in a poorly immunogenic tumor model.* Cancer Immunol Res, 2015. **3**(2): p. 149-60.

35. Mellman, I., G. Coukos, and G. Dranoff, *Cancer immunotherapy comes of age.* Nature, 2011. **480**(7378): p. 480-9.

36. Ledford, H., *Cocktails for cancer with a measure of immunotherapy.* Nature, 2016. **532**(7598): p. 162-4.

37. Boon, T., et al., *Human T cell responses against melanoma.* Annu Rev Immunol, 2006. **24**: p. 175-208.

38. Zitvogel, L. and G. Kroemer, *Anticancer immunochemotherapy using adjuvants with direct cytotoxic effects.* J Clin Invest, 2009. **119**(8): p. 2127-30.

39. Darrasse-Jeze, G., et al., *Feedback control of regulatory T cell homeostasis by dendritic cells in vivo.* J Exp Med, 2009. **206**(9): p. 1853-62.

40. Jiang, A., et al., *Disruption of E-cadherin-mediated adhesion induces a functionally distinct pathway of dendritic cell maturation.* Immunity, 2007. **27**(4): p. 610-24.

41. Palucka, K., J. Banchereau, and I. Mellman, *Designing vaccines based on biology of human dendritic cell subsets.* Immunity, 2010. **33**(4): p. 464-78.

42. Shin, J.Y., et al., *Vascular endothelial growth factor-induced chemotaxis and IL-10 from T cells.* Cell Immunol, 2009. **256**(1-2): p. 72-8.

43. Curiel, T.J., et al., *Specific recruitment of regulatory T cells in ovarian carcinoma fosters immune privilege and predicts reduced survival.* Nat Med, 2004. **10**(9): p. 942-9.

44. Keir, M.E., et al., *PD-1 and its ligands in tolerance and immunity.* Annu Rev Immunol, 2008. **26**: p. 677-704.

45. Gabrilovich, D.I. and S. Nagaraj, *Myeloid-derived suppressor cells as regulators of the immune system.* Nat Rev Immunol, 2009. **9**(3): p. 162-74.

46. Gevensleben, H., et al., *The Immune Checkpoint Regulator PD-L1 Is Highly Expressed in Aggressive Primary Prostate Cancer.* Clin Cancer Res, 2016. **22**(8): p. 1969-77.

47. Butte, M.J., et al., *Programmed death-1 ligand 1 interacts specifically with the B7-1 costimulatory molecule to inhibit T cell responses.* Immunity, 2007. **27**(1): p. 111-22.

48. Carosella, E.D., et al., *A Systematic Review of Immunotherapy in Urologic Cancer: Evolving Roles for Targeting of CTLA-4, PD-1/PD-L1, and HLA-G.* Eur Urol, 2015. **68**(2): p. 267-79.

49. Ott, P.A., F.S. Hodi, and C. Robert, *CTLA-4 and PD-1/PD-L1 blockade: new immunotherapeutic modalities with durable clinical benefit in melanoma patients.* Clin Cancer Res, 2013. **19**(19): p. 5300-9.

50. Akbari, O., et al., *PD-L1 and PD-L2 modulate airway inflammation and iNKT-cell-dependent airway hyperreactivity in opposing directions.* Mucosal Immunol, 2010. **3**(1): p. 81-91.

51. Wang, S., et al., *Molecular modeling and functional mapping of B7-H1 and B7-DC uncouple costimulatory function from PD-1 interaction.* J Exp Med, 2003. **197**(9): p. 1083-91.

52. Topalian, S.L., et al., *Safety, activity, and immune correlates of anti-PD-1 antibody in cancer.* N Engl J Med, 2012. **366**(26): p. 2443-54.

53. Herbst, R.S., et al., *Predictive correlates of response to the anti-PD-L1 antibody MPDL3280A in cancer patients.* Nature, 2014. **515**(7528): p. 563-7.

54. Hodi, F.S., et al., *Improved survival with ipilimumab in patients with metastatic melanoma.* N Engl J Med, 2010. **363**(8): p. 711-23.

55. Wolchok, J.D., et al., *Nivolumab plus ipilimumab in advanced melanoma.* N Engl J Med, 2013. **369**(2): p. 122-33.

56. Ueha, S., et al., *Robust Antitumor Effects of Combined Anti-CD4-Depleting Antibody and Anti-PD-1/PD-L1 Immune Checkpoint Antibody Treatment in Mice.* Cancer Immunol Res, 2015. **3**(6): p. 631-40.

57. Mace, T.A., et al., *IL-6 and PD-L1 antibody blockade combination therapy reduces tumour progression in murine models of pancreatic cancer.* Gut, 2018. **67**(2): p. 320-332.

58. Shalapour, S., et al., *Immunosuppressive plasma cells impede T-cell-dependent immunogenic chemotherapy.* Nature, 2015. **521**(7550): p. 94-8.

59. Woods, D.M., et al., *HDAC Inhibition Upregulates PD-1 Ligands in Melanoma and Augments Immunotherapy with PD-1 Blockade.* Cancer Immunol Res, 2015. **3**(12): p. 1375-85.

60. Muyldermans, S., *Nanobodies: natural single-domain antibodies.* Annu Rev Biochem, 2013. **82**: p. 775-97.

61. Sheridan, C., *Ablynx's nanobody fragments go places antibodies cannot.* Nat Biotechnol, 2017. **35**(12): p. 1115-1117.

62. Zhang, F., et al., *Structural basis of a novel PD-L1 nanobody for immune checkpoint blockade.* Cell Discov, 2017. **3**: p. 17004.

63. Chang, H.N., et al., *Blocking of the PD-1/PD-L1 Interaction by a D-Peptide Antagonist for Cancer Immunotherapy.* Angew Chem Int Ed Engl, 2015. **54**(40): p. 11760-4.

64. Guzik, K., et al., *Small-Molecule Inhibitors of the Programmed Cell Death-1/Programmed Death-Ligand 1 (PD-1/PD-L1) Interaction via Transiently Induced Protein States and Dimerization of PD-L1.* J Med Chem, 2017. **60**(13): p. 5857-5867.

65. Chen, Z., et al., *Discovery of Aptamer Ligands for Hepatic Stellate Cells Using SELEX.* Theranostics, 2017. **7**(12): p. 2982-2995.

66. Lai, W.Y., et al., *A Novel PD-L1-targeting Antagonistic DNA Aptamer With Antitumor Effects.* Mol Ther Nucleic Acids, 2016. **5**(12): p. e397.

67. Tumeh, P.C., et al., *PD-1 blockade induces responses by inhibiting adaptive immune resistance.* Nature, 2014. **515**(7528): p. 568-71.

68. Cheng, K., N. Yang, and R.I. Mahato, *TGF-beta1 gene silencing for treating liver fibrosis.* Mol Pharm, 2009. **6**(3): p. 772-9.

69. Friedman, S.L., *Evolving challenges in hepatic fibrosis.* Nat Rev Gastroenterol Hepatol, 2010. **7**(8): p. 425-36.

70. Bonis, P.A., S.L. Friedman, and M.M. Kaplan, *Is liver fibrosis reversible?* N Engl J Med, 2001. **344**(6): p. 452-4.

71. Lindquist, J.N., W.F. Marzluff, and B. Stefanovic, *Fibrogenesis. III. Posttranscriptional regulation of type I collagen.* Am J Physiol Gastrointest Liver Physiol, 2000. **279**(3): p. G471-6.

72. Yang, C., et al., *Liver fibrosis: insights into migration of hepatic stellate cells in response to extracellular matrix and growth factors.* Gastroenterology, 2003. **124**(1): p. 147-59.

73. Fujii, T., et al., *Mouse model of carbon tetrachloride induced liver fibrosis: Histopathological changes and expression of CD133 and epidermal growth factor.* BMC Gastroenterol, 2010. **10**: p. 79.

74. Cheng, K., et al., *Biodistribution and hepatic uptake of triplex-forming oligonucleotides against type alpha1(I) collagen gene promoter in normal and fibrotic rats.* Mol Pharm, 2005. **2**(3): p. 206-17.

75. Ye, Z., et al., *Receptor-mediated hepatic uptake of M6P-BSA-conjugated triplex-forming oligonucleotides in rats.* Bioconjug Chem, 2006. **17**(3): p. 823-30.

76. Cheng, K., et al., *Enhanced hepatic uptake and bioactivity of type alpha1(I) collagen gene promoter-specific triplex-forming oligonucleotides after conjugation with cholesterol.* J Pharmacol Exp Ther, 2006. **317**(2): p. 797-805.

77. Jin, W., et al., *Discovery of PSMA-specific peptide ligands for targeted drug delivery.* Int J Pharm, 2016. **513**(1-2): p. 138-147.

78. Kato, J., et al., *Ethanol induces transforming growth factor-alpha expression in hepatocytes, leading to stimulation of collagen synthesis by hepatic stellate cells.* Alcohol Clin Exp Res, 2003. **27**(8 Suppl): p. 58S-63S.

79. Nieto, N., et al., *Ethanol and arachidonic acid increase alpha 2(I) collagen expression in rat hepatic stellate cells overexpressing cytochrome P450 2E1. Role of H2O2 and cyclooxygenase-2.* J Biol Chem, 2000. **275**(26): p. 20136-45.

80. Anania, F.A., et al., *Aldehydes potentiate alpha(2)(I) collagen gene activity by JNK in hepatic stellate cells.* Free Radic Biol Med, 2001. **30**(8): p. 846-57.

81. Qin, B. and K. Cheng, *Silencing of the IKKepsilon gene by siRNA inhibits invasiveness and growth of breast cancer cells.* Breast Cancer Res, 2010. **12**(5): p. R74.

82. Tai, W., B. Qin, and K. Cheng, *Inhibition of breast cancer cell growth and invasiveness by dual silencing of HER-2 and VEGF.* Mol Pharm, 2010. **7**(2): p. 543-56.

83. Mahato, R., B. Qin, and K. Cheng, *Blocking IKKalpha expression inhibits prostate cancer invasiveness.* Pharm Res, 2011. **28**(6): p. 1357-69.

84. Borkham-Kamphorst, E., et al., *Dominant-negative soluble PDGF-beta receptor inhibits hepatic stellate cell activation and attenuates liver fibrosis.* Lab Invest, 2004. **84**(6): p. 766-77.

85. Lin, J. and A. Chen, *Activation of peroxisome proliferator-activated receptor-gamma by curcumin blocks the signaling pathways for PDGF and EGF in hepatic stellate cells.* Lab Invest, 2008. **88**(5): p. 529-40.

86. Fontana, L., et al., *Ethanol induces the expression of alpha 1(I) procollagen mRNA in a co-culture system containing a liver stellate cell-line and freshly isolated hepatocytes.* Biochim Biophys Acta, 1997. **1362**(2-3): p. 135-44.

87. Lindquist, J.N., B. Stefanovic, and D.A. Brenner, *Regulation of collagen alpha1(I) expression in hepatic stellate cells.* J Gastroenterol, 2000. **35 Suppl 12**: p. 80-3.

88. Pignatelli, J., et al., *Hic-5 promotes invadopodia formation and invasion during TGF-beta-induced epithelial-mesenchymal transition.* J Cell Biol, 2012. **197**(3): p. 421-37.

89. Lin, X., et al., *Hesperetin derivative-7 inhibits PDGF-BB-induced hepatic stellate cell activation and proliferation by targeting Wnt/beta-catenin pathway.* Int Immunopharmacol, 2015. **25**(2): p. 311-20.

90. Roderfeld, M., et al., *Altered factor VII activating protease expression in murine hepatic fibrosis and its influence on hepatic stellate cells.* Liver Int, 2009. **29**(5): p. 686-91.

91. Bataller, R. and D.A. Brenner, *Liver fibrosis.* J Clin Invest, 2005. **115**(2): p. 209-18.

92. Zhang, M., et al., *Blockade of TGF-beta signaling by the TGFbetaR-I kinase inhibitor LY2109761 enhances radiation response and prolongs survival in glioblastoma.* Cancer Res, 2011. **71**(23): p. 7155-67.

93. Mazzocca, A., et al., *Inhibition of transforming growth factor beta receptor I kinase blocks hepatocellular carcinoma growth through neo-angiogenesis regulation.* Hepatology, 2009. **50**(4): p. 1140-51.

94. Flechsig, P., et al., *LY2109761 attenuates radiation-induced pulmonary murine fibrosis via reversal of TGF-beta and BMP-associated proinflammatory and proangiogenic signals.* Clin Cancer Res, 2012. **18**(13): p. 3616-27.

95. Wang, X., et al., *Inhibitory effect of TGF-beta peptide antagonist on the fibrotic phenotype of human hypertrophic scar fibroblasts.* Pharm Biol, 2016. **54**(7): p. 1189-97.

96. Vogel, S., et al., *An immortalized rat liver stellate cell line (HSC-T6): a new cell model for the study of retinoid metabolism in vitro.* J Lipid Res, 2000. **41**(6): p. 882-93.

97. Xu, J., et al., *New Approaches for Studying Alcoholic Liver Disease.* Curr Pathobiol Rep, 2014. **2**(4): p. 171-183.

98. Yang, H., et al., *Ilexgenin A exerts anti-inflammation and anti-angiogenesis effects through inhibition of STAT3 and PI3K pathways and exhibits synergistic effects with Sorafenib on hepatoma growth.* Toxicol Appl Pharmacol, 2017. **315**: p. 90-101.

99. Liu, C., et al., *A novel pentacyclic triterpenoid, Ilexgenin A, shows reduction of atherosclerosis in apolipoprotein E deficient mice.* Int Immunopharmacol, 2016. **40**: p. 115-124.

100. Lindquist, J.N., et al., *Characterization of the interaction between alphaCP(2) and the 3'-untranslated region of collagen alpha1(I) mRNA.* Nucleic Acids Res, 2000. **28**(21): p. 4306-16.

101. Pinzani, M., et al., *Expression of platelet-derived growth factor and its receptors in normal human liver and during active hepatic fibrogenesis.* Am J Pathol, 1996. **148**(3): p. 785-800.

102. Adachi, T., et al., *NAD(P)H oxidase plays a crucial role in PDGF-induced proliferation of hepatic stellate cells.* Hepatology, 2005. **41**(6): p. 1272-81.

103. Tang, S.L., Y.L. Gao, and X.B. Chen, *MicroRNA-214 targets PCBP2 to suppress the proliferation and growth of glioma cells.* Int J Clin Exp Pathol, 2015. **8**(10): p. 12571-6.

104. Mao, X., et al., *PCBP2 Modulates Neural Apoptosis and Astrocyte Proliferation After Spinal Cord Injury.* Neurochem Res, 2016. **41**(9): p. 2401-14.

105. Ye, J., et al., *Poly (C)-binding protein 2 (PCBP2) promotes the progression of esophageal squamous cell carcinoma (ESCC) through regulating cellular proliferation and apoptosis.* Pathol Res Pract, 2016. **212**(8): p. 717-25.

106. Li, L., et al., *Effect of RhoA on transforming growth factor beta1-induced rat hepatic stellate cell migration.* Liver Int, 2012. **32**(7): p. 1093-102.

107. Bitencourt, S., et al., *Capsaicin modulates proliferation, migration, and activation of hepatic stellate cells.* Cell Biochem Biophys, 2014. **68**(2): p. 387-96.

108. Zhao, M., et al., *Alcohol promotes migration and invasion of triple-negative breast cancer cells through activation of p38 MAPK and JNK.* Mol Carcinog, 2016.

109. Lin, X., et al., *Interplay between PCBP2 and miRNA modulates ARHGDIA expression and function in glioma migration and invasion.* Oncotarget, 2016.

110. Vlieghe, P., et al., *Synthetic therapeutic peptides: science and market.* Drug Discov Today, 2010. **15**(1-2): p. 40-56.

111. Chen, Z., et al., *Discovery of Peptide ligands for hepatic stellate cells using phage display.* Mol Pharm, 2015. **12**(6): p. 2180-8.

112. Dong, H., et al., *Tumor-associated B7-H1 promotes T-cell apoptosis: a potential mechanism of immune evasion.* Nat Med, 2002. **8**(8): p. 793-800.

113. Jain, A., et al., *Comparison of Avidin, Neutravidin, and Streptavidin as Nanocarriers for Efficient siRNA Delivery.* Mol Pharm, 2017. **14**(5): p. 1517-1527.

114. Freeman, G.J., et al., *Engagement of the PD-1 immunoinhibitory receptor by a novel B7 family member leads to negative regulation of lymphocyte activation.* J Exp Med, 2000. **192**(7): p. 1027-34.

115. Zak, K.M., et al., *Structure of the Complex of Human Programmed Death 1, PD-1, and Its Ligand PD-L1.* Structure, 2015. **23**(12): p. 2341-8.

116. Shukla, R.S., et al., *Intracellular trafficking and exocytosis of a multi-component siRNA nanocomplex.* Nanomedicine, 2016. **12**(5): p. 1323-34.

117. Zhang, Y. and O.J. Igwe, *Exogenous oxidants activate nuclear factor kappa B through Toll-like receptor 4 stimulation to maintain inflammatory phenotype in macrophage.* Biochem Pharmacol, 2018. **147**: p. 104-118.

118. Tai, W., et al., *A novel rapamycin-polymer conjugate based on a new poly(ethylene glycol) multiblock copolymer.* Pharm Res, 2014. **31**(3): p. 706-19.

119. Barve, A., et al., *An enzyme-responsive conjugate improves the delivery of a PI3K inhibitor to prostate cancer.* Nanomedicine, 2016.

120. Martin, A.M., et al., *Paucity of PD-L1 expression in prostate cancer: innate and adaptive immune resistance.* Prostate Cancer Prostatic Dis, 2015. **18**(4): p. 325-32.

121. Ghebeh, H., et al., *Doxorubicin downregulates cell surface B7-H1 expression and upregulates its nuclear expression in breast cancer cells: role of B7-H1 as an anti-apoptotic molecule.* Breast Cancer Res, 2010. **12**(4): p. R48.

122. Mittendorf, E.A., et al., *PD-L1 expression in triple-negative breast cancer.* Cancer Immunol Res, 2014. **2**(4): p. 361-70.

123. Dallakyan, S. and A.J. Olson, *Small-molecule library screening by docking with PyRx.* Methods Mol Biol, 2015. **1263**: p. 243-50.

124. Noman, M.Z., et al., *PD-L1 is a novel direct target of HIF-1alpha, and its blockade under hypoxia enhanced MDSC-mediated T cell activation.* J Exp Med, 2014. **211**(5): p. 781-90.

125. Sockolosky, J.T., et al., *Durable antitumor responses to CD47 blockade require adaptive immune stimulation.* Proc Natl Acad Sci U S A, 2016. **113**(19): p. E2646-54.

126. Lau, J., et al., *Tumour and host cell PD-L1 is required to mediate suppression of anti-tumour immunity in mice.* Nat Commun, 2017. **8**: p. 14572.

127. Sagiv-Barfi, I., et al., *Therapeutic antitumor immunity by checkpoint blockade is enhanced by ibrutinib, an inhibitor of both BTK and ITK.* Proc Natl Acad Sci U S A, 2015. **112**(9): p. E966-72.

128. Clayton, J.A. and F.S. Collins, *Policy: NIH to balance sex in cell and animal studies.* Nature, 2014. **509**(7500): p. 282-3.

129. Twyman-Saint Victor, C., et al., *Radiation and dual checkpoint blockade activate non-redundant immune mechanisms in cancer.* Nature, 2015. **520**(7547): p. 373-7.

130. Mandai, M., et al., *Dual Faces of IFNgamma in Cancer Progression: A Role of PD-L1 Induction in the Determination of Pro- and Antitumor Immunity.* Clin Cancer Res, 2016. **22**(10): p. 2329-34.

131. Abiko, K., et al., *IFN-gamma from lymphocytes induces PD-L1 expression and promotes progression of ovarian cancer.* Br J Cancer, 2015. **112**(9): p. 1501-9.

132. Homet Moreno, B., et al., *Anti-PD-1 therapy in melanoma.* Semin Oncol, 2015. **42**(3): p. 466-73.

133. Ahmadzadeh, M., et al., *Tumor antigen-specific CD8 T cells infiltrating the tumor express high levels of PD-1 and are functionally impaired.* Blood, 2009. **114**(8): p. 1537-44.

134. Tseng, S.Y., et al., *B7-DC, a new dendritic cell molecule with potent costimulatory properties for T cells.* J Exp Med, 2001. **193**(7): p. 839-46.

135. Clark, C.A., et al., *Tumor-Intrinsic PD-L1 Signals Regulate Cell Growth, Pathogenesis, and Autophagy in Ovarian Cancer and Melanoma.* Cancer Res, 2016. **76**(23): p. 6964-6974.

136. Pardoll, D.M., *The blockade of immune checkpoints in cancer immunotherapy.* Nat Rev Cancer, 2012. **12**(4): p. 252-64.

137. Schmidt, M.M. and K.D. Wittrup, *A modeling analysis of the effects of molecular size and binding affinity on tumor targeting.* Mol Cancer Ther, 2009. **8**(10): p. 2861-71.

138. Davies Cde, L., et al., *Comparison of IgG diffusion and extracellular matrix composition in rhabdomyosarcomas grown in mice versus in vitro as spheroids reveals the role of host stromal cells.* Br J Cancer, 2002. **86**(10): p. 1639-44.

139. Fujimori, K., et al., *A modeling analysis of monoclonal antibody percolation through tumors: a binding-site barrier.* J Nucl Med, 1990. **31**(7): p. 1191-8.

140. Baral, T.N., et al., *Experimental therapy of African trypanosomiasis with a nanobody-conjugated human trypanolytic factor.* Nat Med, 2006. **12**(5): p. 580-4.

141. Cortez-Retamozo, V., et al., *Efficient cancer therapy with a nanobody-based conjugate.* Cancer Res, 2004. **64**(8): p. 2853-7.

142. De Meyer, T., S. Muyldermans, and A. Depicker, *Nanobody-based products as research and diagnostic tools.* Trends Biotechnol, 2014. **32**(5): p. 263-70.

143. Zolghadr, K., et al., *A fluorescent two-hybrid assay for direct visualization of protein interactions in living cells.* Mol Cell Proteomics, 2008. **7**(11): p. 2279-87.

144. Yau, K.Y., et al., *Selection of hapten-specific single-domain antibodies from a non-immunized llama ribosome display library.* J Immunol Methods, 2003. **281**(1-2): p. 161-75.

145. Baral, T.N., et al., *Isolation of functional single domain antibody by whole cell immunization: implications for cancer treatment.* J Immunol Methods, 2011. **371**(1-2): p. 70-80.

146. Deckers, N., et al., *Nanobodies, a promising tool for species-specific diagnosis of Taenia solium cysticercosis.* Int J Parasitol, 2009. **39**(5): p. 625-33.

147. Lee, C.M., et al., *Selection of human antibody fragments by phage display.* Nat Protoc, 2007. **2**(11): p. 3001-8.

148. Li, X.Y., et al., *A novel bisindolymaleimide derivative (WK234) inhibits proliferation and induces apoptosis through the protein kinase Cbeta pathway, in chronic myelogenous leukemia K562 cells.* Leuk Lymphoma, 2011. **52**(7): p. 1312-20.

149. Ohaegbulam, K.C., et al., *Human cancer immunotherapy with antibodies to the PD-1 and PD-L1 pathway.* Trends Mol Med, 2015. **21**(1): p. 24-33.

150. Yau, K.Y., et al., *Affinity maturation of a V(H)H by mutational hotspot randomization.* J Immunol Methods, 2005. **297**(1-2): p. 213-24.

151. Abiko, K., et al., *PD-L1 on tumor cells is induced in ascites and promotes peritoneal dissemination of ovarian cancer through CTL dysfunction.* Clin Cancer Res, 2013. **19**(6): p. 1363-74.

152. Dougan, M., et al., *Targeting Cytokine Therapy to the Pancreatic Tumor Microenvironment Using PD-L1-Specific VHHs.* Cancer Immunol Res, 2018. **6**(4): p. 389-401.

153. Gainkam, L.O., et al., *Localization, mechanism and reduction of renal retention of technetium-99m labeled epidermal growth factor receptor-specific nanobody in mice.* Contrast Media Mol Imaging, 2011. **6**(2): p. 85-92.

VITA

Hao Liu was born on Nov 6th, 1985 in Tianjin, China. He received his Bachelor of Sciences degree in Pharmaceutics and Bachelor of Law degree from Tianjin Medical University in June 2007. Then, he received his Master of Science in Pharmaceutics from Tianjin University in June 2009.

He joined Tianjin Fountain Medical Development Ltd., which is a Contract Research Organization and worked as a research associate in department of ICON Central Lab-FMD China from 2009 to 2012. Then, he worked as a research associate in Novozymes, Tianjin, China for 10 months.

He started working at Dr. Kun Cheng's lab as a Graduate Research and Teaching Assistant in Division of Pharmaceutical Sciences in University of Missouri-Kansas City in 2013. Hao's project is mainly focusing on 1) Evaluation of the anti fibrotic activity of PCBP2 siRNA in primary hepatic stellate cells. 2) Discovery of small anti-PD-L1 peptide for cancer immunotherapy. 3) Discovery of anti-PD-L1 nanobody for cancer immunotherapy. He participated and published 7 different papers and received awards, including Non-Resident Alien Scholarship (2013-2016), William J. Rost Memorial Graduate Scholarship (2016), Outstanding Leadership Award as Hazardous Material Oversight Committee (2016-2017). He's member of The Rho Chi Society (An Academic Honor Society in Pharmacy) since 2016. He also served as vice-president of the Pharmaceutical Sciences Graduate Student Association (2015-2016) and successfully hosted the 2016 Pharmaceutics Graduate Student Research Meeting.

PUBLICATIONS

1. **H. Liu**, Z. Chen, W. Jin, A. Barve, Y. Wan, K. Cheng, Silencing of αCP2 Reverses the Alcohol- and Cytokine-Induced Fibrogenesis in Hepatic Stellate Cells. Liver Research, 1 (2017): 70-79.

2. Chen Z., **H. Liu**, A. Jain, L. Zhang, C. Liu, and K. Cheng, Discovery of Aptamer Ligands for Hepatic Stellate Cells Using SELEX. Theranostics, 2017. 7(12): p. 2982-2995.

3. Liu, C., L. Zhang, **H. Liu**, and K. Cheng, Delivery strategies of the CRISPR-Cas9 gene-editing system for therapeutic applications. J Control Release, 2017. 266: p. 17-26.

4. Zhao, Z., Y. Li, A. Jain, Z. Chen, **H. Liu**, W. Jin, et al., Development of a peptide-modified siRNA nanocomplex for hepatic stellate cells. Nanomedicine, 2017.

5. Jin, W., B. Qin, Z. Chen, **H. Liu**, A. Barve, and K. Cheng, Discovery of PSMA-specific peptide ligands for targeted drug delivery. Int J Pharm, 2016. 513(1-2): p. 138-147.

6. Barve, A., A. Jain, **H. Liu**, W. Jin, and K. Cheng, An enzyme-responsive conjugate improves the delivery of a PI3K inhibitor to prostate cancer. Nanomedicine, 2016. 12(8): p. 2373-2381.

7. Chen, Z., W. Jin, **H. Liu**, Z. Zhao, and K. Cheng, Discovery of Peptide ligands for hepatic stellate cells using phage display. Mol Pharm, 2015. 12(6): p. 2180-8.